2012

Measuring and filtering microwave radiations using frequency selective surface through energy saving glass

Irfan Ullah
Edith Cowan University

Recommended Citation

Measuring and Filtering Microwave Radiations using Frequency Selective Surface Through Energy Saving Glass

by
Irfan Ullah
BEng (Hons) Mobile Communication

This thesis is presented in fulfillment of the requirements for the degree of
Master of Engineering Science

Center for Communication and Engineering Research
School of Engineering
Edith Cowan University
Western Australia
February 2012

USE OF THESIS

The Use of Thesis statement is not included in this version of the thesis.

In The Name of ALLAH The Most Beneficent The Most Merciful

Dedicated to ALLAH Almighty, my loving parents whose fruitful advises always kept me motivated to achieve engineering goals. Support of my wife, son (Muhammad Hadeed) and daughter (Areeba Irfan) is unforgettable for achieving research milestones.

Declaration

I certify that this thesis does not, to the best of my knowledge and belief:

1. incorporate without acknowledgment any material previously submitted for a degree or diploma in any institution of higher education;

2. contain any material previously published or written by another person except where due reference is made in the text; or

3. contain any defamatory material.

I also grant permission for the Library at Edith Cowan University to make duplicate copies of my thesis as required.

Signed _____

Dated_____

ACKNOWLEDGMENTS

ABSTRACT

This thesis presents the results of our investigation into the measurement and filtering of microwave radiation, and the subsequent development of a microwave reduction solution for modern building architecture utilising Energy Saving Glass (ESG), in conjunction with Frequency Selective (FSS) surfaces through which useful signals can be filtered.

In the investigation, radiation power density levels arising from the three common microwave sources (radio base stations, mobile phones, and microwave ovens) were measured, and the results were compared with the standards provided by the Australian Radiation Protection and Nuclear Safety Agency. For the radio base stations, the relationship between radiation intensity levels and the important location parameters at the measurement point, e.g., line of sight, distance and elevation, are discussed in detail. Our results show that locations having the same elevation level as the RBS receive higher level of radiation, compared to those locations not at the same level.

Power density of the radiation from microwave ovens was measured at various distances and angles. The results indicate that most of the radiation is emitted through the main door of the ovens, with the doors normally being assembled utilising simple float glass. ESG was found to have desirable radiation attenuating characteristics, and was identified as an effective replacement for float glass in microwave oven doors.

In our investigation of the third potentially hazardous source of microwave radiation, the mobile handset, measurements were carried out in order to analyse power density levels during both call and idle times. Our results confirm that some handsets do not change power level, while others use higher power to communicate with the base station during a call. It is our recommendation that the manufacturers label each handset with the specific transmission power level in order to provide users with the relevant information.

The conclusions drawn from our investigations lead us to recommend that ESG be used in buildings close to RBS, so that the levels of unnecessary radiation are reduced. However, useful signals would still be transmitted by utilising the dual bandpass FSS filters designed as part of this work. We designed two distinct models of bandpass FSS filters on hard coated ESG. The first filter that we designed will block microwave signals coming from weather radar, personal communication devices, power transmission lines and emergency service radios, while transmitting useful UMTS and Wi-Fi signals; minimising the radiation impact. Only 7.30% of the coating area of the glass was removed to enable transmission in the U850 and U2100 frequency bands. The second design requires the removal of 12.35% of the coating area to enable transmission in the U800,U850,U1900 and U2100 frequency bands. Simulation results for the two designs show stable frequency responses for both TE and TM polarisations at

normal and oblique incident angles, with attenuation's below 10 dB within the passbands. Parametric studies on geometrical dimensions, substrate permittivity, and thickness help clarify the effects of these parameters upon the overall performance of FSS on hard coating ESG, and help the process of FSS design optimisation.

Contents

List of Figures

List of Tables

Nomenclature

ANSI   American National Standards Institution

ARPANSA Australian Radiation Protection and Nuclear Safety Agency

BCCH Broadcast Control Channel

CCER Centre for Communication Engineering and Research

CDMA Code Domain Multiple Excess

CNS   Central Nervous System

CSIRO Commonwealth Scientific and Industrial Research Organisation

DBP   Dual-Bandpass

DC   Direct Current

DECT Digital Enhanced Cordless Telecommunications

DES   Differential Evaluation Strategies

DL   Downlink

DSL   Double Square Loop

ECU   Edith Cowan University

EME   Electromagnetic Energy

EMF   Electromotive Force

EMI   Eelectromagnetic Interference

EMI   Electromagnetic Interference

EMR   Electromagnetic Radiation

ERP   Effective Radiated Power

ESG   Energy Saving Glass

ESME Energy Smart and Microwave Efficient

EWI Electromagnetic Wave Interceptor

FDD Fequency Division Duplexing

FDTD Finite-Difference Time-Domain

FEM Finite Element Method

FIT Finite Integration Technique

FSS Frequency Selective Surface

GPS Global Positioning System

GSM Global System for Mobile Communication

GT Geometric Transition

ICNIRP International Commission for Non-Ionisation Radiation Protection

IEEE Institute of Electrical and Electronics Engineering

INIRC International Non-Ionising Radiation Committee

IR Infrared

IRPA International Radiation Protection Association

ISM Industrial Scientific Medical

Low-E Low-Emissivity

LTE Long Term Evolution

LTE-A Long Term Evaluation-Advance

MM Mode Matching

MoM Method of Moment

NRPB National Radiological Protection Board

P-CPICH Primary Common Pilot Channel

PCS Personal Communication Devices

PEC Perfect Electric Conductor

RBS Radio Base Station

RCS Radar Cross Section

REM Rapid Eye Movement

RF   Radio Frequency

RFID   Radio Frequency Identification

SAR   Specific Absorption Rate

SRM   Selective Radiation Meter

TD   Time domain

TE   Transverse Electric

TLCD   Top Loaded Cross Dipole

TM   Transverse Magnetic

UK   United Kingdom

UL   Uplink

UMTS   Universal Mobile Telecommunication System

USA   United States of America

UV   Ultraviolet

WCDMA Wideband Code Division Multiple Access

WHO   World Health Organisation

Wi-Fi   Wireless Fidelity

WiMAX Worldwide Interoperability for Microwave Access

Chapter 1

Introduction

The rapid development of the telecommunication sector has seen the replacement of much of the physical cabling by microwave signals. While great benefit has been achieved through the application of modern wireless communication systems, concerns regarding the impact of microwaves on the environment are also increasingly being heard. During the past two decades in particular, microwave radiation saturation has increased dramatically because of high demand for such useful applications, e.g., Wireless Fidelity (Wi-Fi), mobile phones and other communication devices.

Mobile phone communication has become so widespread that it is now considered to be an essential part of our daily life. A mobile phone is a low power Radio Frequency (RF) transmitter, operating at $0.1 - 2$ W, within an operational frequency range of 450-2700 MHz. However mobile phones need to communicate with a base station or Radio Base Station (RBS), which transmits at much higher power levels. These RBSs have become one of the main sources of microwave radiations in the metropolitan and rural areas. Furthermore, while communicating a mobile phone user uses a transmitter close to his or her head, and hence the resulting exposure to the radiation is non-negligible. Serious concerns have been raised about the health impact of the increasing level of Electromagnetic Radiation (EMR) in our environment, and safety hazards resulting from RF exposure have recently become very active research topics.

From an environmental perspective, fossil fuel emission has also become a major global concern relating to sustainable development. During 1990-2007 global emission of CO_2 increased by 34%, arising mainly from the expansion in usage of fossil fuels and activity in the cement industry [75]. Thus, it is necessary to develop efficient ways of energy saving to reduce global CO_2 emissions. Energy Saving Glass (ESG) helps to reduce energy usage, and also reduces carbon emission through the reduction in energy consumption. For example, it has been estimated that each household in United Kingdom (UK) could save about £200 per year, or the equivalent of a reduction of 2 tonnes of carbon dioxide (CO_2) emission [11] by using ESG. Clearly ESG is well placed to meet challenges of radiation and carbon pollution reduction into the future, with the

tasks being accomplished by upgrading the commercial and residential buildings with a variety of different Low-Emissivity (Low-E) glass, or ESG. Importantly, ESG can also be employed to reduce the radiation level within the microwave range, and as such it is a potential useful tool to combat microwave pollution.

1.1   Motivation

In 1993, public concern was focused on mobile phone radiation hazards following the death of a woman in Florida, United States of America (USA) , due to brain cancer; her husband claiming that the cause of her death being due to radiation arising from mobile phone usage[25]. In general, the major sources of radiation pollution are the RBSs which connect the mobile phone users using RF radio waves; and it has been suggested that exposure to high levels of RF radiation could result in long term adverse health hazards. As such it was desirable to find out the RBSs radiation level in different metropolitan areas and to identify the highest exposure locations around and underneath the individual RBSs. As described earlier, the transmitting power level from mobile phones handsets is also a concern. Different types of mobile handset may have different transmitting levels, and those which transmit at higher power could lead to excessive exposure to the user's body and brain.

A second major source of microwave radiation is the microwave oven, which is typically found in every house and work place. The oven door has a special type of metallic mesh of periodic structure (hexagonal or circular), commonly known as a Frequency Selective Surface (FSS), attached to the inside face of the front glass door, which helps to attenuate radiation coming out from the microwave oven. It is important to identify safer distances to stand while food is being cooked.

In order to reduce the hazard of excessive radiation exposure, shielding solutions can be provided which employ ESG in the construction of commercial and residential buildings that are subjected to high level of radiations. ESG can be used as a building material for significantly reducing electromagnetic radiation exposure inside the building, within both the Infrared (IR) and microwave spectrum regions, the radiation can be attenuated up to 30 dB by using ESG with soft coating, and up to 55 dB by using ESG with hard coating (Fig. 2.12).

It is anticipated that the higher frequencies being proposed for future wireless communication systems should also beneficial to the screening capabilities of ESG, as attenuation levels increase with the frequency [65] [26]. A primary benefit of using ESG is that while attenuating IR and microwave radiations, ESG will enable transmission of visible light without attenuation [83][61][110]. Importantly, these thermal insulation materials can help keep buildings warmer in winter and cooler in summer, and in doing so increase their overall energy efficiency.

One of the problems associated with the existing application of ESG is that it will completely block useful mobile phone and Wi-Fi signals which are necessary for communication links. This problem can be resolved by designing a

FSS filter on the coating side of the glass [43][70][100][112][39] to improve signal transmission in the microwave bands [42], while achieving the desired attenuation level. A solution of this nature is particularly important for the locations where excessive radiation levels are present.

The design process for developing FSSs exhibiting suitable properties presents a number of challenges [70]:

- Electromagnetic waves propagating through space can have different transmission directions and polarisations. As such, the FSS should have a stable frequency response with respect to transmission and reflection characteristics for various polarisations and various angles of incidence. Polarisation and angle stable FSS designs for various thickness of glass substrate are also required.

- An important design parameter of a FSS is the percentage of coating area which must be removed. A trade-off is required in order to minimise the area where coating is to be removed, so that the required microwave radiation can be transmitted without significantly affecting the energy saving property of the glass.

This thesis includes measurements of microwave radiation levels in the vicinity of locally installed RBSs at varying angles, distances, and elevations. The intensity of EMR coming directly from microwave ovens of different brands is also measured at various distances, and the results are discussed in detail with recommendations given for a safer level. ESG was used as the shielding material at the front door of the microwave oven, and a significant reduction in radiation was observed. Measurement of the EMR from various types of mobile phones was also carried out and the results are discussed.

Finally, the thesis presents FSS on ESG designs for filtering microwave signals. The designed FSSs show stable frequency response to both perpendicular (Transverse Electric (TE)) and parallel (Transverse Magnetic (TM)) polarization at normal and oblique angles of incidence. Two typical designs of FSSs are presented for comparison purposes, and the results of a parametric scan of FSS and substrate parameters are also presented together along with detailed discussions.

1.2   Organisation of Thesis

An introduction to microwave radiation absorbers is presented in Chapter 2, providing a basic understanding of how the radiation absorbers work, and identifying the range of applications of these absorbers.

Chapter 3 presents our measurement of the microwave radiation power density levels in the vicinity of the Universal Mobile Telecommunication Systems (UMTS) near Telstra Wide-band Code Division Multiple Access (WCDMA)850 and 3GIS WCDMA2100 (local carriers) RBSs, located at Edith Cowan University (ECU), Australia. The relationship between the measured intensity levels

and three important parameters (line of sight, distance and elevation to the antenna level) are discussed in detail. Our results show that locations having the same elevation level as the RBS are more exposed to the radiation, compared to those at ground level. Moreover, the intensity level is expected to increase for higher frequencies (2.8 GHz) in Worldwide Interoperability for Microwave Access (WiMAX) and Long Term Evaluation Advance (LTE-A), whereas current Wi-Fi and UMTS are operating at the maximum frequency of 2.4 GHz.

Chapter 4 discusses the microwave radiation levels measured at varying distances and angles close to the microwave ovens during their operation. Recommendations are given for safe proximity to the microwave oven during operation. The radiation level is also measured using ESG as a shield at the front door of the oven for comparison purposes. Measurements were also carried out on the transmitting power level from different types of mobile phone. Results show that, some phones do not change power level before or during call, while other mobile phones transmit at higher power when communicating with the RBS immediately after the call is initiated. It is our recommendation that manufacturers should label every handset with the transmitting power level in order to supply users with the relevant information.

Chapter 5 presents an introduction to FSSs, including types of FSS element and corresponding frequency response of these structures. The classification of FSSs and techniques of analysing these structures are also discussed in detail.

Chapter 6 illustrates two typical designs of Dual Bandpass (DBP)-FSS filters based on hard coated ESG. The objective is to create a novel design of FSS on ESG, which can be used to block microwave signals from weather radar, personal communication devices, power transmission lines and emergency service radios, while transmitting only useful UMTS and Wi-Fi signals to avoid microwave saturation. The first design of the DBP-FSS presented here has achieved transmission requirements for two specific frequency bands, with stable frequency response for both TE and TM polarisations at normal and oblique incident angles up to 60^0. The optimised design of a Double Square Loop (DSL)-FSS sustains 92.7% energy efficiency of the original ESG by attenuating IR radiations, while transmitting the U850 and U2100 frequency bands with less than 10 dB attenuation. The second design for a Top Loaded Cross Dipole (TLCD)-FSS sustains 87.65% energy efficiency of the original ESG, while allowing the transmission of the U800, U850, U1900 and U2100 frequency bands with attenuation less than 10 dB.

Chapter 7 presents the conclusions and recommendations for future research work.

1.3 Original Contributions

The main contributions of this thesis are outlined below:

- Microwave radiation power density measurements of UMTS bands are conducted with respect to distance, elevation and angles to identify location of the highest level at ECU for the first time (Chapter 3). The results

are compared with Australian Radiation Protection and Nuclear Safety
Agency (ARPANSA) standards to provide a safety guide for the working
environment.

- Two designs of DBP-FSSs, DSL and square loop-TLCD have been de-
  veloped which enable the transmission of useful mobile phone and Wi-Fi
  signals while attenuating all other unwanted microwave signals (Chapter
  4). These designs show stable frequency response to normal and oblique
  incident angles for both TE and TM polarisations. A parametric scan of
  TLCD-FSS and substrate thickness is also conducted for future optimisa-
  tion of the designs.

- The microwave radiation measurements of a selection of microwave ovens
  at varying distances and angles are conducted, and the results are com-
  pared with Australian radiation safety standards to provide an indepen-
  dent survey of oven radiation safety (Chapter 5). Recommendations are
  made based on the results of our investigation. The radiation level from
  each oven with a normal oven glass door is measured. The ovens are then
  retrofitted with ESG and the radiation levels measured. A comparison is
  made between each set of measurements, clearly demonstrating the supe-
  rior attenuating capabilities of ESG. The results show that ESG can signif-
  icantly reduce radiation level without compromising the inside view of the
  oven. It is our assertion that our measurement of the radiation emanating
  from microwave ovens while using ESG as a shielding on the oven door
  constitute original work. Radiation levels of various mobile phones are
  also measured, both before and during the call; for analysing Uplink (UL)
  transmitting power pattern of various types of handsets. Results show
  that some handsets transmit more power to communicate with the RBS,
  while others maintain a constant level. It has been recommended that the
  manufacturer should label each mobile handset with the UL transmitting
  power.

1.4   Research Collaborations

For achieving M.Sc. project milestones and knowledge sharing, collaborative
work was conducted with different organisations and research institutes. Details
of the collaborations are given below,

CSIRO ICT Center, Australia
A collaboration was established with The Commonwealth Scientific and In-
dustrial Research Organisation (CSIRO) Center at Marsfield NSW, to work on
the ESG project. Dr Ghaffer Kiani, a post doctoral fellow at CSIRO helped in
modeling FSS to improve communication through ESG. To set up a long term
collaboration, Dr Kiani has been offered an adjunct senior lecturer position at
the Center for Communication and Engineering Research (CCER), ECU. This

should help the two organisations to further extend collaboration on other research topics in the future.

Viridian Glass, Australia

The assistance of the glass industry was invaluable; without which it would not have been possible to develop our ESG solution. Mr Peter Bland from Viridian glass supplied the glass panels utilised in the testing and design process and provided all necessary information related to the manufacture of Low-E glass.

1.5 List of Publications

Below is the list of publications which are the outcome of this M.Sc. thesis:

Conference papers

1. Irfan Ullah, Daryoush Habibi, Xiaoli Zhao and Ghaffer Kiani, "Design of RF/Microwave Efficient Buildings Using Frequency Selective Surface" ,IEEE International Symposium on Personal, Indoor and Mobile Radio Communications (IEEE PIMRC), Toronto, Canada, 11-14 Sep 2011, Pages: 1-5

2. Irfan Ullah, Xiaoli Zhao, Daryoush Habibi and Ghaffer Kiani, " Transmission Improvement of UMTS and Wi-Fi Signals Through Energy Saving Glass Using FSS", IEEE Wireless and Microwave Technology Conference (WAMICON), Clearwater, Florida, USA, 18-19 April 2011, Pages: 1-4

3. Irfan Ullah, Ghaffer Kiani, Xiaoli Zhao and Daryoush Habibi, "Selective Transmission of RF Signals through Energy Saving Glass using FSS" 12th Australian Symposium on Antenna, Sydney, Australia, 16-17 Feb 2011.

Journal Papers

1. Irfan Ullah, Daryoush Habibi, Xiaoli Zhao, Ghaffer Kiani, "Microwave Radiation Measurements and issues Associated with Radio Base Station Installed in Metropolitan Areas", Journal of Engineering Science and Technology Review (under submission process).

2. Irfan Ullah, Daryoush Habibi, Xiaoli Zhao, Ghaffer Kiani "Mobile Phones Uplink transmitting Power trend and microwave oven Radiation Safety Recommendations: A review", IEEE Transactions on Antenna and Propagation (under submission process).

Chapter 2

Electromagnetic Radiation Absorbers

2.1 Basics of Electromagnetic

In modern science EMR can be defined as the propagation of energy in the form of waves through free space or other mediums. It can be classified into two major types:

- Ionising radiations (gamma rays, X-rays, etc).

- Non-ionising radiations (RF, Ultraviolet (UV), light and IR radiations, etc).

Those radiations which are capable of ejecting an electron from an atom are commonly known as ionising radiations and those that cannot eject an electron but still induce charged ions upon contact with matter are commonly known as non-ionising radiations.

2.1.1 Differential Equations in Free Space

In free space, Maxwell's equations can be expressed in differential forms,
    Faraday's law of induction

$$\nabla \times E = -\frac{\partial B}{\partial t} \tag{2.1}$$

Ampere's law

$$\nabla \times B = \mu_0 J + \mu_0 \varepsilon_0 \frac{\partial E}{\partial t} \tag{2.2}$$

Gauss's law of electrical fields

$$\nabla . E = \frac{\rho}{\varepsilon_0} \tag{2.3}$$
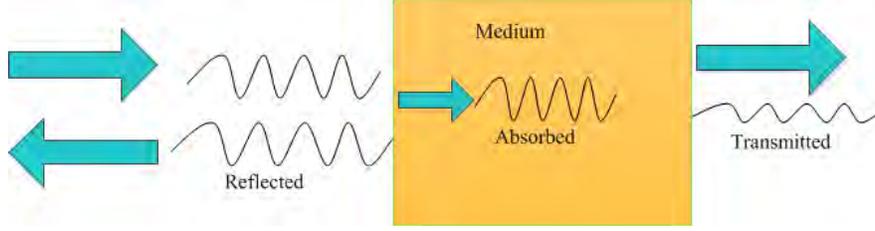
Figure 2.1: The scattering phenomenon of an incident electromagnetic wave by a medium

Gauss's law of magnetic fields

$$\nabla.\bar{B} = 0 \tag{2.4}$$

Where E is the electric field intensity, B is the magnetic flux density, $\nabla.$ is the divergence operator, $\nabla\times$ is the curl operator, $\frac{\partial}{\partial t}$ partial derivative with respect to time, ε_0 and μ_0 are permittivity and permeability of free space respectively. The simplified mutual relationship between E (electric field) and D (electric flux density), as well as that between H (magnetic field) and B (magnetic flux density) in free space can be expressed as,

$$D = \varepsilon_0 E \tag{2.5}$$

$$B = \mu_0 H \tag{2.6}$$

where $\varepsilon_0 = 8.854\times10^{-12}$Farad/meter is the permittivity, and $\mu_0 = 4\pi\times10^{-7}$ Henry/meter is the permittivity of free space respectively. The equations of electric and magnetic field propagation can be derived from the above equations,

$$\nabla^2 E = \varepsilon_0\mu_0\frac{\partial^2 E}{\partial t^2} \tag{2.7}$$

$$\nabla^2 H = \varepsilon_0\mu_0\frac{\partial^2 H}{\partial t^2} \tag{2.8}$$

2.1.2 Scattering of EMR

When a wave traveling in a free space strikes the surface of a medium, a certain portion of the wave is reflected back and the remainder is transmitted through, or is absorbed by the medium, as shown in Fig. 2.1. This process is termed scattering, and its nature is dependent on the properties (i.e. the conductivity, permittivity and permeability) of the medium.

The relationships between the propagation parameters and the medium parameters can be summarised as:

$$Z = \frac{Z_0}{\sqrt{\varepsilon_r}} \tag{2.9}$$

$$\lambda = \frac{\lambda_0}{\sqrt{\varepsilon_r}} \tag{2.10}$$

$$V = \frac{c}{\sqrt{\varepsilon_r}} \tag{2.11}$$

$$Z_0 = \frac{\mu_0}{\varepsilon_0} \tag{2.12}$$

where $Z_0 = \frac{\mu_0}{\varepsilon_0} = 377\Omega$ is the impedance of free space, λ_0 is the wavelength in free space, λ is the wavelength, v is the velocity of wave traveling inside the material, c is the speed of light in free space, and ε_r indicates the relative permittivity of the material. The main factor affecting scattering of waves from a medium is the impedance mismatch between the medium and the free space. According to equation 2.9, the material impedance Z is normally lower than the free space impedance (Z_0). Scattering of waves in free space and inside the material are the main factors to be considered during the design process of electromagnetic absorbers, because various materials have different wave attenuation, or material losses, due to different relative permittivity and permeability characteristics. Materials or mediums may be categorised into different types such as lossless, homogenous or heterogeneous, dispersive or non-dispersive, and isotropic or anisotropic. The free space can be normally treated as a linear, isotropic, homogenous, lossless, and non-dispersive medium.

2.1.3   Power of EMR in Free Space

Wave propagation in free space has minimal attenuation which typically arises from moisture or the response of molecules in the open environment. The power density of the electromagnetic wave can be calculated using a simple power equation. The starting point is the general electrical power expression,

$$P = \frac{E^2}{R} \tag{2.13}$$

where, P is the power density in watt (W), R is the resistance in Ohms (Ω), and E is the electric potential in volts (V). For electromagnetic waves, the term R in the above equation is replaced by impedance (Z) of free space. For example, if the electric field intensity is 10 V/m and the free space impedance value is 377Ω, the power density P_d of the signal traveling through space would be,

$$P_d = \frac{10}{377} Watts/meter^2 = 0.265 \frac{W}{m^2} \tag{2.14}$$
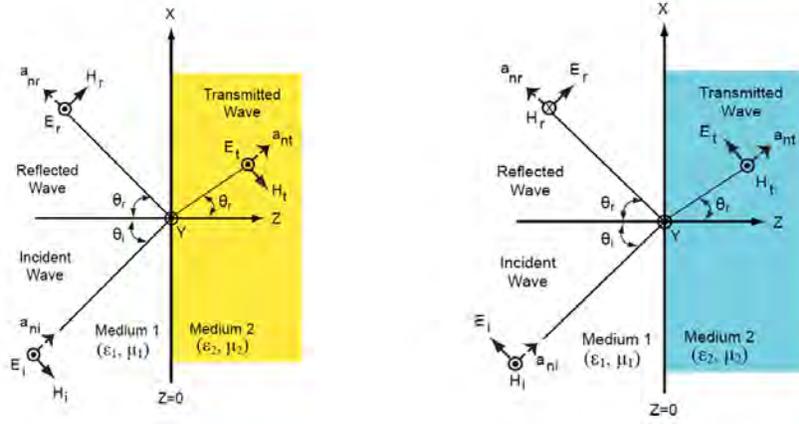
Figure 2.2: (a) Transmission and reflection of a TE incident wave with an oblique angle through (from) a dielectric surface, (b) transmission and reflection of a TM incident wave with an oblique angle through (from) a dielectric surface [38]

2.1.4 Polarisation and Oblique Angle of Incidence

RF, IR, and UV waves are all transverse electromagnetic waves, but the RF wave has a longer wavelength and lower frequency compared to IR and UV waves. The term polarisation in radio waves describes the fact that the direction of electrical or magnetic oscillation is within a plane which is orthogonal to the direction of wave propagation. Polarisation is categorised into TE and TM, which are mutually orthogonal. In a wave with TE polarisation, the induced electric field is perpendicular to the incident plane, as shown in Fig. 2.2(a), where mediums 1 and 2 can be described as less dense and more dense respectively. The incident wave hits the boundary between the two mediums with an oblique incident angle θ_i and is reflected with angle of reflection θ_r, equal to the incident angle. Conversely for a wave with TM polarisation, the induced magnetic field is perpendicular to the incident plane [14] as illustrated in Fig. 2.2(b).

The refractive index of medium 1 and 2 are represented by η_1 and η_2 respectively, where $\eta_1 = \sqrt{\frac{\varepsilon_1 \mu_1}{\varepsilon_0 \mu_0}}$ and $\eta_2 = \sqrt{\frac{\varepsilon_2 \mu_2}{\varepsilon_0 \mu_0}}$, ε_1, ε_2 are relative permittivity, and μ_1, μ_2 relative permeability of medium 1 and medium 2, respectively. The characteristics impedance of medium 1 and 2 are expressed as $\eta_1 = \sqrt{\left(\frac{\mu_1}{\varepsilon_1}\right)}$ and $\eta_2 = \sqrt{\left(\frac{\mu_2}{\varepsilon_2}\right)}$ respectively.

2.2 Applications of Microwave

Microwave radiation is a sub-class of EMR within the frequency range between 300 MHz-300 GHz, with the wavelength varying from 1m to 1mm. Microwaves play a significant role in modern industry and daily life. Currently, the most

important applications of microwaves include mobile phones, microwave ovens, Wi-Fi and radar systems. It was estimated that at the end of June 2010, there were a total of 292.8 million mobile phone users in the USA alone [56]. Initially, the major standard frequency bands for mobile phones were the Global System for Mobile Communication (GSM) 900 MHz and GSM 1800 MHz bands, which have since been upgraded to UMTS with operating frequencies of 850 MHz and $1920 - 2200$ MHz, in most countries. The new frequency bands provided higher data rate, higher channel capacity, and improved frequency reuse efficiency. When using mobile phones, the voice data is sent by handsets through the air medium to the radio base stations in UL, and the base stations broadcast back to the senders in Downlink (DL). The Wi-Fi is another major application using microwaves. However in this application, it is the data instead of the voice that is being transmitted. using a microwave system complying to the IEEE 802.11 standard (sub classification 802.11a for operating frequency of 5GHz and 802.11b and 802.11g for 2.4 GHz). Microwave ovens use microwaves to heat food by transmitting waves towards a food container. The energy of the microwaves is absorbed by the food without affecting the container appreciably. Another application of microwave radiation is microwave therapy, which has been adapted to minimise the toxic effects of chemotherapy in cancer treatment [54].

2.3   Standards for Microwave Radiations Exposure

Potential health risks from microwave radiation prompted the radiations regulatory agencies to develop, and continue to update standards concerning microwave usage on a regular basis. Some organisations distinguish these standards as public and occupation standards [4], but others have identified them by distinguishing the area under consideration; for example, controlled areas, and uncontrolled areas, instead of categories or groups of people [35].

The absorption and transmission of microwave radiation in human tissues depends entirely upon the body structure and tissue boundaries involved. However for general evaluation, the term Specific Absorption Rate (SAR) is used to define the safety standards. Usually SAR is expressed in watts per unit mass in tissue (W/kg). For example, if the weight of a human body is 80 Kg and the total power dissipation in the body is 8W, the average whole body SAR can be evaluated as 8/80 W/kg or 0.1 W/kg.

Absorption of microwaves within by human tissues will result in a temperature increase. The relation between energy absorption and temperature rise can be expressed as [91],

$$T = J/(c \times 4180) \tag{2.15}$$

where T = increase in temperature in ^0C, J = specific energy absorption in J/Kg, c = relative heat capacity = 0.85 $J(kg^0C)^{-1}$. Thus, for a person of 60

Exposure category	Frequency range	E-Field (V/m rms)	H-field strength (A/m rms)	Power density (mW/cm^2)
	100 KHz-1 MHz	614	$1.63/f$	N/A
	1 MHz-10 MHz	$614/f$	$1.63/f$	$100/f^2$
	10 MHz-400 MHz	61.4	0.163	1.0
	400 MHz-2 GHz	$3.07 \times f^{0.5}$	0.00814	$f/400$
Occupational	2 GHz-300 GHz	137	0.364	5.0

Table 2.1: Occupational reference levels for time average exposure to the RMS electric and magnetic field [4]

kg in weight, a SAR of 2 W/Kg in 30 minutes will rise the body temperature by 1^0C, when cooling effects were ignored. The majority of the western standards include additional safety margins. Worldwide standards allocation bodies are listed below:

- Australian radiation protection and nuclear safety agency, an agency of Commonwealth department of health, who established a radiation standard series in 2002 [4].

- International Commission for Non-Ionisation Radiation Protection (IC-NIRP) [34].

- The American National Standards Institution (ANSI).

- The Institute of Electrical and Electronics Engineering (IEEE) C95.1 (RF safety standard name) standard group, which worked under ANSI for a long time but recently have started to work independently [35].

- The International Non-Ionising Radiation Committee (INIRC) - the International Radiation Protection Association (IRPA). This body has been in operation for several years. In May 1991 IRPA announced the establishment of an ICNIRP standard [34], which specifically deals with RF/non-ionised radiations and defines safety standards against saturation. IRPA is a non-government and non-political organisation formed by professional bodies concerned with ionised and non-ionised radiations.

- The UK National Radiological Protection Board (NRPB), which is working as a legal adviser for the health and safety commission on both ionised and non-ionised radiations.

- The commission of the European community's, which is also drafting standards for ionised and non-ionised radiations.

Exposure category	Frequency range	E-Field strength (V/m rms)	H-Field strength (A/m rms)	Power flux density
	100 KHz-150 KHz	86.8	4.86	N/A
	150 KHz-1 MHz	86.8	$0.729/f$	N/A
	1 MHz-10 MHz	$86.8/f^{0.5}$	$0.729/f$	N/A
	10 MHz-400 MHz	27.4	0.0729	0.2
	400 MHz-2 GHz	$1.37 \times f^{0.5}$	$0.00364 \times f^{0.5}$	$f/2000$
Non-Occupational	2 GHz-300 GHz	61.4	0.163	1.0

Table 2.2: Non-occupational reference levels for time average exposure to the RMS electric and magnetic field [4]

2.4 Microwave Radiation Absorbers

There are several commercial microwave radiation absorbers available which can significantly reduce radiation impact, either as narrow band or broadband absorbers. Narrow band absorbers are usually built using a large number of lumped resistors, in order to allow tuning options for different frequencies. However, the cost of resistors in large quantity is prohibitive, and external Direct Current (DC) sources are also required, which adds complexity to the implementation [95].

Typical examples of these absorbers are the Salisbury screen absorber, the resonant absorber, and the Dallenbach absorber. They are formed from three layers, with the thickness of each layer being a quarter of the wavelength ($\lambda/4$) of the absorbing frequency. The main disadvantage of this type of screen is their large thickness, which is at least 2.5 cm if the wavelength range is between 1 mm and 10 cm (within the microwave range). Other disadvantages are: 1) this type of screen absorbs only a single frequency, 2) they do not remain effective if radiation frequency changes, and 3) they do not provide good angular stability. Researchers are working to rectify these problems in order to enhance the absorption bandwidth and angular stability of narrow band absorbers. Recently the FSS technique has been utilised to enhance the capability of the Salisbury screen absorber. A FSS fabricated sheet was placed in the outer layer of the resistive sheet and ground plane, which was designed to create extra reflection nulls at defined frequencies. Results showed three narrow absorption bands having widths in the range of 24-32% at the normal incident angle, which can be increased to 117% by loading resistive FSS with −10 dB reflectivity for incident angles ranging between $0^0 - 40^0$[12].

Traditional microwave absorbers are designed to dissolve a wave by reducing the reflectivity factor. The property of absorbing electromagnetic energy at varying frequencies can be achieved by modifying the geometry and structure of certain type of materials [46]. The laws governing wave propagation, reflection, absorption, and transformation of energy are summarised by Maxwell's equations, in conjunction with constitutive equations, definition of impedance,

and Helmholtz wave equations. The optimum design for a microwave absorber requires an appropriate material of specific dimensions, which is characteristic of a specific application. Two major types of microwave absorbers for differing applications will be discussed below.

2.4.1 Narrowband Absorber

This type of absorber is usually designed in two parallel surface layers, and provides good absorption characteristics for any particular frequency for which the absorber is configured. The structure of these absorbers is designed in such a way that the reflected wave from the outer (primary) surface interfere with waves reflected from the inner (secondary) surface. The absorption frequency of a narrowband absorber depends upon a variety of different parameters, such as the dimensions of the pattern and period, the materials and the thickness of the conducting layer and the substrate, etc. This type of absorber can also be built using many lumped resistors, which allows more tuning capabilities [95]. Salisbury screen absorbers, resonant absorbers and Dallenbach absorbers are typical examples of the narrow band absorbers.

Salisbury Screen Absorber

W.W Salisbury of MIT radiation laboratory is the inventor of this absorber, which was patented in 1952 [70]. A Salisbury screen includes a resistive sheet placed a quarter of the wavelength from the ground plane. The ground plane is an important part of the absorber, supplying backing to the absorber sheet to avoid any uncertainty. The Salisbury screen design uses the following equation,

$$\hat{Z}(z) = \hat{\eta} \frac{1 + \hat{\Gamma}(z)}{1 - \hat{\Gamma}(z)} [\Omega] \tag{2.16}$$

equation 2.17 illustrate the reflection ration as follows,

$$\hat{\Gamma}(z) = \frac{\hat{Z}(z) - \hat{\eta}(z)}{\hat{Z}(z) + \hat{\eta}(z)} \tag{2.17}$$

The reflection ration at any point of absorber can be obtained using 2.18 expression,

$$\hat{\Gamma}(z') = \hat{\Gamma}(z) e^{2\gamma(z'-z)} \tag{2.18}$$

where, $\hat{\Gamma}(z)$ and $\hat{\eta}(z)$ are the respective reflection and refractive coefficients at location z, z' is the imaginary part and γ is the gamma function.

In a Salisbury absorber, an incident wave is reflected from metal in zone 4 (Fig. 2.3). Assuming that the metal conductivity is infinite ($\sigma = \infty$), then the total impedance would be zero Ω in zone 4, and the impedance in the air region (zone 3) would be 377 Ω. The resistance of Zone 2 (thin resistive sheet) can be considered equivalent to the resistance of the parallel edges of a square over a surface [101], which can be represented as,

14

$$R_s = \frac{1}{\sigma d_1} \tag{2.19}$$

where d_1 is the thickness of resistive sheet as expressed Fig. 2.3. The compatibility goal can be achieved by matching the impedance in zone 2 and zone 3, which means that the resistive sheet impedance should be equal to or close to 377 Ω, as illustrated in Fig. 2.3; the distance between the metal and the resistive sheet is $d_2 = \lambda_0/4$ which is one quarter of a wavelength. A wave with its wavelength equivalent to an even multiple of the $\lambda_0/4$ gap will be transmitted, while waves with other frequencies/wavelength will be blocked. In this way a narrow band absorber is realised. Salisbury absorbers cannot be used for low frequencies due to the $\lambda_0/4$ distance requirement.

A Salisbury screen can result in a standing wave in space before the perfect electric conductor, caused by the interaction between the incident and the reflected waves. According to electromagnetic theory, the maximum electric field will be induced in a plane with a distance of one quarter of the wavelength before the conductor (metal), which takes place in the region of a lossy dielectric material. The maximum magnetic field will be induced at the metal edge. Absorption properties of the Salisbury screen do not depend upon the permittivity and permeability of the material. If the Salisbury screen resistance is equal to the impedance of free space ($Z0$), then the optimal thickness t can be presented as,

$$t = \frac{1}{z_0 \sigma} \tag{2.20}$$

where σ presents the electrical conductivity of sheet.

Resonant Absorber

This type of absorber structure normally has a one-quarter wavelength thickness. Resonant absorbers do not depend on the match of impedance between the free space and absorbing material. Thus both transmission and reflection start from free space at the air-absorber interface. In the next phase, an incident wave inside the medium exhibits multiple reflections, which in turn creates several evolving rays back to the incident point as presented in Fig. 2.4. The destructive interference of this reflected wave will produce absorption characteristics.

When the incident wave impinges onto the surface of the first medium, part of the wave is reflected back with a phase angle of $180^0 (\pi)$ and the remaining part transmits through the first medium. When the transmitted wave strikes the second medium it is again effected with a phase angle of π. If the distance covered by the reflected wave equals an even multiple of $\lambda_0/2$, then the reflections from the first and the second interfaces would be out of phase, and there will be destructive interference at the first interface. When designing absorbers, material thickness and properties should be selected in such a way that, the incident wave and the reflected waves should be equal in magnitude but be reversed

Zone 1 | Zone 2 | Zone 3 | Zone 4

Resistive sheet

Metal

Incident EM wave

$d_2 = \lambda_0/4$

d_1

Z_0

Short

R

d_2
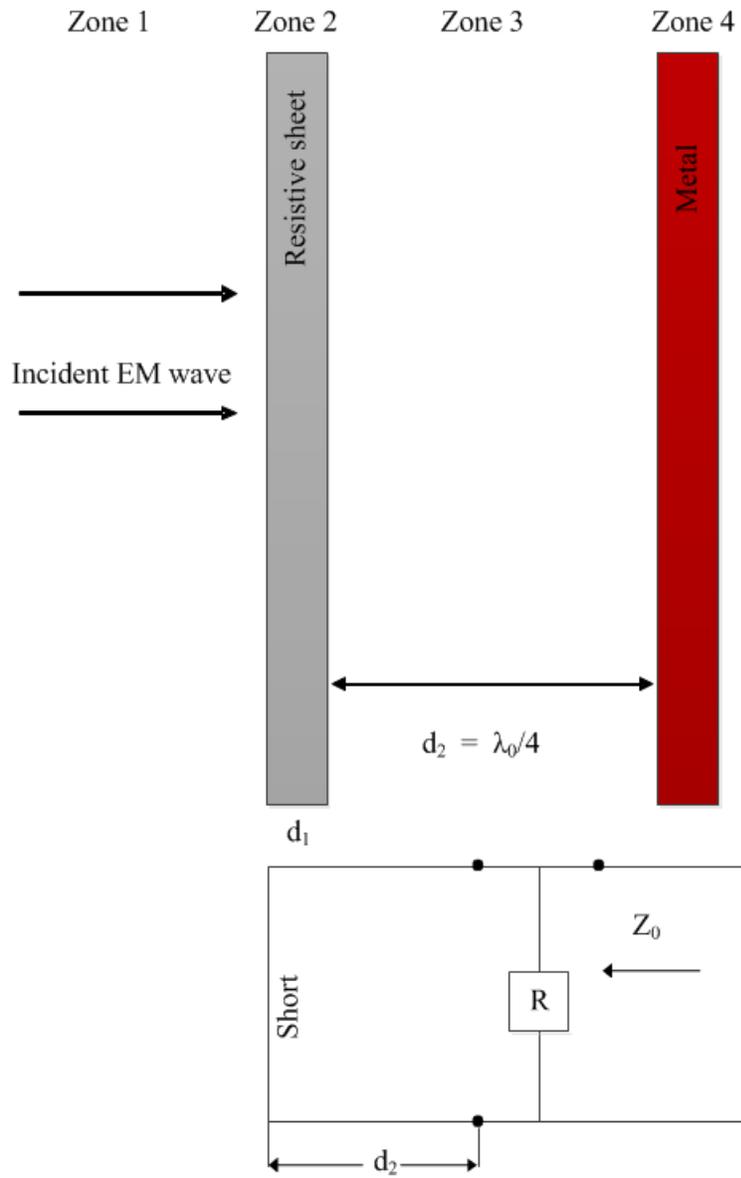
Figure 2.3: Salisbury screen absorber with a resistive sheet placed at a distance d_2 from the metal surface, adjacent is an equivalent circuit of the absorber
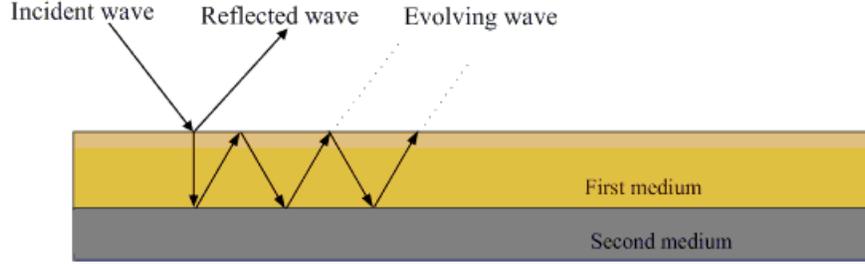
Figure 2.4: The reflection and evolving wave mechanism of an incident wave for a mulch-layered structure made of different absorbing medium.

in phase at the first interface. This can be achieved when the first layer has a thickness of one quarter of the required wavelength, producing a 180^0 phase angle difference. The absorber condition of one quarter wavelength restricts it to absorbing at only specific frequencies, without providing good stability at oblique incidence angles.

Dallenbach Absorber

A Dallenbach absorber is a single homogenous lossy absorbing layer backed by a conducting plane (metal), as illustrated in Fig. 2.5.

It can also be categorised as a resonant absorber, where waves of thickness of one quarter of the wavelength of reflected waves from the first and the second boundary with a phase difference 180^0, resulting in destructive interference. Part of the incident wave is absorbed in the air-medium interface. Good impedance matching reduces reflection, resulting in more complete wave absorption. The absorption properties can also be modified using multiple absorbing layers which improve the impedance matching from the air to the conductor (substrate), resulting in an expansion of absorber bandwidth. The equation for attaining zero reflection (maximum absorption) can be expressed as,

$$\Gamma = \frac{ztan\gamma d - z_0}{ztan\gamma + z_0} = 0 \tag{2.21}$$

$$Ztan\gamma d - z_0 = 0 \tag{2.22}$$

where Γ is the reflection coefficient at front interface, z_0 is the impedance of the air, Z is the impedance of the conductive material, d represents the thickness of absorber, and γ is the propagation constant of the electromagnetic wave.

Conductive materials can be optimised to obtain impedance matching (reducing reflection and increasing absorption) characteristics. This can be realised by altering the thickness, permittivity and permeability properties in order to achieve lower reflectivity and larger bandwidth. The electromagnetic wave reflective properties of a single layer absorber have already been discussed [72].
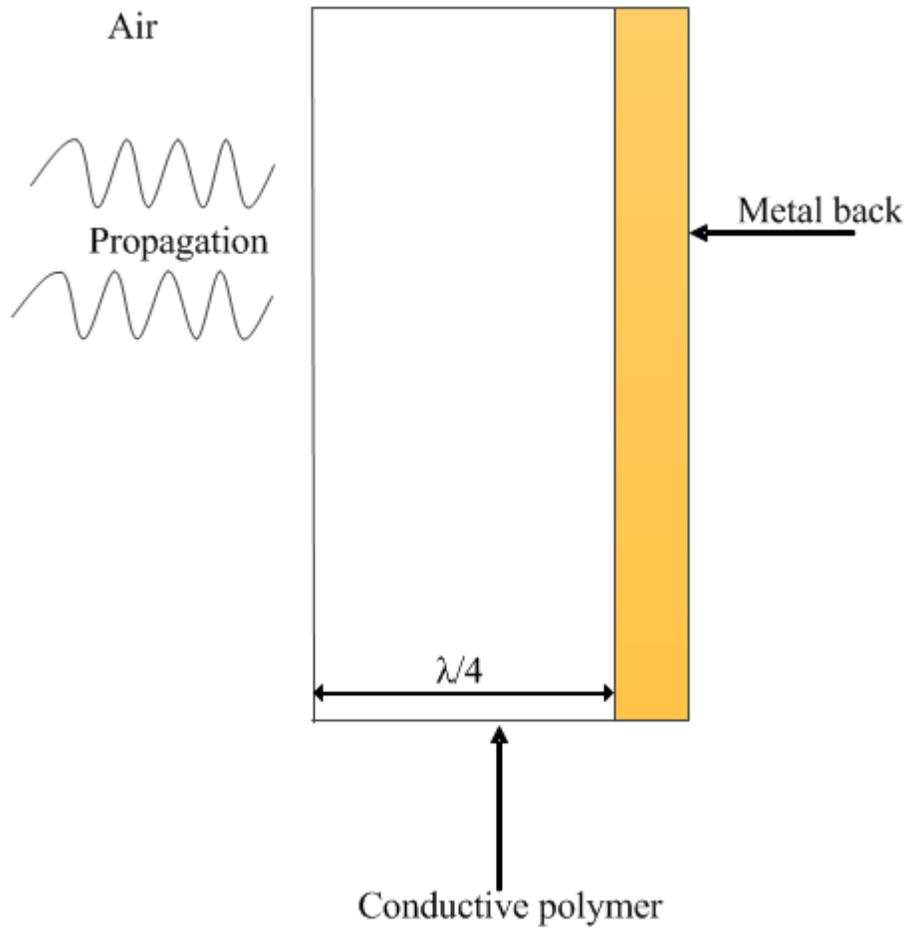
Figure 2.5: Dallenbach radar absorber consisting of magnetic material on a metal back layer.

Broadband absorption in a Dallenbach absorber cannot be attained with a single layer only, though multiple layers can provide enhanced bandwidth [59]. The Lagrangian optimisation method with constraint variables has been used to design multilayer Dallenbach absorbers. Furthermore, reflectivity issues have been resolved by using the Powell method [101].

2.4.2 Broadband Absorbers

This type of absorber generally has a broadband absorption capability, which is achieved by exploiting the basic properties of the material, and by changing the structure and layer patterns.

Jaumann Absorber

A Jaumann absorber is a combination of different resistive sheets that are layered together with equal separation between the layers (see Fig. 2.6). This absorber also exhibits resonance characteristics, and the cancellation of reflected waves is achieved by using interference technique. The distance between any adjacent layers of this absorber (reflecting surface and ground plane) is $\lambda/4$.

Geometric Transition Absorbers

This type of absorber can be further classified into four different configurations: pyramidal type, truncated pyramidal type, wedge type, and convoluted type, as shown in Fig. 2.7. The pyramidal type absorber is more common due to its good performance at higher frequencies. Foams, filled with electrically lossy materials such as carbon, are the primary material for all four configurations. These absorbers are made from two-dimensional arrays of lossy foam pyramids, cones and wedges. They are mainly used in anechoic chambers for reducing wall reflection. The broadband nature of these absorbers gives attenuation of up to -50 dB, when the thickness is 10λ. Moreover, these absorbers sustain arbitrary incident angles and polarisation direction. The materials used for these absorbers help to reduce impedance mismatch at the air absorber boundary. These absorbers do not perform well at lower frequencies (GSM) unless modified into the configuration of Geometric Transition (GT) absorbers, which contain a group of multilayer wedges [114] or range of double periodic curved pyramids [115]. The performance of GT absorbers with loaded FSS elements with respect to tolerance variation has also been investigated [23]. Their larger size limits the application of the absorbers.

Inhomogeneous Graded Dielectric Absorber

In this type of absorbers, the medium is not homogenous, and the basic electromagnetic properties (permittivity, permeability) vary at different locations. The absorber consists of a combination of different layers, with different material properties, which are stacked together on a metal surface back plane . The optimal design of layer stacking amplifies the loss tangent towards the direction
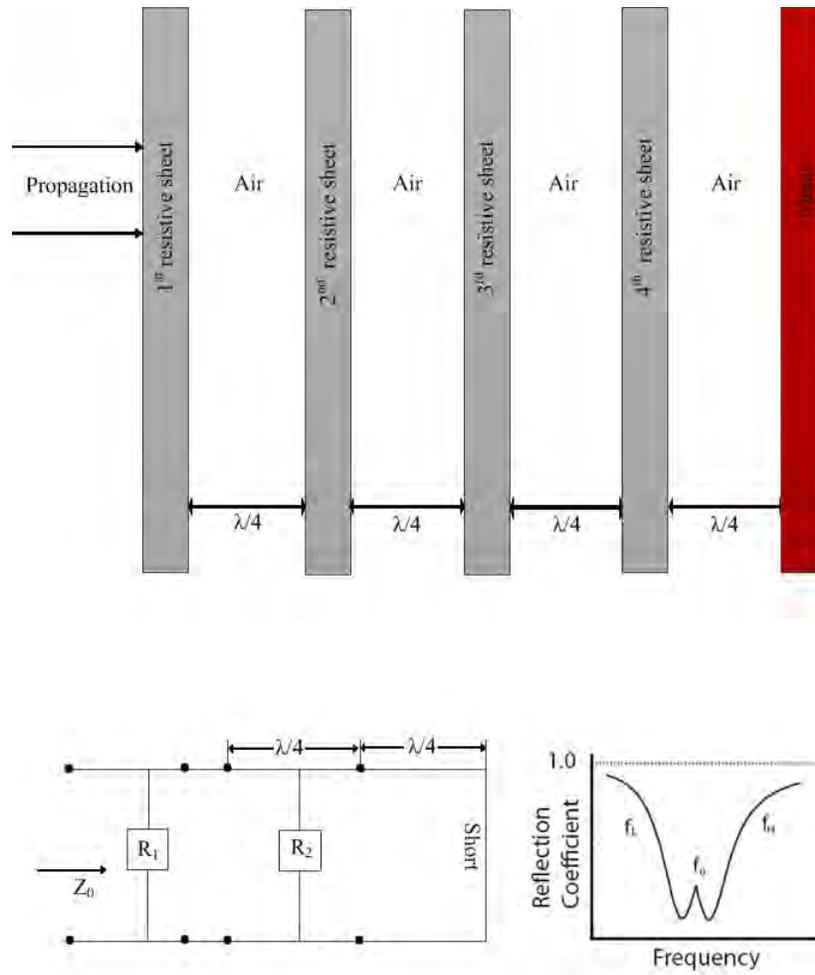
Figure 2.6: Four layer resistive sheet of Jaumann absorber backed with a conductive ground, equivalent circuit and frequency response.
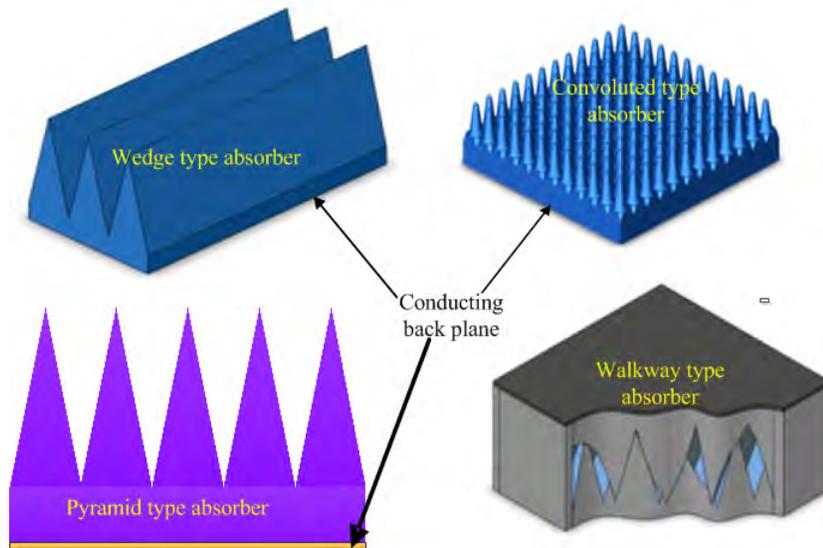
Figure 2.7: Four different types of geometric transition absorber backed with conductive ground

of the conducting layer (metal). However, it still remains a challenge to control spatial variation of electromagnetic properties (permittivity and permeability) in the material during the fabrication process.

Electromagnetic Shielding Paint

This type of absorber consists of a thin conductive coating layer painted on normal building materials, such as walls. The painting liquid is made from metal (Ag, Ag hybrid, Cu, Ni) flakes and some additives (water, pure acrylic binder, graphite, carbon black). The electromagnetic shielding paint is an alcohol–soluble broadband absorber, which can maintain its performance even at high temperatures, and has better adhesion to a range of specific materials for different applications. The viscosity of this absorber is within the range of 1000-2000 cps, while the surface resistance of single layer is $10 \ \Omega/m$. The attenuation of the absorber depends upon the number of layers and frequency range. Measured results presented in Fig. 2.9 shows that HSF 54 [117] can attenuate up to 60 dB at 2 GHz and 120 dB at higher frequencies (6 GHz). The main disadvantage of this type of absorber is that it is not transparent to visible light (Fig. 2.8), and is normally black in colour, which makes it unsuitable for use on windows (the main pathway to Electromagnetic Interference (EMI)).

Figure 2.8: Transmission measurement setup for HSF 54 shielding paint using log periodic antennas.
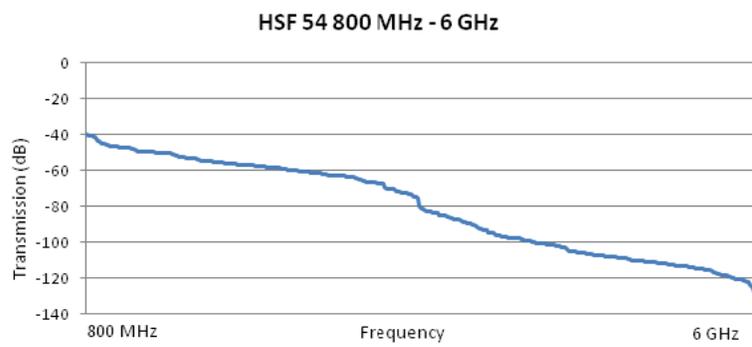
Figure 2.9: Measured transmission result of HSF 54 shielding paint with single layer coating on one side

Figure 2.10: Energy saving glass in a modern architect used to save energy and to secure indoor wireless communication system (photo courtesy of Oracle)

Energy Saving Glass

Electromagnetic shielding windows are now used as absorbers in many modern buildings (Fig. 2.10). EMI shielding windows can be classified in three types, knitted wire mesh screens, woven mesh screen, and transparent conductive coating. The third type of transparent conductive coating is known as ESG. Its manufacturing process does not require any wire mesh for EMI shielding. Instead, conductive material (metal oxide) is deposited onto the surface of ordinary glass substrate, in order to achieve thermal and microwave isolation, while allowing transmission of the visible light spectrum. It exhibits different attenuation capabilities according to the material used in the manufacturing process. For example, measurement result for Viridian ComfortSave^{TM} [102] shows 55 dB attenuation for the frequency range of 800 MHz - 3 GHz (Fig. 2.12) attenuation. For illustration purposes, the measurement setup is presented in Fig. 2.11.

ESG is considered to be the best radiation absorber which can attenuate electromagnetic waves in the IR and microwave region, while transmitting in the visible light spectrum. Another characteristic of ESG is to enhance the original beauty of building (Fig. 2.10).
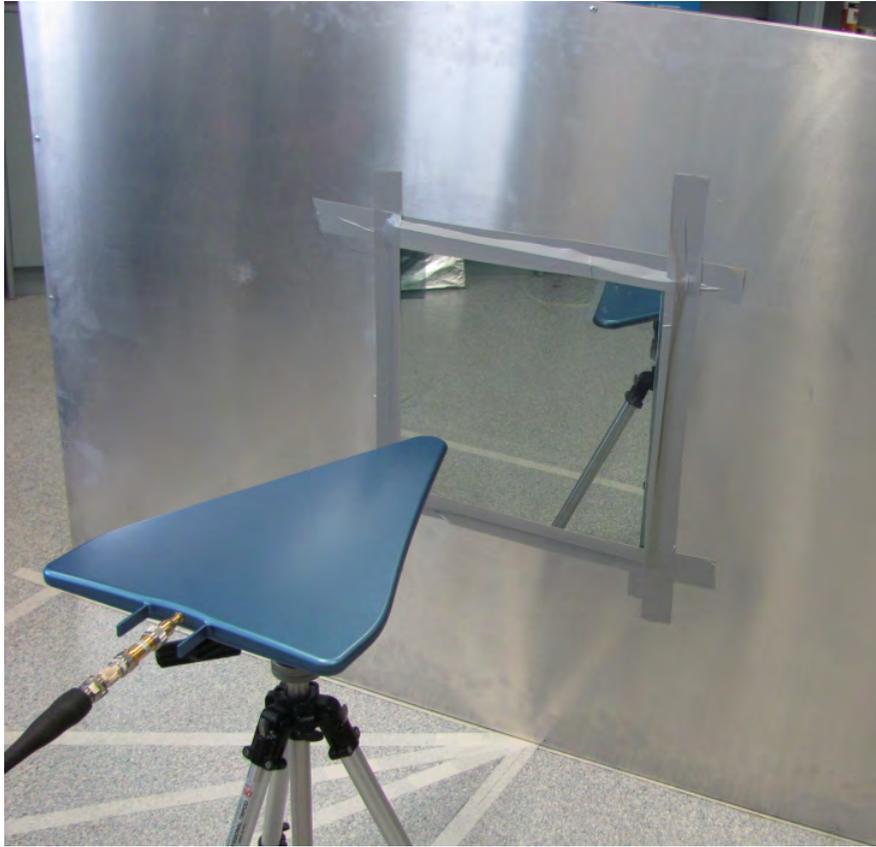
Figure 2.11: Transmission measurement setup for ComfortSave^{TM} ESG in the frequency range of 800-3000 MHz using log periodic antennas.
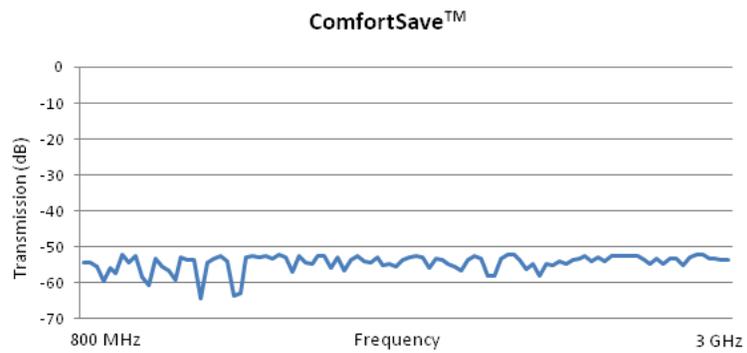
Figure 2.12: Measured transmission result of ComfortSave^{TM} ESG with full coating on one side.

Chapter 3

Microwave Radiation Measurements

3.1   Potential Microwave Radiation Hazards

The number of mobile phone users worldwide has dramatically increased during recent years, especially after the upgrading from GSM to UMTS. The benefits for using UMTS are that it can effectively used for voice, video communication and net browsing due to its higher data rate/channel capacity than that GSM provides. This increase has led to more RBSs being installed in metropolitan areas, in the very locations that citizens may be concerned about associated potential hazards; i.e. near their homes or workplaces. Due to the ongoing conflict between the demands for more communication facilities and the community opposition to these RBSs, telecommunication enterprises have been forced to take these prospective risks seriously. A general consensus has been achieved that the radiation exposure guidelines should be based on the worst case scenarios [94].

For more than two decades researchers have examined disease impacts of RBSs on human beings; for example, cancer and brain tumors as well as more subtle potential effects such as headaches, body temperature increase, sleep disorders and other unexpected health symptoms.

In the early stages of the introduction of mobile phones, research (1994) on health impacts of microwave radiation reported that electromagnetic radiation could induce a blood brain barrier [88], promote the development of brain tumors [26][87], promote the development of tumors with neuronal features [73], and cause damage to DNA [84]. In 1995, research on the effect of exposure to radiation on human brain activity during sleep revealed a correlation between reduction of sleep latency and percentage of Rapid Eye Movement (REM), and the increase in radiation power flux density near a GSM base station. REM sleep in turn, has a significant impact on information handling in the brain, specifically on the learning processes [55]. Heating due to microwave radiation

may disturb human biological infrastructure. However not all mechanisms directly linked to heating produce significant effects at higher exposure levels, for example, electrical induction in body cells and electroporation [24]. The World Health Organisation (WHO) conducted a broad study in 2005 to identify effects of short-term usage of mobile phones[108] and found no major adverse health effects. However, more research work is needed to elucidate the effects of long-term exposure to microwave radiations, which can increase the thermo-embolic risks in the endothelial cell line [10]. Hinrichs et al. discussed the influence of a GSM 1800 base station in a far field exposure experiment of double-blind design type. A vertically polarised electromagnetic field from the GSM 1800 MHz band continuously radiated 13 subjects for 2 nights. No significant adverse health impacts were identified during sleep. However it was suggested that different carrier frequencies should also be tested, specifically at higher frequencies, such as the UMTS bands which could be critical in sleep disturbance. As sleep and working patterns may be affected, it was recommended that these factors be considered in motivation and alertness studies [31].

In 2005 a broad review conducted by Moulder [67] revealed cancer occurrence relating to RBS radiation. Referring to the biological considerations, it had been proven theoretically that radiations initiated by mobile phones and radio base stations have significant effects when interacting with the human body. However, the epidemiological facts for an informal association between cancer and microwave energy were not strong enough to support the conclusion. Results of animal studies were not sufficiently consistent to verify potential hazards of microwave radiations. This review was not able to clarify an exact association between cancer and RBS, but it was suggested that more research on epigenetic effects should be conducted. To date, studies on the effects of mobile phone radiations (GSM 900 and 1800 MHz) have revealed cognitive impacts, however the debate is still ongoing.

In 2007, a meta-analysis was conducted in which a total of 19 studies were tabled for consideration, with 10 studies which fulfilled the criteria for relevant robust research being analysed in detail. The study concluded that electromagnetic radiations emanating from a GSM base station may impact on human concentration; and that response times for computational subtraction tasks could be affected. A further issue was associated with working memory, as measured by the N-back test. As both effects were very small, further study employing a double blind study structure was recommended, in order to focus specifically on changes to attention and working memory [7].

An interview-based study which considered subjects at risk of brain tumor due to mobile phone radiations was published in 2010. It was conducted between 2000-2004 in 13 countries including Australia, on 2708 glioma and 2409 meningioma patients. This research was funded and monitored by the International Agency for Research in Cancer. In this study, questionnaires were based on different topics, such as basic demographics, usage of mobile phone and other wireless communication equipment, occupational exposure to Electromotive Force (EMF) and links to other risk factors: 1) location of residence from ionised radiation transmitter, and 2) family history of cancer. All cases were determined

in neurological and neurosurgical treatment facilities. In the case of glioma patients, 60% were men and 40% were women, whereas for meningioma patients, 24% were men and 76% were women. No risk of either glioma or meningioma arising from the usage of mobile phone was discovered. However, risk of glioma or meningioma was suspected to arise due to higher RF-Electromagnetic Energy (EME) exposure. It was suggested that further investigations are required on the long-term health hazards of heavy mobile phone usage [27]. Another study was published on the effect of GSM 1800 MHz radiation transmitting antenna on children immature Central Nervous System (CNS) in 2010. The cell stress and glial responses in the brain of growing rats were computed after the rats were exposed to GSM 1800 MHz signal transmission for 2 hours at the SAR range of 1.7- 2.5 W/kg. From the results it was not possible to identify any cortical cell responses indicating that short-term exposure can induce neurotoxic effects in growing rat brains. However, this could have negative effects on neural cell signaling or gene expression in the development and maturation of glial cells and neuronal infrastructure. It was also recommended that further research be conducted on repetitive exposure at different developmental stages [105].

A study conducted by Heinrich, examined the effects of RF-EME exposure to mobile base station transmissions, by selecting and personal interviewing 3022 young people and children in 4 different cities in Germany. Each user operated a mobile phone for a short period of time each day (half of the children and all adults owned mobile phones). In this research no association between exposure and chronic symptoms during normal waking hours were identified. However, an association was observed between self-reported usage of mobile and Digital Enhanced Cordless Telecommunications (DECT) phone and impatience in young people [30]. Radiation level was measured by keeping a dosimeter near the bed of each participant during the night, resulting in a constant and arbitrary measurement; because valid readings can only be recorded by moving the dosimeter. In this study a dosimeter was kept with each participant for 5 hours of the 24 hours cycle. It was suggested that both long term exposure and keeping the dosimeter for a longer duration with each participant should be assessed for both children and adolescents [30].

A recent study also focused on the effects of RBSs (using UMTS and GSM 900) on the macro structure of sleep. This study consisted of an adoption night (worked as a screening night) and an adjustment night in a testing environment. The study was conducted for 9 nights, with a gap of 2 weeks, on 30 men with ages ranging from 18-30 years, who were subjected to three different radio frequency exposures (WCDMA/UMTS, GSM 900 and sham). Potential health effects were observed on the human nervous system by examining a period of 8-hours of continuous sleep, and found no change to the sleeping patterns. This research was conducted on the assumption that the handset was transmitting at a maximum power with is less than the SAR = 2.0 W kg-1 specified under guidelines of ICNIRP [33].

A report published online in 2011, stated that the total brain tumor (benign and malignant) incidents were 18.71 per 100,000 persons per year, with 11.52 per 100,000 persons diagnosed with a benign tumor, and 7.19 per 100,000 with a

malignant tumor. Past studies on brain tumors were reviewed and indicated the exact relationship between development of brain tumor and RF-EME radiation exposure [76].

The impact of the position of the user of the mobile handset, in closed and free space environment over SAR in the human head-phantom, generated by mobile phone transmitting antenna, was studied in 2011. The SAR distribution within the human head-phantom was simulated using a Finite Difference Time Domain (FDTD) technique, and found no significant difference between the exposure of human head in closed space and free space [5].

In summary, global attention has focused on the potential health hazards of microwave radiation due to rapidly increasing numbers of RBSs and mobile phone users. Direct links between exposure to radiation and health disorders have been confirmed in some cases, and require further investigations in other cases. Therefore the need for shielding buildings from microwave radiations has become a serious public concern.

3.2   Effects of Radiation Exposure

Due to the rapidly increasing number of mobile phone users, operators in various countries have upgraded frequency spectrum according to new standards. The early analogue services used the frequency range near 850 MHz, GSM standard bands used the 900 MHz and 1800 MHz ranges, while UMTS used the range above 2000 MHz in most countries, as shown in Table 3.1. These operating frequencies are close to the Industrial Scientific Medical (ISM) bands (915 and 2450 MHz) used in USA for microwave ovens and medical equipments respectively.

The RBSs transmit microwave signals at a required power level, commonly known as Effective Radiated Power (ERP), which is a measure used to determine the power intensity of radiated signals (typically 200-2000 W). However, ERP is not constant for each micro cell. For example, in metropolitan areas transmitting power can be 10 W, whereas in rural areas this value may increase more than 10 W. In metropolitan areas, small micro cells are used for providing better coverage within a radius of a few hundred meters, which is in contrast to the multiple kilometer radius utilised in rural areas.

The amount of microwave energy absorbed by the human body is measured as the SAR value, which can be described as power absorbed (W) by per kilogram of tissue (W/Kg). The measurement condition requiring that the subject be within the far field, or more than one wave length away from the antenna. The intensity of the microwave radiation beam is measured in power density (power per meter square W/m^2). The exposure can increase when the subject is closer to the RBS, which should be always below the specified limit (defined for both general public and occupational categories).

As previously noted, countries including the USA, Canada and Australia have already established microwave radiation standards to provide for a green

Frequency bands	Uplink frequency (MHz)	Downlink frequency (MHz)	Region
2100	1920-1980	2110-2170	Oceania, Europe, Asia
1900	1850-1910	1930-1990	North America
850	824-849	869-894	Australia, Hong Kong
800	830-840	875-885	Japan

Table 3.1: Worldwide frequency allocation table of the paired Universal Mobile Telecommunication System (UMTS)-FDD Bands.

environment, However, the long term health effect of radiation is still not a clear issue, and further investigation is required.

3.3 Problem Description

During recent years, RBSs have been installed densely in metropolitan areas to provide better coverage. For example, at ECU Joondalup campus, Telstra Corporation and 3GIS Pty Limited (local operators) have installed a roof top RBS on building 21 to transmit radio signals of WCDMA850 and WCDMA2100 bands respectively for mobile phones communication.

Several other buildings are located within 100 m of the RBS. In these buildings most of the staff members, students, and even the children at the childcare center, spend approximately 8 hours every day of a normal working week. Concerns have been raised, as previous studies suggested the presence of potential health hazards for those who remain at a location within 300 m from RBS for a minimum of 1 hour a day [89]. Furthermore, those students and children who spend most of the time outside buildings receive more exposure to microwave radiation, compared with those who stay inside the buildings. This is because the radiation level is reduced considerably inside the buildings, due to the absorption property of the building walls [83]. Therefore it is desirable to measure the microwave radiation level at different locations near building 21 (where RBSs are installed), including areas inside building 21, outside of building 19, and public places within 100 m radius of the RBS transmitting antenna. The measured results should be compared with the ARPANSA standards and the potential health hazards assessed. It is also desirable to provide an Electromagnetic Interference (EMI) shielding solution, in order to reduce current levels of radiation in the vicinity of the RBS. The proposed shielding solution will be employed in future Energy Smart and Microwave Efficient (ESME) buildings.

Other sources of microwave radiation include microwave ovens to be used in the prospective ESME. Safe distance and safe angle from the microwave oven

door should be defined, and then observed by the operator while the ovens are in use. Transmitting power behavior of various mobile phones must also be analysed, in order to obtain a clear understanding of the effects of microwaves on the user's heath while communicating with mobile phones.

3.4 Effect of Geographical Location of Microwave Radiation Transmitter

Radiation intensity at a specific point can be influenced by a range of factors, including: 1) distance between the transmitting antenna and the object, 2) number of RBS channels in use, 3) quality of received signals (poor reception handsets transmit more power to communicate and vice versa) and 4) angle of exposure. Research results relating to radiation induced cancer and leukemia have raised concerns, specifically for those who are living in close proximity to a mobile phone base station or radio or TV transmitter. A national debate was started in Italy following a media report concerning the growth in diagnosis of leukemia within a 10 km radius of Vatican radio station. However, debate could not go farther because analysis was only focused on small group and defined area as a substitute of exposure [62]. Cancer clusters were also identified in the vicinity of an FM/TV broadcasting base station during a 1997 study conducted in UK. Incidence of leukemia declined with increasing distance from the transmitting antenna [20]. An Australian study also reported a higher rate of leukemia in children and adults within 2 km of a radio base station [32]. Most of these studies utilised a single line of sight and distance from an antenna, as a substitute indicator for radiation exposure. However, the radiation pattern from a broadcasting antenna is highly dependent on the angle i.e., they are angle dependent, with beam intensity also changing due to reflections from objects and the terrain along its direction of propagation. Exposure is also dependent upon the total time which one spends while he stays at one particular location. Radiation power density should be measured at a selection of geographical locations surrounding an antenna, in order to identify the locations with the highest radiation levels. Thus, a questionnaire based survey was conducted on 530 residents (male and female) living close (50 m, 100 m, 300 m or > 300) to the roof top antenna of a mobile base station for 1 year or longer. More symptoms of headache, nausea, loss of appetite, sleep disturbance, depression, discomfort and visual interruption were found in people living within 100 m of the base station. These symptoms declined with increasing distance. For example, at 200 m only headaches and sleep discomfort were identified. At a distance of more than 300 m these effects were significantly reduced, particularly for those living in a house which is not facing towards the antenna [89]. It was suggested that a minimum distance from roof top RBS to the exposed subject should be at least 300 m. However, the candidate could not identify any published study which addressed the influence of radiation pattern and angular power distribution in a substantive manner. The radiation pattern of a RBS is determined by

its directionality. Research shows that the radiated power from the azimuthal direction of an RBS could be designed as a Gaussian function [22] or a Laplacian function [15]. Thus, it is necessary to measure the radiation power density surrounding the base station transmitting antenna, which is of concern.

3.5   Purpose of the Measurements

Since RBSs in metropolitan areas are installed close to each other, and it is necessary to determine exposure levels, proximity, location, and angle to depict the most affected area; this research only focuses on RBSs installed at the Joondalup campus, ECU. The base station antennas under consideration have been installed on the roof of Building 21. It has been reported that potential hazards exist for those who stay at least 1 hour a day at a location which is within 300 m of a RBS [89]. GSM-RBS measurements were conducted in Palestine in 2010 for radiation power density following ICNIRP and FCC standards; results were recorded at 3, 6, 10, 15, and 20 m away from the transmitting antenna. It was determined that there was an inverse linear relationship between exposure and distance. It should be noted that the receiver was on the ground and the antenna was mounted on a 17 m high mast [68]. It has been determined that when evaluating the level of RF-EME within the vicinity of the RBS at ECU, the measurements are taking over longer periods of time and at different selected locations. Our initial results at ECU showed that higher levels of radiation are measured at locations which are at same height as the transmitting antenna. This is an important consideration when attempting to effectively shield buildings or apartments closer to the roof top RBS.

3.6   Measurement Methods

For comparison purpose, this research only focus on RBSs installed at the Joondalup campus, ECU. EMR power density measurement was performed using Selective Radiation Meter (SRM)3006. A calibrated isotropic antenna and a 1.5 m RF cable were used with a tripod at 1.5 m height above the ground to reduce interference as shown in Fig. 3.1 & 3.2.

UMTS measurements require configuring channels at code level since they use Code Domain Multiple Access (CDMA), in which the Primary Common Pilot Channel (P-CPICH) shares the same spectrum with other traffic channels, which makes it difficult to measure P-CPICH powers separately. Whereas GSM channel can be measured easily using a selective receiver because the Broadcast Control Channel (BCCH) is separated from the traffic channel while utilising constant power. In our measurement, power of P-CPICH was measured by using an option which enables identification of the number of scrambling codes, and their subsequent power levels. Bandwidth ranges for the Telstra base station and the 3GIS were set to 884.7 MHz $- 889.7$ MHz and 21101 MHz $- 21151$ MHz respectively. The radiation power density was measured during normal

Figure 3.1: Irfan Ullah (L) and Dr Xiaoli Zhao (R) measuring RF-EME levels for the Telstra WCDMA 850 and 3GIS WCDMA2100 inside Building 21 at ECU using a selective radiation meter 3006.

Figure 3.2: The selective radiation meter 3006 used to measure the RF-EME level from the Telstra WCDMA 850 and 3GIS WCDMA2100 (in line of sight).

working days, when the majority of staff and students were present in the University. Only DL bands of the UMTS cellular base station was measured. The resolution bandwidth was set to 200 KHz, and the measured frequency band (at 350 measurement points) was scanned in each 30 sec interval to generate the maximum and average data during the specified time period. All measurements were conducted using the ARPANSA guideline [4]. ARPANSA is an agency responsible for establishing the general public and occupational radiation protection standards. Levels were observed at more than 200 locations inside and outside of Building 21 where the roof top RBSs are installed, for a duration of 1 minute each, to locate the highest radiation levels and identify the most important locations for carrying out further detailed measurements. After four such locations were determined, measurements were carried out for 2 hours at each selected location, and then 24 hours at the locations with the highest level, for each of the two base stations. The level of power density was given in W/cm^2.

3.7   Results and Discussion

According to the ARPANSA standards, the RF-EME general public limit for the Telstra WCDMA850 service is 0.44 mW/cm^2 and the 3GIS WCDMA2100 service is 1 mW/cm^2. The measured results at 100 m distance from ground floor of the building adjacent to the RBS, building 19 are shown in Fig. 3.3 (for 3GIS WCDMA2100) and Fig. 3.4 (Telstra WCDMA850). The approximate angle formed between the vertical line and the line joining the RBSs and radiation meter was 45^0. For the 3GIS band power density was remained within the range of 0.70 - 0.75 nW/cm^2 for the 2 hour measurement period, except at one instance when it approached to 1 nW/cm^2. During the 2 hour time period the power density of the Telstra band (Fig. 3.4) was higher than that of the 3GIS (Fig. 3.3), while the exposure limit of the Telstra band (0.44 mW/cm^2) was less than that of the3GIS band (1 mW/cm^2). The Telstra radiation level was relatively stable (2.0 - 2.3 nW/cm^2) and was lower than the limit specified by the ARPANSA guidelines.

Fig. 3.5 presents the results of measurements taken for the Telstra base station when conducted inside the top floor (Room 21.521) of Building 21, with the SRM 3006 placed at an approximate angle of 30^0, and 30 m distance from the Telstra base station. In this case, the reflection and attenuation of signals when passing through the roof need to be considered in conjunction with the directionality of the antennas. It was noticed that even when the measurement location was closer to the transmitting antenna (RBS), the radiation power density was lower (150 - 170 pW/cm^2) than in Fig. 3.4 (100 m). This effect was due to the attenuation of the radiation by the building roof, as well as the directionality of the RBS antenna. The measured level for the 3GIS (Fig. 3.6) at the same location was again lower (50 - 60 pW/cm^2) than that of the Telstra unit. The radiation levels for both bands were well below the limits specified in the standard. Compared to the previous level (Fig. 3.3 & 3.4), it was concluded that staff who work immediately below the roof top antenna in rooms at the top
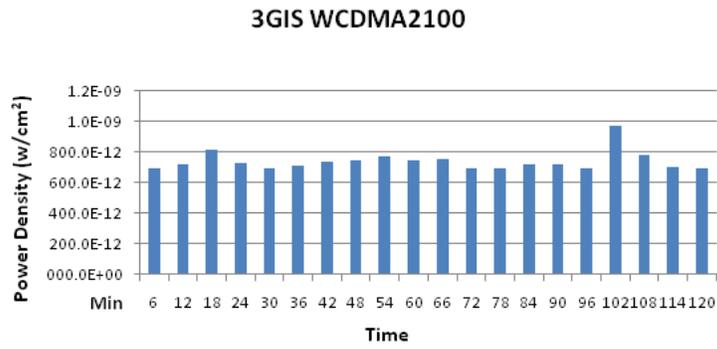
3GIS WCDMA2100

Figure 3.3: RF-EME measured level of 3GIS WCDMA2100 band over 2 hours period, outside of building 19 at ground floor in line of sight to the transmitting antenna.
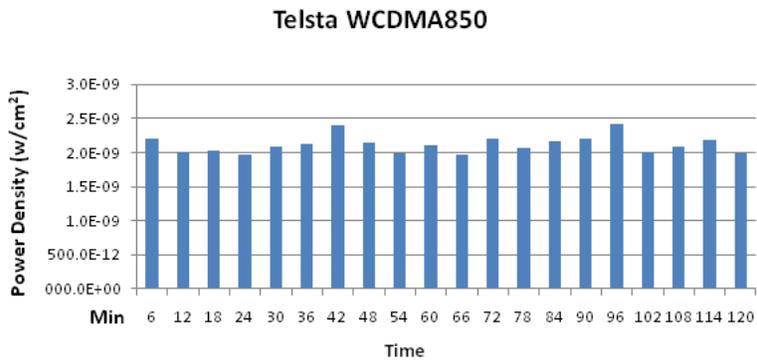
Telsta WCDMA850

Figure 3.4: RF-EME measured level of Telstra WCDMA850 band over 2 hours period, outside of building 19 at ground floor in line of sight to the transmitting antenna.
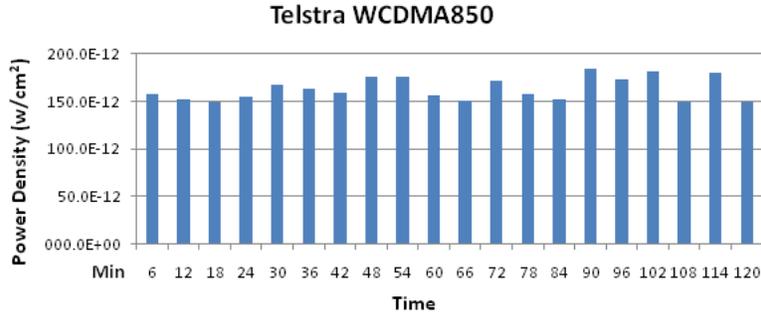
Telstra WCDMA850

Figure 3.5: RF-EME measured level of Telstra WCDMA850 band over 2 hours period, inside the room number 21.521 on top floor of building 21 at an angle of 30^0 and 30 m away from the transmission point.

level of Building 21 received less radiation exposure per unit time than students outside of the adjacent buildings.

Fig. 3.7 presents the measurement results for the Telstra base station which were again contained on the top floor of Building 21 (Room 21.501), below the RBSs at a 170^0 angle. These results (Fig. 3.7) clearly indicate that at the same floor and through the same roof construction material, the radiation level becomes even lower (60 - 65 170 pW/cm^2) as compared to that in Fig. 3.5 (30 m away from transmitter). However, for the 3GIS bands the difference in the levels (Fig. 3.8) was not significant. All the measured levels remained below the ARPANSA defined limit. Therefore, among all the locations where measurements were taken, the location with minimum radiation exposure was immediately below the RBS. This location was later assigned to research students, who normally work more than 8 hours a day there.

The last measurement point for the Telstra base station (DL) was in Building 19, outside room 19.388. The location was 100 m away from the antenna, and at approximately 180^0 in the line of sight as shown in Fig. 3.9. Out of the four selected locations this was the highest exposure point in the vicinity of the base station. The maximum level reached was more than 70 nW/cm^2 on 2 occasions, whereas most of the readings were between 40 - 60 nW/cm^2 and two readings at > 70 nW/cm^2, as illustrated in Fig. 3.9. This point was at the same distance and direction as the measurement point where the result was shown in Fig. 3.4, the only difference being the angle for the line of sight. In Fig. 3.4 (at ground level of Building 19) the maximum level was below 2.5 nW/cm^2, when a 45^0 angle was formed between measurement meter and RBS. However, at a 180^0 angle the radiation level exceeded 70 nW/cm^2, which shows a large variation in radiation exposures due to a change of relative orientation between the RBS and the measuring antenna. To verify this conclusion, measurements were conducted over 24 hours for Telstra and 3GIS RBSs separately. Fig. 3.10 & 3.11 show the 24 hours result for the Telstra base station. The radiation level always remained

35

3GIS WCDMA2100 Band
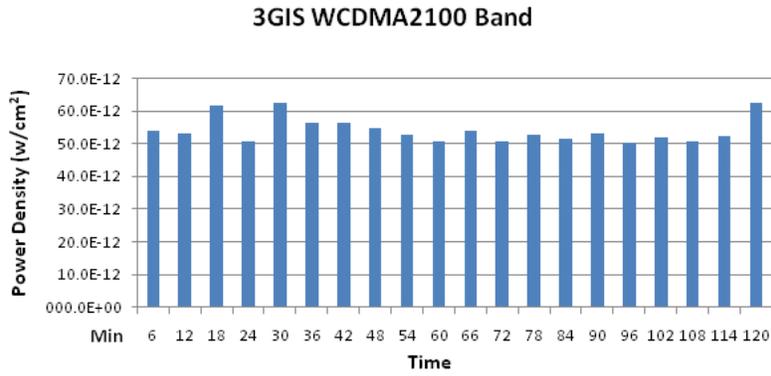
Figure 3.6: RF-EME measured level of 3GIS WCDMA2100 band over 2 hours period, inside the room number 21.521 on top floor of building 21 at an angle of 30^0 and 30 m away from transmission point.
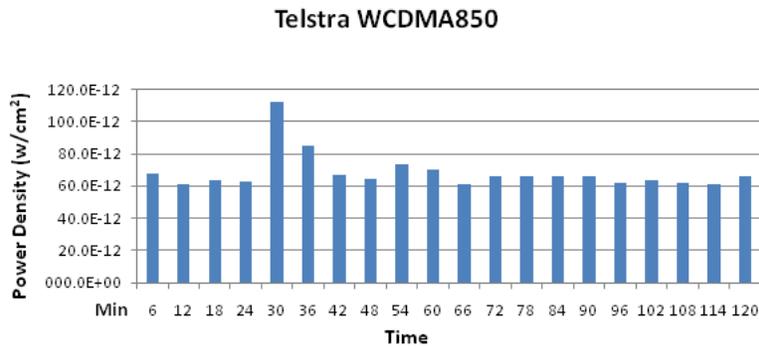
Telstra WCDMA850

Figure 3.7: RF-EME measured level of Telstra WCDMA850 band for 2 hours, in the room below the transmitting antenna (room number 21.501), on the top floor of building 21.
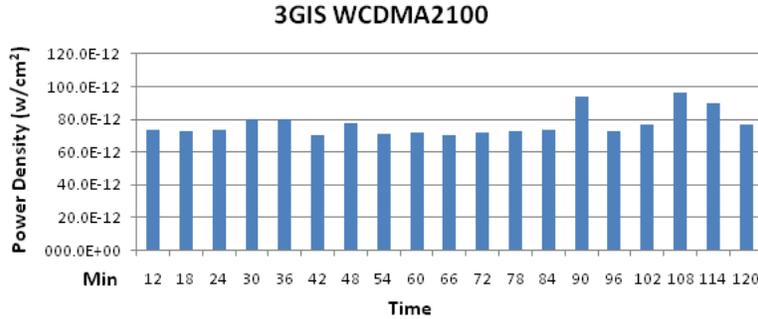
Figure 3.8: RF-EME measured level of 3GIS WCDMA2100 band over 2 hours period, in the room below the transmitting antenna (room number 21.501), on the top floor of building 21.

within the range of 40 - 50 nW/cm^2, except during the night time when fewer communication channels are in use, when readings were about 20 30 nW/cm^2 (Fig. 3.11), higher than the measured result of Fig. 3.4. The same trends were also observed in the 3GIS measurement results at the same location; during the 2 hour time period the level remained between 8 - 14 nW/cm^2 as shown in Fig. 3.12, whereas in Fig. 3.3 (at 45^0 angle) the level was less than 0.8 nW/cm^2. This relationship was further examined over 24 hours (Fig. 3.13 & 3.14). The intensity fluctuated around 8 - 15 nW/cm^2, and never falls below 8.0 nW/cm^2, which confirms that the higher level readings were observed on the upper level of Building 19, when compared to the that on the ground floor.

Thus, an EMI shielding solution is desirable at the top levels of the adjacent buildings, even though these radiation levels are still below the ARPANSA standards. As noted in previous studies, the RBSs can still produce potential health hazards in daily life and possibly adverse long term effects even at the lower levels. This is especially the case in a typical office environment where staff and students spend more than 8 consecutive hours in a typical working day. As published research works showed that if the distance between the subject and the transmitter is below 100 m, the exposure limit is reached quicker when both are in the line of sight [29]. Due to the geographical restrictions, the candidate could not measure radiation levels at other locations which are less than 100 m in line of sight at an angle of 180^0. As clearly indicated by our results, those residential apartments which are at close proximity (30 m) to the base station, at the same height and at an angle of 180^0 will be receiving a higher radiation level.

In summary, measurement results of RF-EME levels at all selected locations did not exceed the ARPANSA general public exposure limit for the frequencies being transmitted by the RBS. The highest measured level was 82 nW/cm^2 on the 3rd floor of Building 19 (room 19.388) where the receiving antenna was in
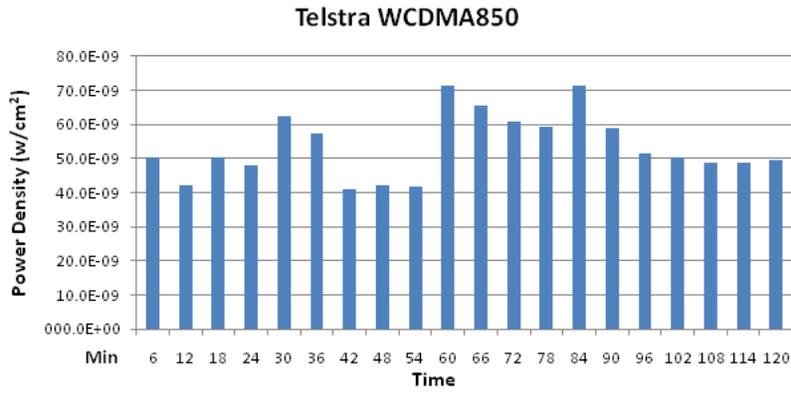
Figure 3.9: RF-EME measured level of Telstra WCDMA850 band over 2 hours period, outside of building 19 on 3rd floor in line of sight and almost at the same elevation as the transmitting antenna.
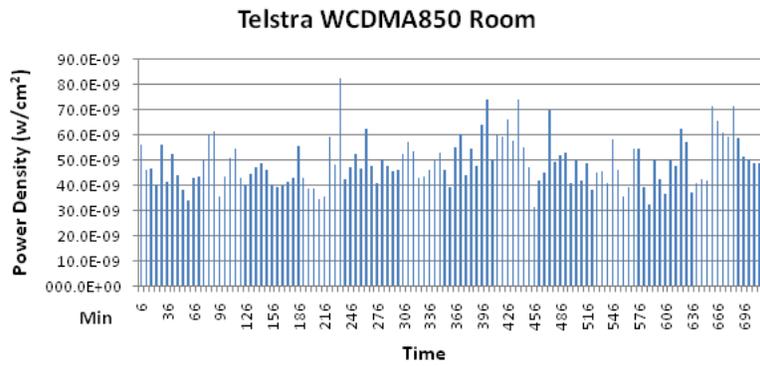
Figure 3.10: RF-EME measured level of Telstra WCDMA850 band for a period of 1-12 hours, outside of building 19 on 3rd floor in line of sight and almost at the same elevation to the transmitting antenna.
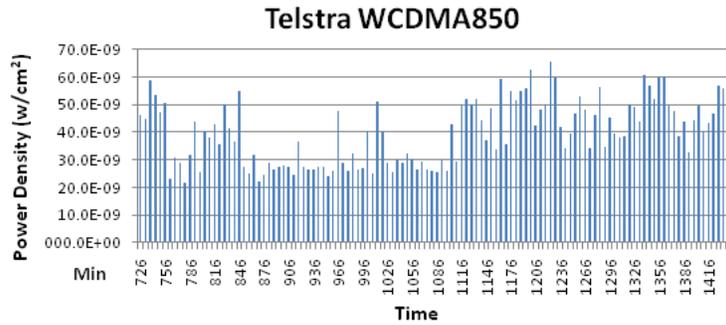
Figure 3.11: RF-EME measured level of Telstra WCDMA850 band for a period of 12-24 hours, outside of building 19 on 3rd floor in line of sight and almost at the same elevation to the transmitting antenna.
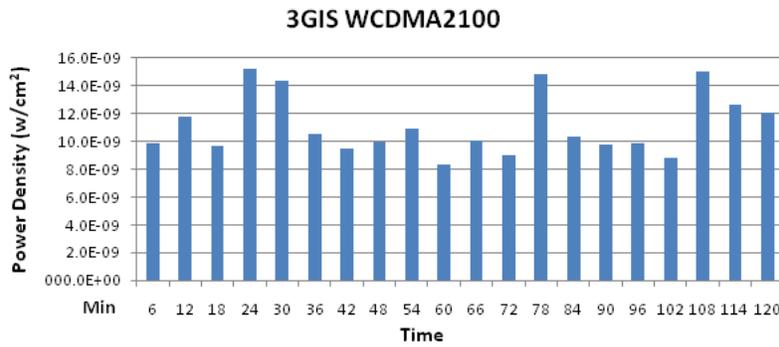
Figure 3.12: RF-EME measured level of 3GIS WCDMA2100 band for a period of 2 hours, outside of building 19 on 3rd floor in line of sight and almost at the same elevation to the transmitting antenna.
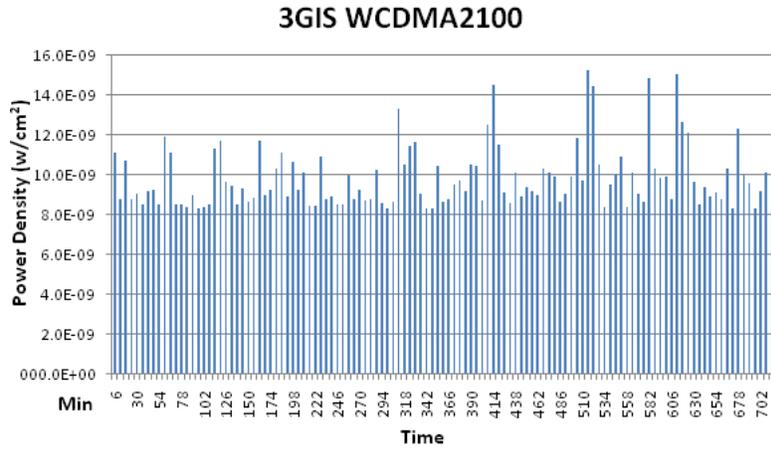
Figure 3.13: RF-EME measured level of 3GIS WCDMA850 band for a period of 1-12 hours, outside of building 19.388 on 3rd floor in line of sight and almost at the same elevation to the transmitting antenna.
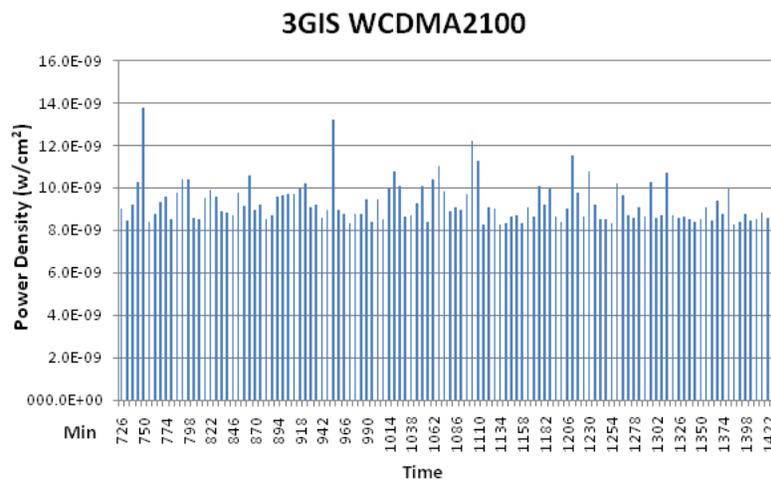
Figure 3.14: RF-EME measured level of 3GIS WCDMA850 band for a period of 12-24 hours, outside of building 19 on 3rd floor in line of sight and almost at the same elevation to the transmitting antenna.

40

line of sight with the Telstra WCDMA850 transmitting antennas. The minimum measured exposure was 60 pW/cm^2 immediately below the roof top Telstra WCDMA850 base station.

3.8   Conclusion

The RF-EME levels for the Telstra WCDMA850 and the 3GIS2100 (local carriers) were measured at 4 selected locations inside the University campus, close to where the RBSs are installed. All the measurements were conducted for each service provider separately, for a period of 2 hours, and then 24 hours at the dominant location. Results were compared with ARPANSA standards, where the thresholds of 0.44 mW/cm^2 and 1 mW/cm^2 were defined for Telstra and 3GIS, respectively. The measured exposure was below the thresholds defined by the standards, even after multiplying a safety factor of 10 for long term radiation exposure, the maximum power density becoming 0.1 mW/cm^2. Potential health hazards associated with chronic exposure were discussed extensively during the past, but exact quantification of radiation exposure limits is still a difficult issue. Adverse effects of non-thermal radiations on humans cannot be gathered or excluded at this stage, because only very limited toxicological information is available, despite the enormous growth in mobile phone use. The demands of proven scientific research on adverse health effects and dose response for humans requires the amending and upgrading of new standard guidelines. Unfortunately there is currently an inadequate limit of detection, an insufficient dosimetry, and a lack of exposure management risk assessment for long-term health hazards. It is highly expected that updated officially drafted standards could limit the consequences of potential adverse health hazards within the economical impact.

3.9   Recommendations

The candidate's recommendation is to pursue the prevention rule, which includes the implementation of an exposure reduction strategy inside the University wherever staff and researchers are working more than 8 hours a day. There is a need to adopt a radiation strategy (in conjunction with non-thermal effects) which is more rigorous than the officially defined standards, especially within Universities, Hospitals and Schools environment. Local operators should also take the issue of reducing radiation to the minimum possible level seriously, in order to avoid the consequences of long-term effects.

41

Chapter 4

Measurement of Radiation from Mobile Phones and Microwave Ovens

4.1 Working Principle of Mobile Phone

Researchers have been working to improve overall network quality since the analogue mobile phone was first introduced in the United States of America in 1983. The transmission type was subsequently upgraded from analogue to digital (1986 in Japan and 1991 in USA). Since then the number of users have been gradually increasing year by year as illustrated in Fig. 4.1. Voice data is sent by handsets through the air medium to a RBS (UL), and then base stations broadcast back to the sender (DL). In these processes microwaves are used as the carrier. The mobile phone is a low power RF transmitter which operates within the power range of 0.1 - 2 W, with an operational frequency range between 450 - 2700 MHz. Immediately after the mobile phone is turned on, it starts searching for the closest RBS that can provide the strongest communication signal. For areas with less coverage, mobile handset transmission power will be higher in order to communicate with the base station effectively [37]. One of the most effective means to improve telecommunication network performance is to install extra base stations throughout the metropolitan areas, which also allows mobile phones to transmit less power while maintaining communication performance at a required level.

4.2 Mobile Phone Radiation

When human bodies are exposed to mobile phone RF waves, heat is generated due to movement of the charged particles within tissues. This process is known as thermal effect [86]. Thermal effect can be harmful to the body after long

Figure 4.1: Mobile phone subscriber's per 100 inhabitants 1997-2007[111]

exposure, especially when the phone is placed near to the skull area. Skin temperature will also increase gradually until it is equivalent to the rate at which it is dispersed via the circulation of the blood [58]. As explained in chapter 3, the SAR value is the dosimetry measure, which indicates the absorption rate of microwave radiation per unit mass by the affected part of a body. The SAR value decreases when the distance between the mobile handset and the body increases. In other words, a lower SAR value and good network coverage can reduce exposure significantly.

4.2.1 Radiation Levels in Assorted Types of Mobile Phones

It has been reported in previous research work that mobile handset radiation can be absorbed in the human head, resulting in a significant increase in body temperature during a long phone call [58]. For example, during a 15 minutes phone call, body temperature was increased by 2.6 ^0C - 3.7 ^0C , the radiation consequences remaining for a considerable period of time.
'

In this study, radiation power density from mobile phone handsets is measured in W/cm^2. Various types of mobile handsets (smart and legacy), using WCDMA850 and WCDMA2100 frequency bands, were used as transmission sources. All the measured results were in the frequency domain, and the radiation distribution was measured along the physical structure of mobile handset. The measurement equipment used was a SRM3006 [74] as illustrated in Fig.4.2.

For handset-A the level was measured for Telstra WCDMA850 band, with the frequency ranging between 884.7 - 889.7 MHz as depicted in Fig.4.3. The resolution bandwidth was set to 2 KHz. Readings were recorded for a total duration of 8 minutes. In the first 2 minutes the mobile phone was in standby mode, and during the next 6 minutes a call was connected to the handset. Results showed that, the level in standby mode remained between 100 - 130×e^{-15}, and then suddenly increasing slightly to 150×e^{-15}, but remaining below this level after the call was connected (transmitting mode). The difference was an indication of the radiation level variations before and after making call. It can be concluded that, handset-A does not transmit a significantly higher power while communicating with RBS.

In handset-B, radiation power density was also measured for total duration of 8 minutes. During the first 2 minutes the level almost remained the same (1.20×E^{-13}) whilst in standby mode, as illustrated in Fig.4.4. However, immediately after the call was made (transmitting and receiving mode), radiation

Figure 4.2: Selective radiation meter measuring mobile handset radiation level in standby, transmission and receiving mode
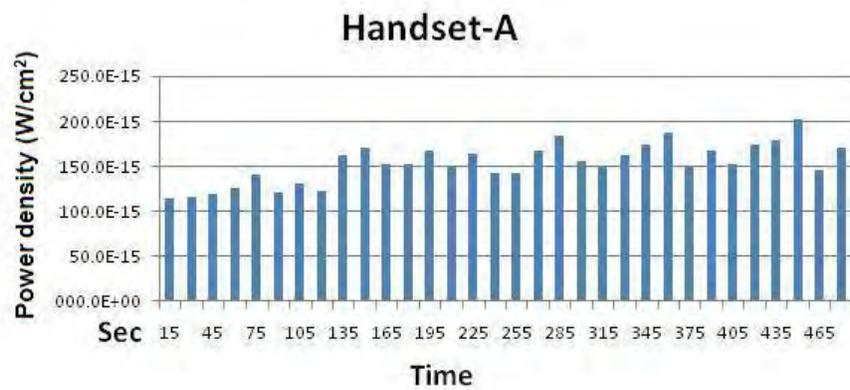
Figure 4.3: Measured radiation level of mobile Handset-A for a total duration of 8 minutes (2 min standby mode, 6 min transmitting mode).
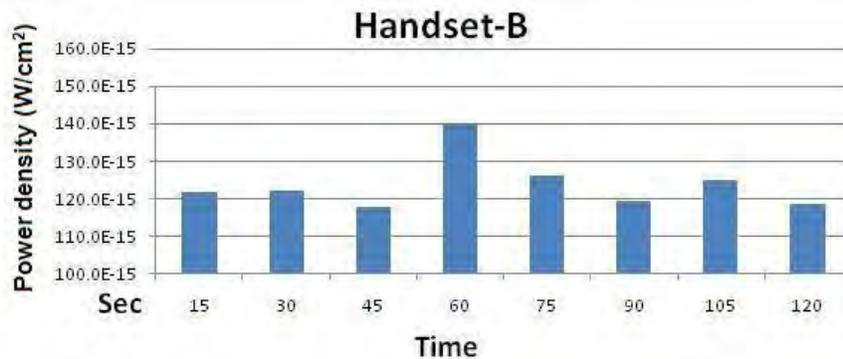
Figure 4.4: Radiation level measured for 2 min in Handset-B during standby mode.

level jumped to $1.5 \times e^{-12}$, and at one stage it reached $2.0 \times e^{-12}$. In Fig.4.5, a total of 8 minutes of readings were presented, which clearly showed the dramatic increase of the radiation level once the call was connected. The comparison indicated that handset-B transmitted at a higher power when communicating with the RBS, while handset-A transmitted at approximately the same power during both communication and standby/idle modes.

In our 3rd handset measurement (handset-C), significant differences were observed (during transmission and receiving) before (standby mode) and after activating the call. For illustration purposes, readings from the first 2 minutes are presented separately in Fig. 4.6 and results of the total 8 minutes time span are shown in Fig. 4.7. In standby mode radiation power density remained at $120 \times e^{-15}$, but the level reached $150 \times e^{-12}$ as soon as the call was connecting and did not fall below $50 \times e^{-12}$. In this handset the radiation level was much higher and fluctuated throughout a larger range, when compared to both handset-A & B.

Our results here indicate that there would be a significant difference between the radiation exposure for operators using these particular mobile handsets; 3 orders of magnitude difference was observed between handset-A and handset-C. The level may increase further if handsets having external antennas are to be used [118]

4.2.2   Recommendations

It is recommended that manufacturers specify the transmit power for each mobile handset; as measured while it is communicating with a RBS. Electromagnetic Wave Interceptor (EWI) which is a special type of EMR attenuating polymers painted on the receiving side of the handset, should also be installed in mobile phones. EWI could also be in the form of electric tags pasted on the back plate. A brief description of mobile phone health hazards and basic expo-
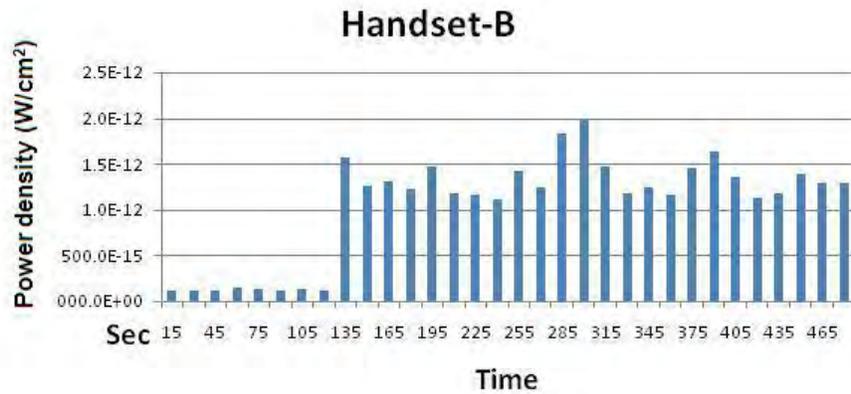
Figure 4.5: Measured radiation level for mobile Handset-B for total duration of 8 minutes (2 min standby mode, 6 min transmitting mode).
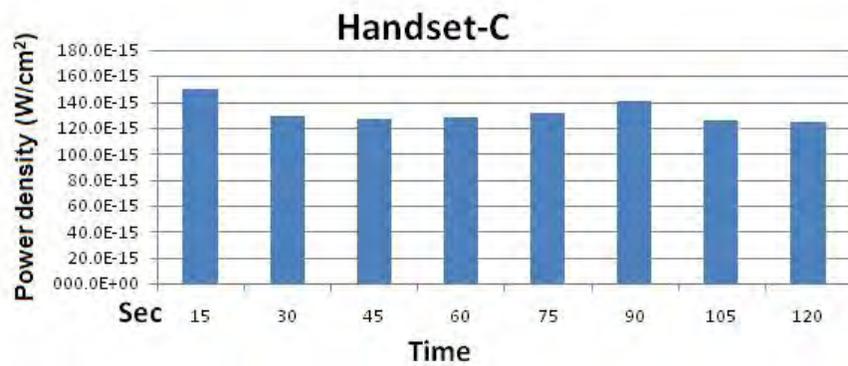
Figure 4.6: Radiation level measured for 2 min in Handset-C during standby mode.
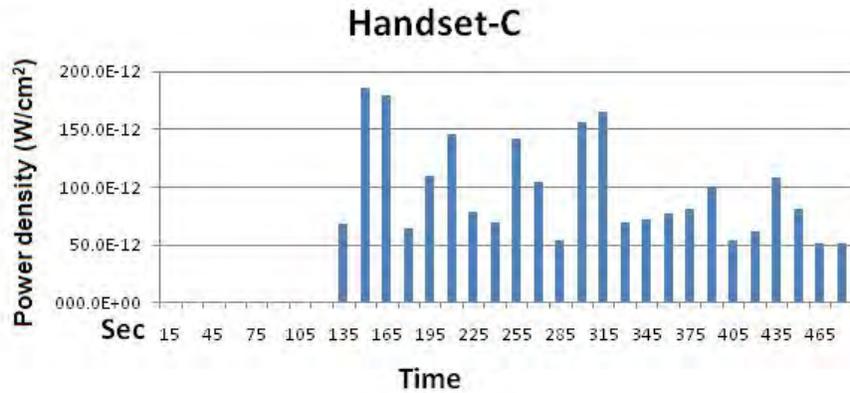
Figure 4.7: Measured radiation level of mobile Handset-C for total duration of 8 minutes (2 min standby mode, 6 min transmitting mode).

sure reduction techniques should also added to mobile handset manuals, so that users can be made to aware of potential health impacts.

4.3 Operation of Microwave Oven

Microwave ovens work at the frequency range around 2450 MHz (120 mm in wavelength). They work by transmitting radiation towards food placed in the middle of the oven cavity. Materials behave differently when exposed to microwave radiation. Metallic material completely reflect microwaves, whereas, some non-metallic materials, such as glass or plastic, are partially transparent to the microwave. On the other hand, materials containing moisture, such as food or the human body, can absorb microwaves radiation, resulting in a temperature rise.

4.3.1 Energy Distribution

The magnetron is the electric device in each microwave oven which generates and transmits microwaves. It is surrounded by metal walls which direct the waves towards the food. The time required for cooking depends upon the shape, contents and volume of food. Most of the non-metallic cooking utensils used inside microwave ovens do not absorb energy, so that only the food absorbs energy and is heated up.

4.3.2 Safety of Radiation Leakage

In Australia and New Zealand, radiation safety agencies have defined standards (AS/NZS60335.2.25:2002) for maximum levels of microwave leakage, aimed at

reducing the impact of exposure. As a result, manufacturers have been making a constant effort to improve and optimise designs, minimising the radiation levels coming from the microwave ovens. All microwave ovens are assembled with two types of safety interlock switches, which help eliminate radiation escaping from the oven when the door opens. Even though the magnetron ceases emission of radiation once the electric power is turned off, radiation leakage still occurs, as it is difficult to stop radiation leakage through the door completely.

4.4   Radiation Outside of Microwave Oven

4.4.1   Radiation Levels of Various Types of Oven

It has been observed that the radiation level (or leakage) outside a microwave oven, depends mainly upon the quality of the door seal, the type of the glass used in front door, and the configuration of metallic mesh pasted inside of oven door to attenuate radiation. Exposure for a person near a microwave oven can also be angle and distance dependent. Fortunately, it is possible to reduce the leakage level by modifying these parameters. In this work we have measured radiation levels for various brands of ovens. Measurements of the radiation from each oven were taken, both in their original unmodified state, and after ESG shielding was placed in front of the oven doors. These measurements were used for comparison purposes.

4.4.2   Measurements Setup

Measurements were conducted using an SRM 3006, as illustrated in Fig. 4.8. All results were measured in mW/cm^2 (which is the rate of energy flow per unit area), within the frequency range between 2445 - 2455 MHz. Two liters of tap water were placed inside a microwave oven, then readings were recorded for a total duration of 8 minutes (microwave oven-A) for the best case scenario (minimum reflection inside the room), where minimum radiation should be leaked into the environment. For the first 2 minutes the oven was not in a running state, and data was recorded from other microwave sources. During the next 6 minutes the microwave oven was operated at full power, while data was recorded continuously. For microwave oven B and C, results were only recorded for the 6 minutes of oven operation.

4.4.3   Results and Discussion

For microwave oven-A, the radiation was measured using a 0.67 m face to face distance between the SRM 3006 receiving antenna and the oven door. The level recorded for the first 2 minutes was very low, but during the next 6 minutes (operating mode), the level reached at ~ $1.1 \times e^{-6}$mW/cm^2, and remained at approximately this level throughout, as shown in Fig. 4.9. Radiation exposure was also measured with ESG pasted in front of, and parallel to, the microwave oven glass. A significant reduction in radiation coming out from the microwave

Figure 4.8: Microwave oven radiation power density measurements using selective radiation meter 3006.
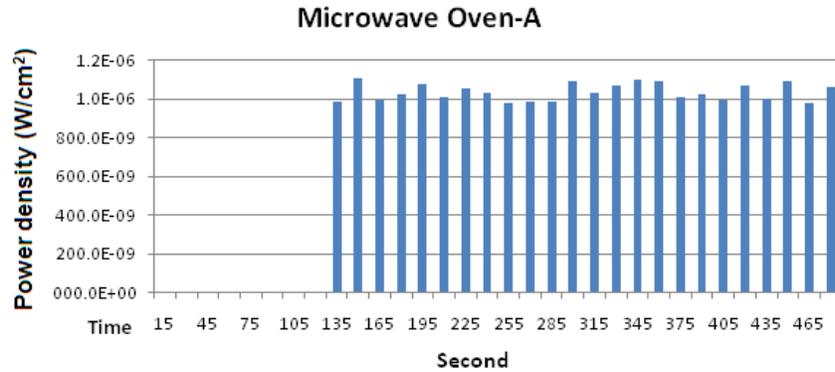
Figure 4.9: Radiation power density measurements of microwave oven-A with 2 feet distance, during normal working condition for total period of 8 minutes.

oven was observed (Fig. 4.10 illustrate), while transparency was maintained to provide an inside view.

In the case of microwave oven-B, the radiation was measured face to face with the oven door, and the receiving antenna being placed at varying distances. For the distance of 0.67 m and 180^0 angle (face to face), the radiation level climbed to $1.5 \times e^{-6}$ mW/cm^2, (Fig. 4.11) which was higher than the value measured for microwave oven-A (Fig. 4.9). This indicated that oven-A has better safety measures in comparison to oven-B and that those who are using oven-B will receive higher exposure to radiation. Radiation level was also measured at a 1.67 m distance from microwave oven-B as plotted in Fig. 4.12, showing a gradual reduction in radiation intensity with increase of distance. It confirms that the subject will receive less radiation if he moves away from the front door of the oven.

In microwave oven-C, the radiation was also measured at 0.67 m distance (Fig.4.13), which is the typical distance the subject stands whilst waiting for food to be cooked. In this case, the radiation level was the lowest at the 0.67 m distance, among the three ovens measured. Measurements were also conducted at the same distance (0.67 m), but at 45^0 angle away from the center line of the microwave oven. A significant reduction in radiation level was observed in comparison to that obtained at a 0^0 angle; as shown in Fig. 4.14. Hence, it can be concluded that the major pathway of radiation emission from oven cavity was through the glass door.

In summary, ovens produced by different manufacturers have varying abilities to shield radiation from the oven cavity. Furthermore, one can reduce radiation exposure by using the recommended techniques, such as: 1) standing at a larger distance from the oven (> 1.67 m) during its operation, 2) standing at 45^0 or larger angle instead of facing the front panel, etc. One of the most effective ways of reducing the radiation level from a microwave ovens is to replace
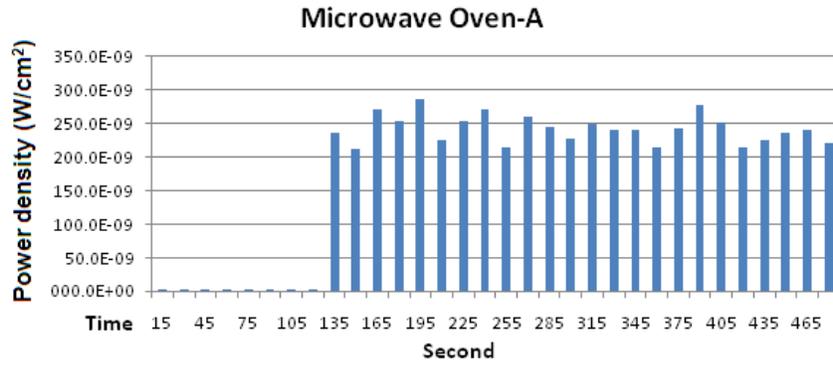
Figure 4.10: Radiation power density measurements of microwave oven-A with energy saving glass pasted on front door for period of 8 minutes.
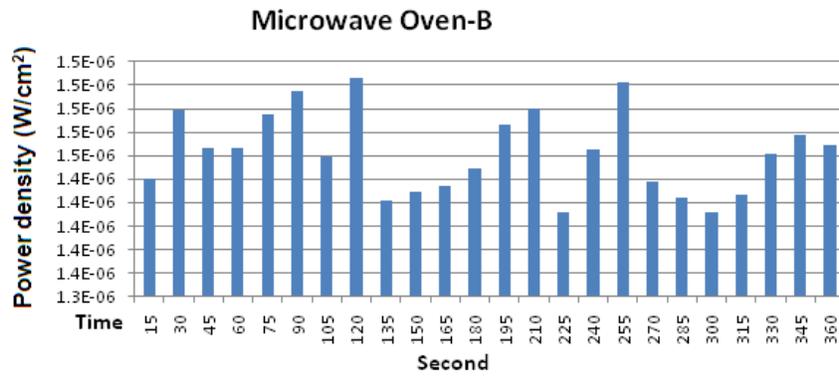
Figure 4.11: Radiation power density measurements of microwave oven-B with 2 feet distance, during normal working condition for total period of 6 minutes.
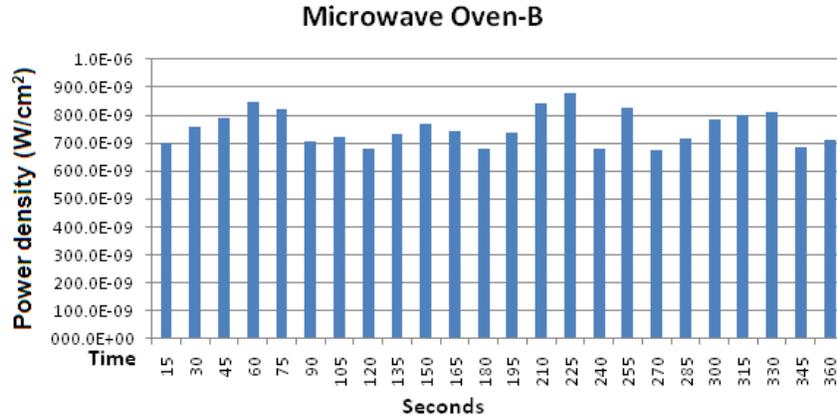
Figure 4.12: Radiation power density measurements of microwave oven-B with 5 feet distance, during normal working condition for total period of 6 minutes

standard float glass with ESG.

4.5 Conclusion

Radiation levels from two major microwave devices; mobile phones and microwave ovens were measured, and the results have been discussed in detail. Radiation levels from various type of mobile handsets have been measured in both standby and operating modes, and the results were compared. It was concluded that different brands of handset have different transmission powers and radiation levels. It has been recommended that the transmission power of the handset be specified in the user guide. Radiation emission from another source, the microwave oven, has also been discussed in detail. ESG has been proved to be a good radiation attenuator on the microwave oven, significantly reducing radiation exposure in comparison to the standard float glass. Importantly, this has been achieved while maintaining a clear inside view of the oven. Finally, it has been determined that subjects can be less exposed to radiation by standing 1.67 m or further away, and at an angle of 45^0or above from the front door of a microwave oven.
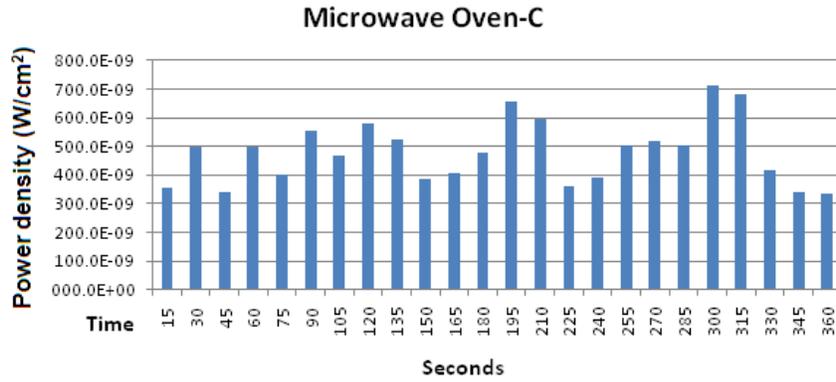
Figure 4.13: Radiation power density measurements of microwave oven-C with 2 feet distance, during normal working condition for total period of 6 minutes.
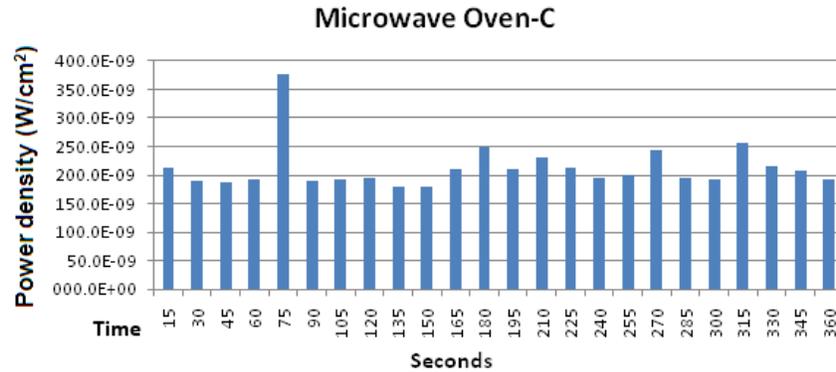
Figure 4.14: Radiation power density measurements of microwave oven-C with 2 feet distance and 45^0angle, during normal working condition for total period of 6 minutes

Chapter 5

Frequency Selective Surface

5.1 Definition

FSSs are a planar periodic array of identical metal-dielectric patch or aperture elements, arranged in a 1D or 2D plane. During plane wave transmission, resonance will be induced if the length of the elements is a multiple of half of the incident wavelength, i.e $\lambda_g/2$ [70][98]. This array of elements acts as a spatial electromagnetic filter and exhibits capacitive and inductive frequency characteristics, as shown in Fig. 5.1. The frequency response of these structures is determined by several factors, including the periodicity along the X-axis and Y-axis, and the manner by which the periodic surface is exposed to the EMR (for example, incident angle etc). In term of functionality, periodic structures can be classified into four major categories; 1) lowpass, 2) highpass, 3) bandpass, and 4) bandstop filters. In each of these four instances, the resonance phenomenon remains the same [70].

5.2 Geometry and Response of FSS Elements

Based on their geometric configuration, FSS elements are categorised as aperture-type and patch-type as shown in Fig. 5.2. Aperture/slot type FSSs produce a capacitive response, reflecting lower frequency radiation while transmitting at higher frequencies, clearly demonstrating the properties of a highpass filter. On the other hand, patch FSSs act as lowpass filters, transmitting at lower frequencies and reflecting at higher frequencies [112]. The performance of one type is complementary to the other. Alternate element geometries can result in a similar resonance frequency, but exhibiting different bandwidth performance. In addition, some elements show more tuning options than others. Effective FSSs should exhibit stable resonant frequencies, at both normal and oblique angles of incidence.

Broad bandwidth and close separation between the reflection and transmission bands are desirable properties for the FSS. The selection of the most
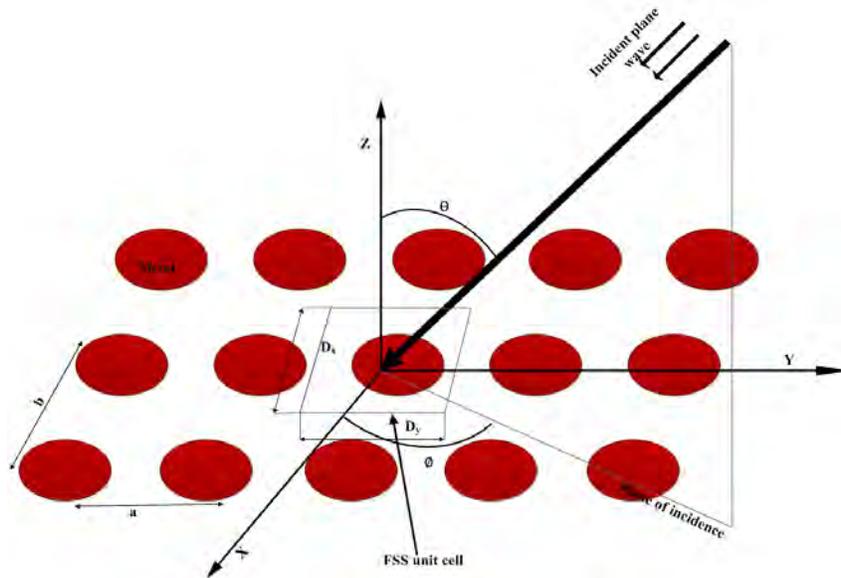
Figure 5.1: Geometry of a two-dimensional FSS periodic array, where Dx and Dy are the length and width of the unit cell, respectively [85]
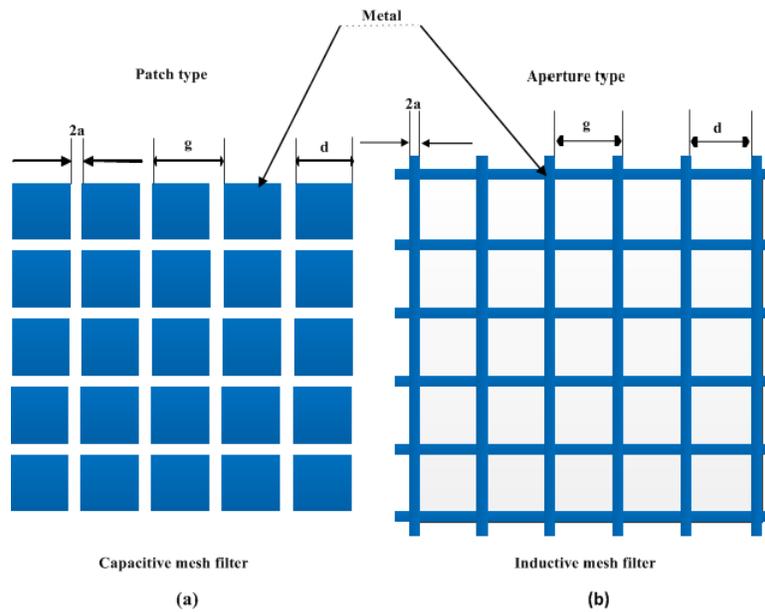
Figure 5.2: (a) Layout of an aperture type FSS (b) Layout of a patch type FSS

suitable element type depends largely upon the particular requirement, and is to some extent governed by the prior experience of the designer.

5.3   Types of FSS element

The physical shape of the FSS elements can be divided into four different types [70]. Each element type exhibiting its own frequency response characteristics. For example, some types allow fast transition between stopband and passband but are sensitive to the polarisation angle. The combination of these types can be used to generate new elements with a range of specific properties, such as elements for multiband FSSs, polarisation independent FSSs and miniaturised element, and so on. In this thesis we utilise Munk approach for distinguishing element groups, as shown in Fig. 5.3, which can be further classified into four basic types [70].

5.3.1   Center Connected or N-poles

The main element of this group is a tripole array as shown in Fig. 5.3. These are formed by a combination of three poles of equal length having the same center point. In general, tripole elements generate larger bandwidth by reducing inter element spacing. The individual element properties of this class have been discussed in various research papers, for example: 1) tripole element stability of the center frequency in the reflection band during changing of the mode of the plane of the electromagnetic wave [6], 2) current from a single tripole element has also been calculated with a 4:1 frequency range [64], and 3) also along one arm of the tripole with 45^0 angle and band spacing 2:1 [99]. Researchers have also investigated the performance of the cross-dipole, which provides reasonable bandwidth for the transmission of mobile phone signals (900,1800 MHz band) while blocking 5 GHz wireless signals[45, 44]. The cross-dipole can also be used as a dual polarised element, dependent on the angle of incidence [77]. The Jerusalem cross is the third most important element in the N-poles class, and provides more tuning options for obtaining the required response [97]. The modal technique has been used for calculating the plane wave transmission coefficients of the Jerusalem cross in frequency ranges up to 40 GHz [79]. In [9], the performance of the Jerusalem cross was compared with the concentric ring, and it was found that the Jerusalem cross gives higher bandwidth the concentric ring does. More details and significance of the Jerusalem cross has also been investigated in a range of prior research works [60][82][92][1].

5.3.2   Loop Type

The looped tripole, the ring, and the square loop are the main members of this family; as shown in Fig. 5.3. The length of the two orthogonal poles should be equal in order to provide for proportionality in the loop type structures. Since the last decade, these structures have attained significant attention from

researchers due to their better performance in angle stability, ease of fabrication, and higher bandwidths. As an example, the plane wave transmission curve of the square loop gives a band spacing in the range of 1.5 to 2.2 GHz [49]; and the single FSS screen for four band FSS of DSL element is fabricated to transmit signals from the X and Ka-band, while blocking the Ku band [113]. The effect of concentric rings was compared to the simple ring [78], and it was observed that the concentric ring provides more center band frequency with a ratio of 1/1.3, but having a more complex transmission curve. Ring characteristics have also been discussed in other literature [81]. The third element of this class is a looped tripole [71]. Transmission line theory can be used to analyse the basic characteristics of loop type elements. The half-wave dipole exhibits the property of a shorter dipole which is reactance loaded (ZL). The property of reactance is to absorb the radiation of shorter wavelengths. When referring to the total impedance of the dipole, it should have a value of zero at resonance. As the half-wave dipole shows capacitive characteristics at the resonant frequency[48], the load ZL should in turn have inductive characteristic, in order to make the overall impedance equal to zero. However, inductance can be induced by shorting the transmission line.

5.3.3   Solid Interior/Plate type

The solid interior/plate types are a patch consisting of a metallic array which can be either a circular disk, square, rectangular, or hexagonal in shape (Fig. 5.3), and having a $\lambda_g/2$ element length. This class of FSS element captured the attention of designers, as reported in an early study [47]. The circular elements of this class are generally reflecting arrays, while the behaviour of the square patch tends to be transparent to radiation [57, 66]. These elements are not recommended for general purpose filter designs because of their poor angle stability and early onset of grating lobes [70]. This type exhibits characteristics which are more useful for the design of miniaturised FSS elements [90].

5.3.4   Combination Types

The design of the combination type of element is intended to overcome the performance shortcomings (angular stability, bandwidth, and so on) of FSS structures. They are formed from a combination of: 1) solid interior shape, 2) loop, or 3) center connected [69, 16, 93] (Fig. 5.3) and typically have a wide range of elements. A combination of any two elements from the first three types make a new element which is categorised as a combination type.

5.4   Selection Criteria of Elements

The selection of elements is mostly dependent upon two factors; the designer's experience, and the ease of fabrication. In general, preference is given to those elements which are not dependent on angle of incidence and polarisation. The
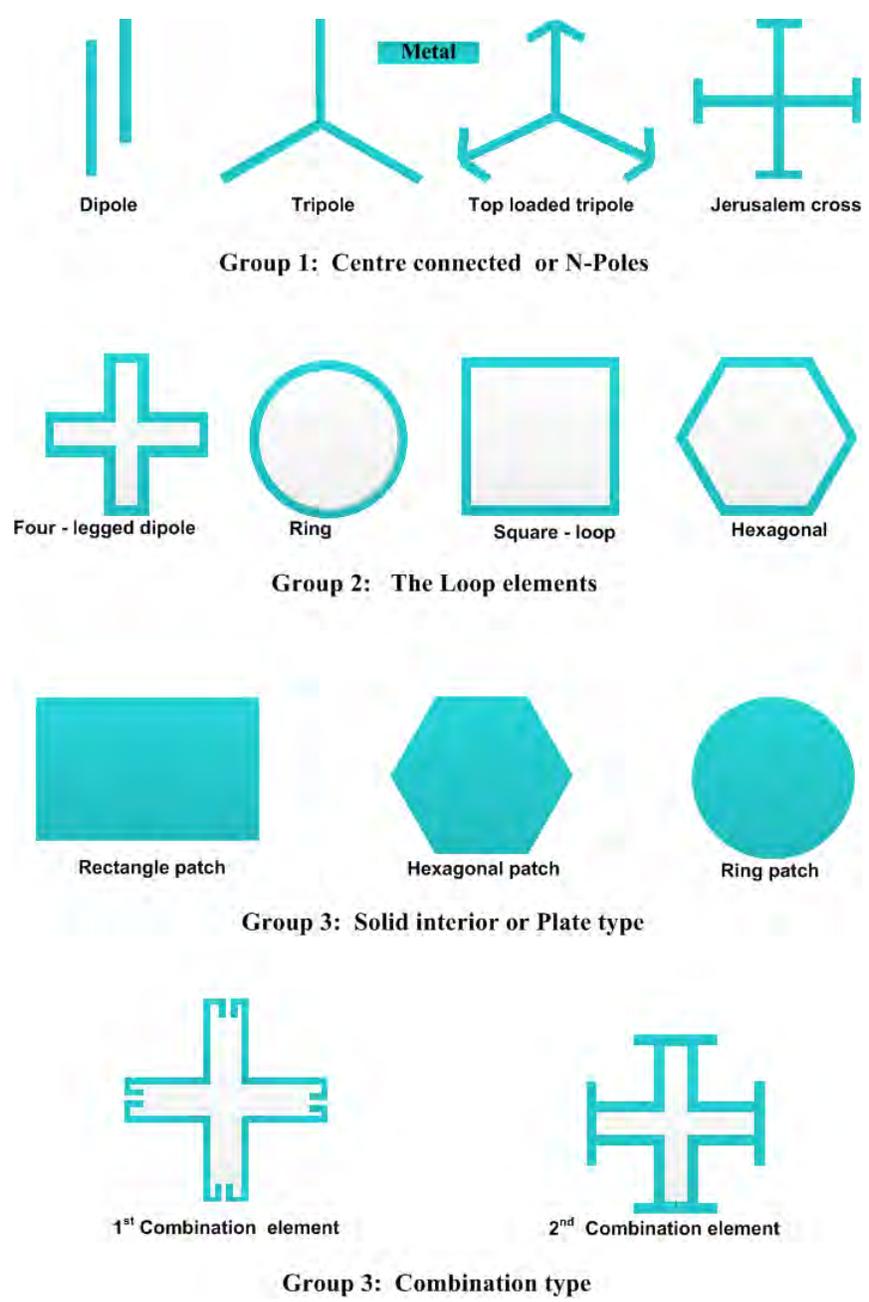
Figure 5.3: The groups of traditional type of FSS elements

Element shape	Angular stability	Cross polarisation level	Larger bandwidth	Small band separation
Dipole	4	1	4	1
Cross dipole	3	3	3	3
Loaded dipole	1	2	1	1
Tripole	3	3	3	2
Jerusalem	2	3	2	2
Ring	1	2	1	1
Square loop	1	1	1	1

Table 5.1: Performance analysis of different shapes of FSS elements [112]
Rating: 1 = best, 2 = second best
Based on the free standing single screen's performance

required angular stability can be achieved by reducing the inter-element spacing with reference to the wavelength. Wider element spacing creates more grating lobes, which in turn causes an increase in angular instability. Loop type elements are considered to be useful for achieving high levels of angular stability [70].

5.5 Performance Analysis of FSS Elements

Table 5.1 presents a comparison of the different shapes for various FSS elements. The square loop shows the best performance characteristics in terms of obtaining larger bandwidth, angular stability, polarisation, and sensitivity in comparison to all other elements. If the side length of the loop is equal to a multiple of half of the wavelength, the element behaves as a dipole. In the case of a square loop, we can define resonance points at the stage that the lengths of two sides of the square reach a multiple of $\lambda_0/2$.

5.6 Normal and Oblique Incidence Plane Wave

The behaviour of the incident wave after striking the periodic structures at an oblique angle is illustrated in Fig. 5.4, where the element separation is indicated as d. The oblique incident wave induces a characteristic current distribution upon coming into contact with the surface of a periodic structure. The response is significantly different to that caused by a normal incident wave [28], and depends on two primary factors, the separation between the elements, and the thickness of the elements.
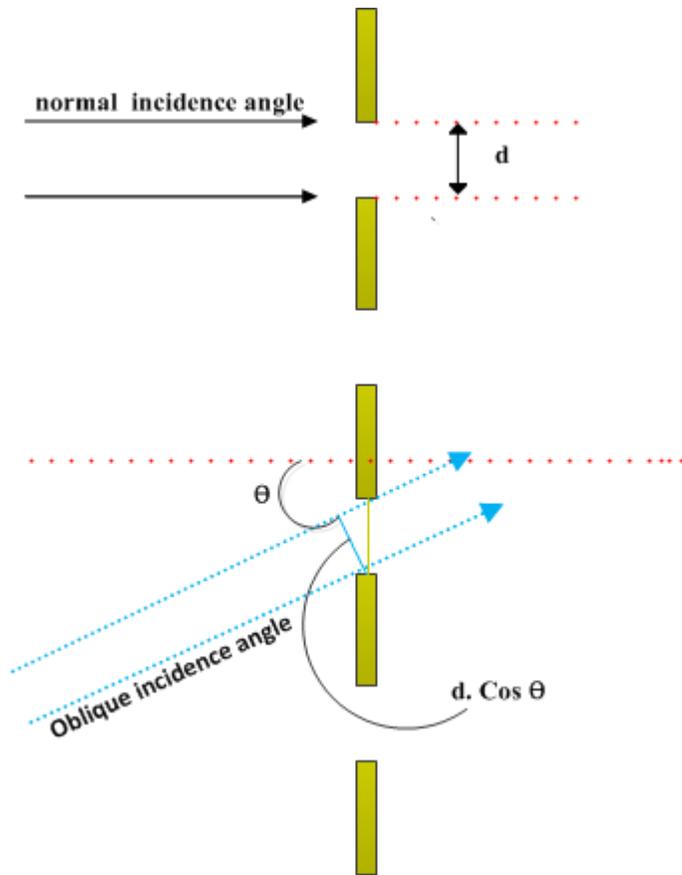
Figure 5.4: Effect of normal (top) and oblique (bottom) incidence, where d is the distance between the two conductive periodic strips [38].

Figure 5.5:   F-117 nighthawk stealth strike aircraft (photo courtesy of en. Wikipedia)

5.7   Applications of FSSs

The enhanced applications of FSSs have contributed substantially to a higher quality of life and further advances in technology, including:

- Usage in Radio Frequency Identification (RFID) tags, collision prevention systems, and photonic band-gap structures; and have enabled the achievement of a significant reduction in Radar Cross Section (RCS) [104].

- Stealth aircraft technology (Fig. 5.5), where it is used to create interference to radar waves. FSS structures create lower visibility in IR, visual and in RF spectrum.

- Microwave ovens, where FSS metallic mesh is pasted inside the door. This FSS layer acts as a highpass filter, reflecting microwave energy at 2.45 GHz [112], while passing visible light (400 THz-700 THz) to enable an inside view, as shown in Fig. 5.7.

- Wireless communication security, for example the radome (formed by radar and dome), which is a special cover fabricated from FSS for military applications (such as aircraft), works as a bandpass filter to reduce the radar cross section of an antenna outside its operating band [103]. In the design of all aircraft the antenna is mounted in front of the fuselage and is covered by a radome. The radome is configured to operate in two modes, known as transparent mode and opaque mode. The transparent mode enables useful signals for the antenna to pass through the radome body. The opaque mode reflects the signals in specular (strong reflection), or bi–static direction, because the unique radome shape generates very weak signals in the back scatter direction to avoid interference with incoming signals. This technique is utilised in order to reduce the radar cross sectional area.

- FSSs are also used in the design of sub-reflectors for spatial communication [70][112]. In FSS sub-reflector designs, two separate feeds send signals to the main sub-reflector, which in turn only passes one frequency by attenuating other as shown in Fig. 5.6. This technique allows for the design of lightweight periodic wire grid reflector antennas, instead of the traditional parabolic antennas, which are much heavier in weight.
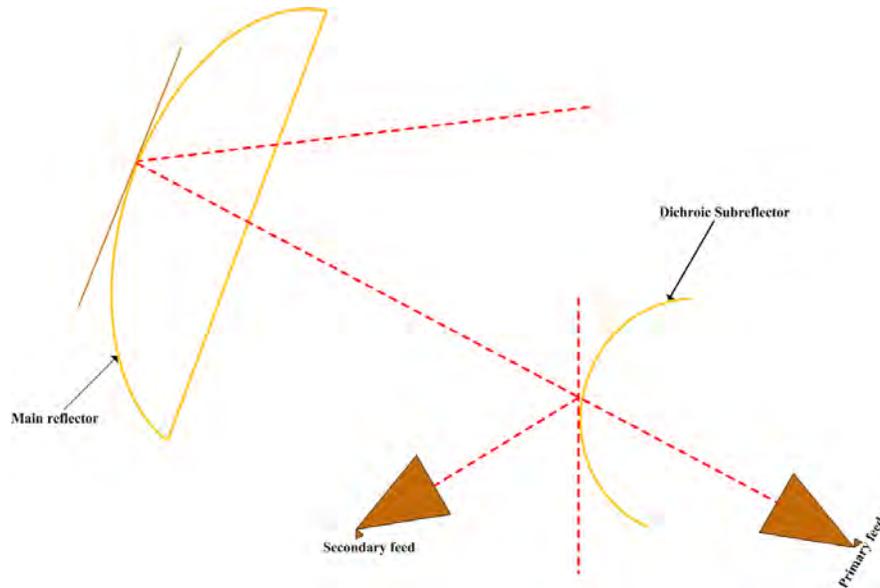
Figure 5.6: Dual feed frequency selective surface reflector antenna. The operating frequencies of primary and secondary feed are differ from others [85]

5.8 FSS Classification

Based on their configurations and applications, FSS structures can be classified as either (a) Passive or (b) Active .

5.8.1 Active FSS

An active FSS is formed by incorporating active elements such as varactor and pin diodes between the FSS elements. These diodes enable the creation of impedance surfaces having tuning characteristics that can easily be configured after insertion. This property was first explained in [112], but a detailed study of scattering properties of corrugated surfaces loaded with microwave solid state amplifiers was published in [51]. However, these types of structures exhibit certain disadvantages, i.e., they require a continuous DC power source, they are expensive to produce due to the cost of the diodes, and it is difficult to design complex structures. One of the advantages of an active FSS is that it can be configured for two frequency responses.

5.8.2 Passive FSS

The frequency response of a passive FSS is fixed at fabrication, and it is not possible to be subsequently altered. This type is not recommended for filtering smaller cross section areas (such as windows), because more space is required

Figure 5.7: The metallic mesh of microwave oven door that exhibit high-pass filtering property to reflect microwave energy while transmit visual light for inside view [36]

to fabricate the elements. The main advantages of the passive FSS are: it is cheaper to fabricate than the active FSS, and it is easy to design.

5.9   Methods Used for Analysing FSS Structures

To date the reflection and transmission characteristics of electromagnetic waves through FSS structures have been analysed and evaluated extensively. Different methods of evaluation have been employed which assume: 1) that the FSS behaves as a planar double periodic structure, 2) that the FSS has an infinite number of arrays of equal dimensions, and 3) that the unit cell can be simulated by applying boundary conditions. However, all evaluation methods have their characteristic advantages and limitations, which are discussed below.

5.9.1   Equivalent Circuit Method

This method utilises FSS filter responses as shown in Fig. 5.8., which are ideally applicable for those periodic structures whose thickness, periodicity, and dimension of inductive patch and capacitive gaps are less than the excitation wavelength [3]. This technique does not calculate cross polarisation and wide angle response; but the oblique incident angle of less than 45^0 with respect to normal incidence, has previously been evaluated [50]. The focal point of impedance in an active FSS can be predicted in a periodic grid on dielectric substrate, but multilayer thin planar FSS cannot be solved using this technique.

5.9.2   Method of Moments

This method is used to determine the electric and magnetic surface currents of thin metallic arrays of random shape [8]. The Method of Moment (MoM) result requires post-processing for achieving transmission and reflection response.

5.9.3   Mode Matching

This procedure is associated with the growth of boundary conditions and scattering from cavities. Initially this technique was implemented to solve the demanding waveguide scattering problems [107], where each side of a broken field diverge in a wave guide mode. The Mode Matching (MM) technique was developed to solve this problem. This technique uses test functions to minimise the integral equation into a matrix form. Consequently it can be used for evaluation of multilayer FSSs. In the FSS periodic structures, the field is expanded into floquet modes on both side of the unit cell [2]. The procedure is associated with the growth of boundary conditions and scattering from cavities.

5.9.4   Finite Element Method

This method divides the element structure into smaller elements, and reconnects them back through nodes (which holds the elements). This method was
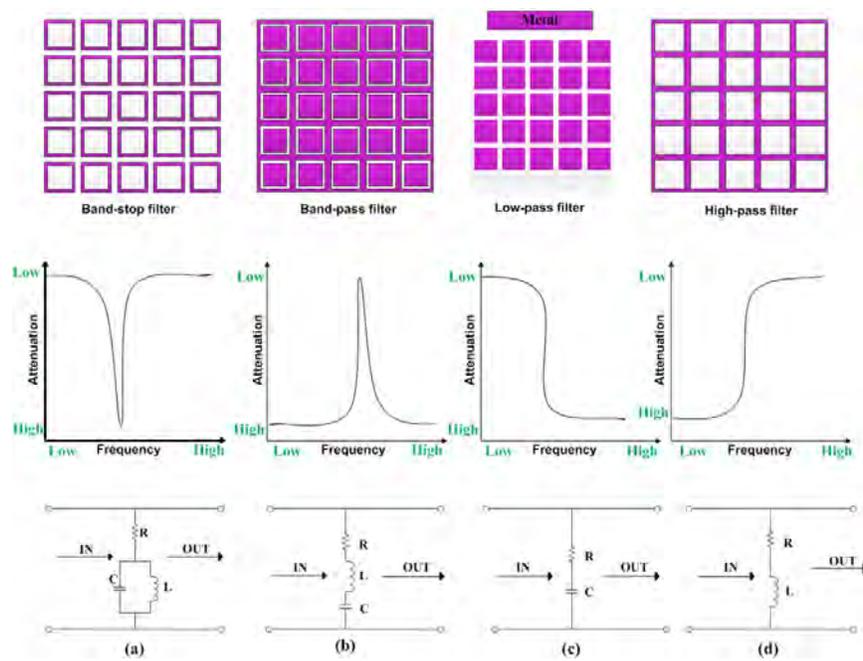
Figure 5.8: (a) Bandstop (b) Bandpass (c) Lowpass and (d) Highpass FSS filters with corresponding frequency responses and equivalent circuits [38]

originally used for simplifying closed domain problems, as it is appropriate for evaluating the eigenvector of random structures. The Finite Element Method (FEM) performance becomes complex in three-dimensional periodic scattering, with diminishing accuracy at oblique incident angles. To overcome these issues, a hybrid of FEM and the boundary element [52] or boundary integral [21] can be utilised. The computational methods of this technique require substantial computer time to evaluate the structures.

5.9.5   Finite Difference Time Domain

Time domain (TD) is suitable for determining the broadband response of periodic structures; but the TD method is not suitable for oblique excitation of periodic scattering, because of the required phase shift among adjacent periodic boundaries. Phase shift in the frequency domain transforms to time delay, by storing data of all time intervals along appropriate periodic boundaries. In [18], comprehensive detail of FDTD has been provided for solving FSS structures. This method is not well suited for oblique incident angles, as it requires an independent FDTD run for each unique frequency point.

5.9.6   Finite Integration Technique

The Finite Integration Technique (FIT) method is pretty much similar to FDTD and FEM. Some researchers have attempted to promote FIT, though, FEM has established better solver techniques [106]. In FIT, the solver domain is separated into two grids. The space between grids is designed in such a way that corner of one grid is placed in the middle of a cell in the other grid [17]. The changed grid conditions correspond to the grid electric voltage vector (E); the magnetic voltage vector (H), magnetic induction flux (B) and electric displacement flux (D) are presented as the grid condition variables of FIT. The FIT circuit model does not have coupling for connecting separate branches, whereas these coupling relations exits in FEM. However, two dimensional structure coupling design can convert into a coupling free model equivalent; but in the case of three dimensional FIT, equivalent FEM does not seems effective [19].

5.9.7   Network Analysis

The network approach is being utilised; since the scattering properties of waves from multi-layered dielectrics were initially observed, where each layer is considered as a transmission line with unique impedance characteristics. The combination of network method with other techniques has the capability of analysing thin metallic dielectric scattering structures with negligible losses. The oblique excitation of slim and broad FSS structures with random aperture cross section and longitudinal gap, has already been investigated in previous research work [109].

66

5.10 Conclusion

The background and history of periodic structures have been discussed in this chapter. The geometry of different group elements and their characteristics have been highlighted in order to choose the most suitable design. These elements are divided into four groups known as: a) center connected or N-poles (dipole , tripole and top-loaded tripole), b) loop type (four-legged dipole , ring , square loop), c) solid interior or plate type (rectangular patch, hexagonal patch, ring patch), and d) combination (mixture of any previous element). Different elements behave differently upon contact with electromagnetic waves, and each element has its own unique characteristics (angular stability, higher bandwidth, lighter in weight). Four basic FSS filters (lowpass, highpass, bandstop, and bandpass) with their responses and equivalent circuits have also described. Further classification of FSS structures into passive and active forms has been described, according to their functionality and implementation. A number of FSS characterisation and analysis techniques for evaluating the scattering properties of periodic structures are briefly discussed.

Chapter 6

Frequency Selective Surface Absorber and Transmitter

ESG can be used to reflect and attenuate microwave radiations coming from different sources, such as: 1) RBSs, 2) weather radar, 3) emergency services radio communication devices, 4) AM and FM radio, 5) Personal Communication Devices (PCS), 6) Global Positioning Systems (GPS), 7) satellite TV, 8) Wi-Fi, and 9) long distance telephone transmission. It also attenuates useful mobile phone and Wi-Fi signals. Usually the soft coating layer on ESG attenuates microwave signals up to 30 dB [43], whereas the hard coating layer blocks up to 200 dB within the same spectrum region. This will probably be more effective when used to accentuate higher frequencies in future wireless communication systems, as attenuation level increases with frequency [65]. However within normal commercial and residential buildings this effect is not desirable, since mobile and Wi-Fi signals with sufficient power level are required for effective communication.

One of the solutions to this problem is to design a band-pass FSS [70][43] on the coated side of the ESG, to improve transmission of mobile phone and Wi-Fi signals, whilst blocking other signals. Thus microwave radiation saturation can be avoided without greatly affecting the IR and UV attenuation properties of the ESG [42], while the transmission of mobile and Wi-Fi signals are enabled. As described in the previous chapter; in order to achieve various spectral responses and angular stability, different types of FSS elements can be selected for the required filter design.

This chapter describes the design and simulation results of two FSS systems, which can be used to fulfill the objectives mentioned above:

- Bandpass-FSS model 1, which is a combination DSL for transmitting WCDMA850 and WCDMA2100 bands at normal and oblique incident angle; achieved by removing 7.3% of the coating area.

- Bandpass-FSS model 2, which is a combination of a square loop and TLCD

Band No	Frequency band	Name	UL Frequencies	DL Frequencies
1	2100	IMT	1920-1980	2110-2170
5	850	CLR	824-849	869-894

Table 6.1: Frequency allocation of Universal Mobile Telecommunication System (UMTS)-FDD bands for Australia

Parameters	$P_x \times P_y$	$D_x \times D_y$	$L_x \times L_y$	w_1
Values	40×40 mm	37.5×37.5 mm	20.5 mm	0.5 mm
Parameters	w_2	$g/2$	ϵ_r	h
Values	0.5 mm	1.25 mm	6.9	6 mm

Table 6.2: Parameters of the dual-bandpass FSS unit cell.

for transmitting most of the GSM, UMTS Frequency Division Duplexing (FDD) globally used frequency bands (WCDMA800, WCDMA850, WCDMA1900, WCDMA2100); achieved by removing 12.35% of the coating area.

6.1 Reflecting and Transmitting FSS: Model 1

6.1.1 FSS Requirement

In order to improve the transmission of UMTS-FDD band radiation through ESG windows, two FSS passbands centered at $f_c = 887$ MHz and $f_c = 2112$MHz need to be designed for transmitting the mobile phone bands of the local carriers (Table 6.1), and while blocking all other frequency bands. For these frequencies passbands it is necessary to select an optimum design, which does not affect the performance of the ESG significantly within the IR range. The design is selected by considering the linear relationship between the percentage area removed and the percentage increase in IR transmission [42].

6.1.2 Design and Analysis

In the first model, DSL-FSS has been selected for designing the DBP filter, which has already been analysed and optimsed using various techniques. For example, beside parametric analysis, some other tuning techniques can also be employed for DBP; i.e. optimized algorithms and Differential Evaluation Strategies (DES) [53].

The geometry of our optimised final design for a DBP-FSS unit cell is presented in Fig. 6.1, and the parameters are illustrated in Table 6.2. The cell structure is modeled as two square through-cuts, of different side lengths, on the coating layer. The relative permittivity (ϵ_r) and conductivity (σ) of glass are 6.9 and $5 \times 10^{-4} S/m$, respectively [40].

The periodic array is arranged in two dimensions with periodicity of $P_x = P_y$. The distance between the boundary of the unit cell and the larger square is $g/2$. For the first bandpass filter where $f_c = 887$ MHz band, the length along x - axis and y - axis is equal to $D_x = D_y$ and the width is equal to w_2. Whereas for the second bandpass filter tuned at $f_c = 2112$ MHz band, the length along x - axis and y - axis is equal to $L_x = L_y$, and the width is equal to w_1. The values of these parameters are listed in Table 6.2 for the center frequencies given above. In this design 7.12% of coating area was removed from the total area of unit cell. As a result an extra 7.13% IR energy will be transmitted through the ESG, which represents an insignificant percentage of the total radiations [42].

The parametric analysis of DSL shows that the resonant frequency of the first passband (outer square loop with a resonance frequency of f_1), does not depend on lengths L_x and L_y of the inner square loop which has a higher resonance frequency, but it is dependent on the aperture width w_2. On the other hand, the resonant frequency of the inner square loop, having a resonance frequency f_2, is depend on L_x and L_y; and f_2 increases with the decrease of L_x and L_y. The control of the resonant frequency of the passband (at frequency f_T) is also dependent on the relative spacing between the first and the second resonance loop. These observations agree with the results in previous studies obtained using different substrates [49].

6.1.3   Simulation Procedure

In this research the frequency domain solver of CST MW Studio2010 [63], a fully featured electromagnetic analysis and design software, was used for designing, simulating and optimising the FSS model. The full wave simulation technique was used for DBP-FSS, and for various polarisation modes and incident angles. To utilise the computational resources effectively, whole infinite periodic surface was analysed by only considering a periodic cell (see Fig.6.1). The performance of the complete structure was evaluated by applying a periodic boundary condition at the four boundaries of the unit cell, which are perpendicular to the FSS plane, and grouped into two pairs; each consisting of two opposite boundaries labeled as source and destination. The incident wave was assumed to be a plane wave, and different transmission modes (TE and TM) at different incident angles were simulated. Due to the fact that the thickness of the coating layers is of the order of ~ 10 micrometers, zero thickness is used as an approximation throughout the modeling process. The coating is treated as a Perfect Electric Conductor (PEC). Other physical parameters and the geometrical parameters are discussed in the next section.

6.1.4   Results and Discussion

The simulation results of transmission patterns for the DBP-FSS are presented in Fig. 6.4 and 6.5. The optimisation process was carried out step by step using fine tuning. The transmission coefficients for TE and TM polarisation were then
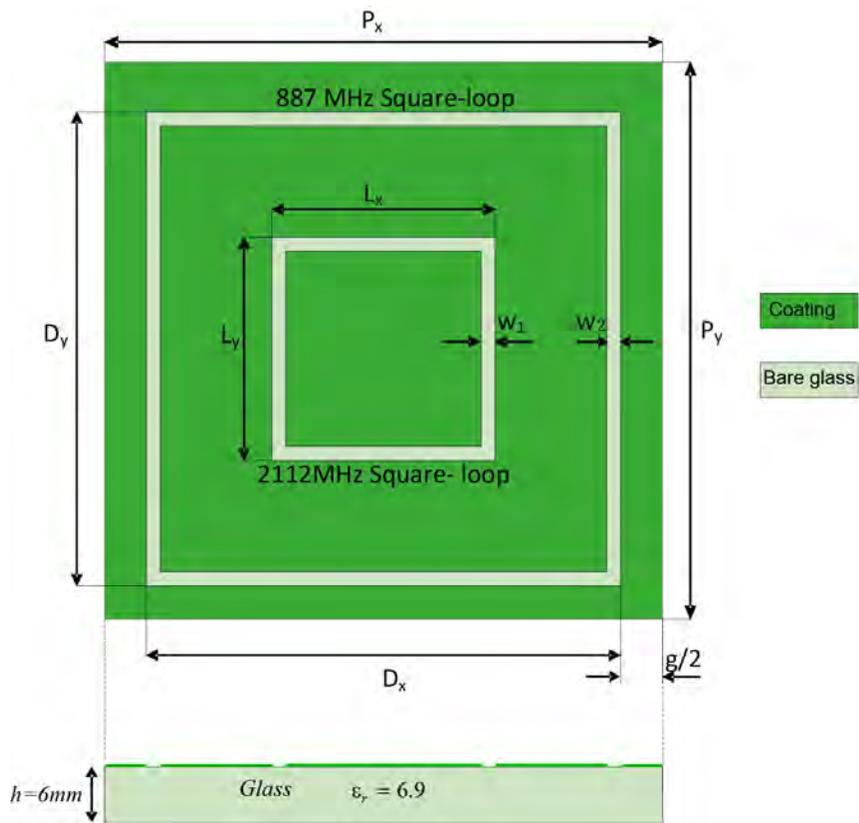
Figure 6.1: Top − double square dual-bandpass FSS. Bottom − cross sectional view at the center line.
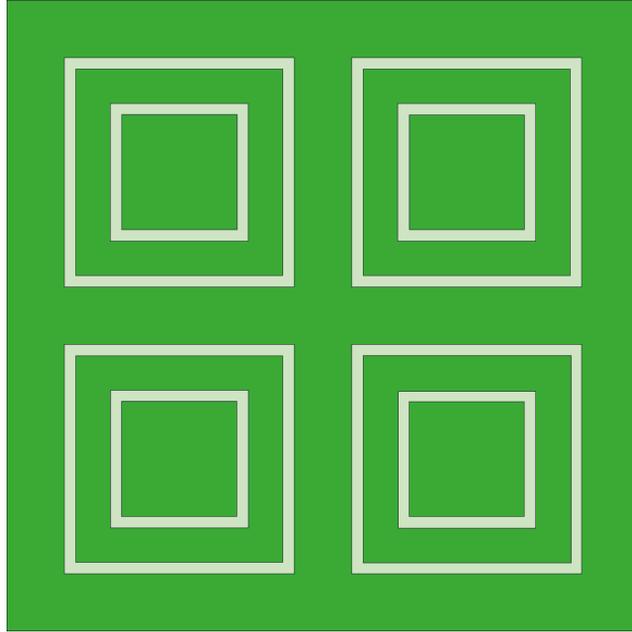
Figure 6.2: Layout of a portion of FSS in an infinite 2D array, showing 2×2 unit cells.
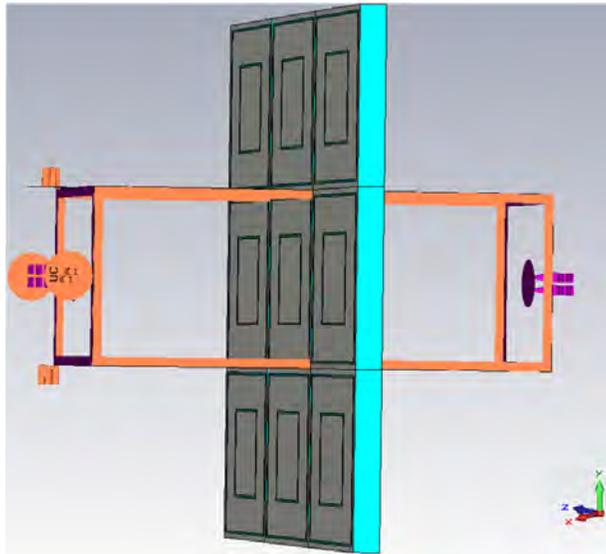
Figure 6.3: FSS unit cell source and destination boundary presentation in CST MW studio2010.

evaluated and recorded for the 0 - 3 GHz frequency band at both normal and oblique incident angles.

TE Polarisation

In Fig. 6.4 transmission coefficients (in dB) for TE polarisation are given at normal and oblique incident angles. The resonant frequencies and the corresponding bandwidths are listed in Table 6.3. At all four resonant frequencies plotted, negligible attenuation is observed for transmission of the required mobile phone signals. In order to minimise unwanted absorption throughout the entire range of the two UMTS bands, the FSS is designed in such a way that the widths of -10 dB passbands of the filters are significantly wider than those of the corresponding UMTS bands, with the center frequencies being slightly tuned in order to optimize the response. The final design gives a maximum attenuation of only 4 dB over the full WCDMA850 band (824-894 MHz, see Table 6.1), while the -10 dB passband width is between 388 - 651 MHz for different incident angles (Table 6.3). For the full WCDMA2100 band, the maximum attenuation at oblique incident angle is 11 dB, while the -10 dB passband width ranges between $357 \sim 923$ MHz for different incident angles. Note that for a particular mobile base station, only a smaller range of the full band is used; and such smaller attenuation can be achieved locally by adjusting the center frequencies. For examples, at ECU site the local band for WCDMA850 is $884.7 - 889.7$ MHz, and over this range the maximum attenuation is reduced to 1 dB. Similar reduction is observed for the WCDMA2100 band, with a maximum attenuation of 3 dB. These results satisfy the design requirements of transmitting the f_c =887 MHz and f_c = 2112 MHz UMTS bands. As for different incident angles, the first bandstop center frequency is between $1629 \sim 1644$ MHz, with attenuation ranging between -62 $\sim$ -73 dB. On the other hand the second bandstop center frequency is between $3132 \sim 3264$ MHz, with attenuation ranging between -40 to -54 dB. By using a FSS, the complete WCDMA850 and WCDMA2100 bands with a TE polarisation can be transmitted with less than 6 dB attenuation, for an incident angle $\leq 60^0$. There is only a slight shift of resonance frequency of about 2% in the case of the first passband, and 3% in the case of the second passband, for different incident angles; which confirms the stability of the FSS from $0^0 - 60^0$. On the other hand, with the increase of the incident angle, there is a significant decrease in the bandwidth for both of the passbands: ~ 40% for the first passband, and ~ 60% for the second passband. As such, in the case when large incident angles are required, variation of other parameters is necessary in order to achieve desirable performance.

TM Polarisation

Fig. 6.5 presents transmission coefficient (dB) for TM polarisation at normal and oblique incident angles. The resonant frequencies and the corresponding bandwidths are listed in Table 6.4. Again, for all the four resonant frequencies listed, negligible attenuation is observed. Similar discussions with the corre-
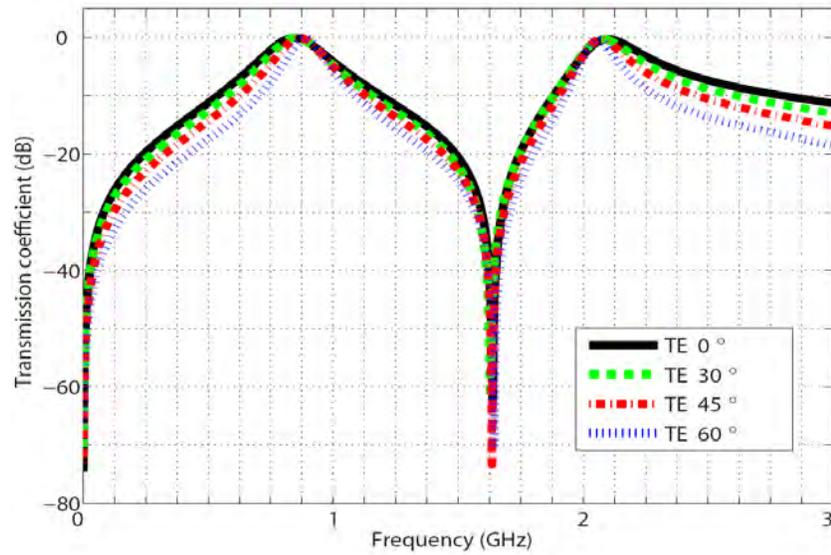
Figure 6.4: Transmission coefficient of dual-bandpass FSS at normal and oblique incidence angles for TE polarization.

	887 MHz		2112 MHz	
Angle	Resonance (MHz)	BW (MHz)	Resonance (MHz)	BW (MHz)
0^0	875	651	2112	923
30^0	866	581	2092	730
45^0	885	500	2100	565
60^0	891	388	2076	357

Table 6.3: -10dB transmission bandwidth at 887 MHz and 2112 MHz for TE Polarisation.

74
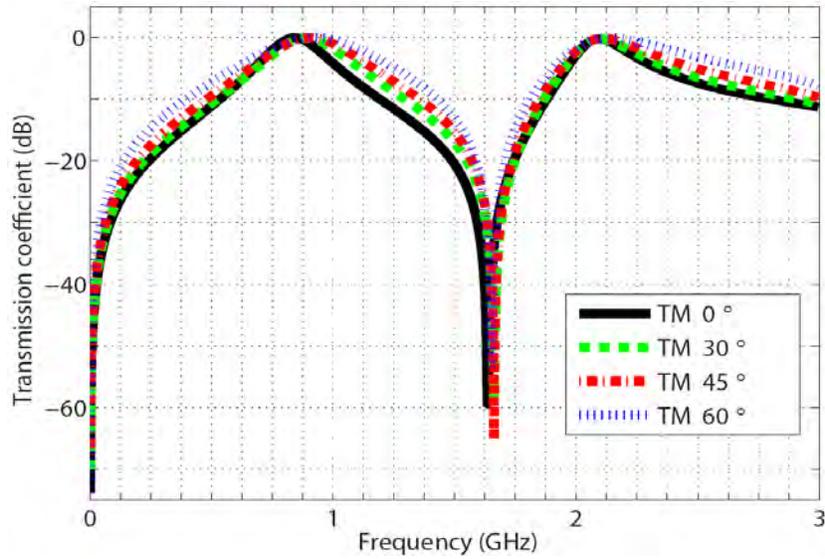
Figure 6.5: Transmission coefficient of dual-bandpass FSS at normal and oblique incidence angles for TM polarization.

sponding TE case are applicable for the passband resonant frequencies. On the other hand, compared with the TE polarisation, larger bandwidths of the two passbands were observed for the TM polarisation. The bandwidth obtained for the $f_c = 887$ MHz band ranges between $655 \sim 1046$ MHz, while that for the 2112 MHz band ranges between $921 \sim 1252$ MHz, with respect to a -10 dB transmission coefficient. There is a decrease in the attenuation at both bandstop centers. Here the first bandstop center frequency is between 1637   1652 MHz, with attenuation ranging between -47 $\sim$ - 63 dB. The second bandstop center frequency is between 3094 $\sim$ 3269 MHz, with attenuation ranging between -34 $\sim$ -47 dB. Again, by using a FSS, the complete WCDMA850 and WCDMA2100 bands with a TM polarization can be transmitted with less than 8 dB attenuation, for an incident angle $\leq 60^0$. The resonant frequency is also stable from $0^0 - 60^0$. Furthermore, as discussed above, at a large incident angle (60^0), more than 60% increase in bandwidth can be achieved as compared with 0^0 when using TM polarisation. When a large bandwidth is required, this factor can be taken into account in the design process.

In summary, the transmission results of both TE and TM polarisation satisfy the design requirements. Under different circumstances the design requirements may change, which can be accommodated by using parametric analysis and the optimisation process.

Angle	887 MHz		2112 MHz	
	Resonance (MHz)	BW (MHz)	Resonance (MHz)	BW (MHz)
0^0	861	655	2111	921
30^0	899	766	2105	1032
45^0	909	872	2118	1149
60^0	942	1046	2162	1252

Table 6.4: -10dB transmission bandwidth at 887 MHz and 2112 MHz for TM Polarisation.

Frequency Bands	UL Frequencies (MHz)	DL Frequencies (MHz)	Zone
2100	1920-1980	2110-2170	Oceania, Europe, Asia
1900	1850-1910	1930-1990	North America
850	824-849	869-894	Australia, Hong Kong
800	830-840	875-885	Japan

Table 6.5: Worldwide frequency allocation table of the paired universal mobile telecommunication system (UMTS)-FDD

6.2 Reflecting and Transmitting FSS: Model 2

6.2.1 Configuration

For the second model, TLCD-FSS has been selected to design a DBP filter, which transmits almost all useful mobile phone frequency bands being used around the world.

TLCD-FSS normally provides: 1) higher bandwidth [13], 2) excellent angular stability, and 3) more tuning options for optimisation. Separation between two adjacent elements can be much smaller than that between two elements of other types, which helps to increase mutual capacitance.

In previous research, TLCD's [80] and their characteristics have been analysed for achieving broad-band and flat top frequency responses, but the angular stability and polarization effects have not been discussed [116].

In this study the relative performances of square loop and TLCD-FSS are analysed and compared, assuming that the two passband frequencies are well apart.

6.2.2 Frequency Bands for Mobile Communication

In our previous FSS model, the filter design was only focused on two bands, with operating frequencies ranges between 884.7-889.7 MHz and 21101-21151 MHz respectively [96]. However, the enhanced bandwidth capability of TLCD allowed transmission of the required microwave signals (GSM, UMTS and Wi-Fi) of the different frequency bands in use worldwide. Standard GSM normally operates
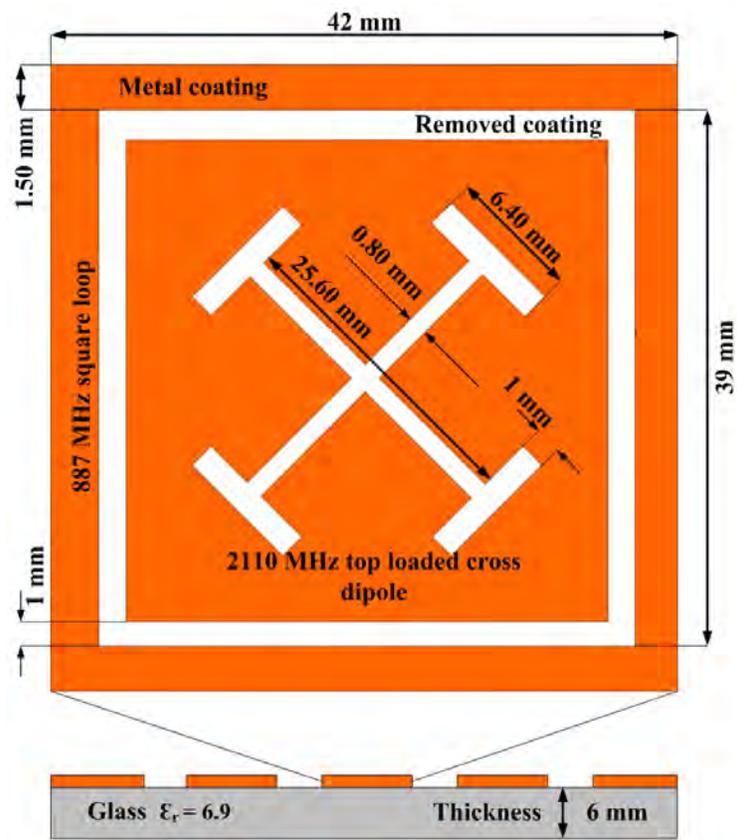
Figure 6.6: Top – The dimensions of the square loop and top loaded cross dipole designed for dual bandpass-FSS filter. Bottom – cross sectional view at the middle line.

in two frequency bands, GSM 900 and 1800 MHz, whereas Wi-Fi works at 2400 MHz. The UMTS-FDD frequency allocation spectrum varies for different regions, as presented in Table 6.5.

6.2.3 FSS Unit Cell

The requirements of this work can be described as an enhanced first pass-band with an improved bandwidth, and a minimised etching area. Based on these requirements, we have selected the combination of a square loop and a TLCD that is designed on coated side (hard coating) of ESG. The front view of our proposed unit cell is presented in Fig. 6.6. The periodic array is positioned in two dimensions (X and Y) with a periodicity of 42 mm in both directions. These dimensions are smaller than the fundamental mode ($\lambda_g/2$), because of capacitive characteristics of the top loaded element. The relative permittivity (ϵ_r) of glass used in the simulation is 6.9, the conductivity (σ) is $5 \times 10^{-4} S/m$ and the thickness of the glass is set to 6 mm [41]. The two unit cells are 3 mm apart from each others in both X and Y directions. The square loop center frequency is tuned to $f_c = 887$ MHz and the TLCD is tuned to $f_c = 2110$ MHz. As mentioned earlier, the TLCD exhibits more tuning options and behaves as a parallel equivalent circuit, which is utilised for obtaining higher bandwidth. It is also possible to increase the equivalent capacitance and angular stability by rotating the TLCD 45^0 from its original orientation [70]. In this FSS design only 12.35% of the coating area was removed from the total unit cell area, enabling transmission of most of the globally used UMTS-FDD frequency bands.

6.2.4 Results and Discussion

TE Polarisation

Results of simulated signal transmission (dB) through ESG for perpendicular polarization (TE) at 0^0, 30^0, and 60^0 incident angles and the corresponding bandwidths are presented in Fig. 6.7 and Table 6.6. The square loop and TLCD-FSS design on coated (hard) side of the glass was optimsed to obtain the required bandwidth for transmitting UMTS and Wi-Fi signals. Signal attenuation's less than 10 dB were considered to be satisfactory for both band-pass filters. The center frequencies were slightly adjusted to optimise the locations of the transmission bands in the first passband, the signal within both UMTS-FDD 800 and 850 frequency bands (Table 6.5) was fully transmitted with 3 dB attenuation at different incident angles. However, the total bandwidth at 0^0 (749 MHZ) is gradually reduced by 43% at an angle of 60^0. For the second passband, the signal within the complete UMTS-FDD 1900 and 2100 frequency bands (Table 6.5) passed with a maximum of 9 dB attenuation at oblique incident angles, with a shrinking of 54% bandwidth at 60^0 compared to that at the normal incident angle.

Table 6.6 shows the total bandwidth achieved at various angles in both band-pass filters. Although steady declines in bandwidths were observed with
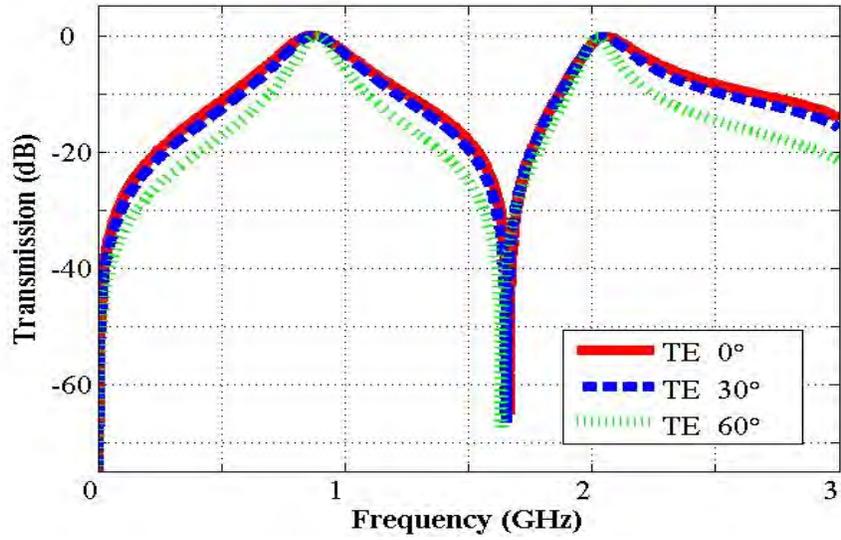
Figure 6.7: Theoretical TE transmission results of dual band-pass FSS, modeled on hard coated energy saving glass.
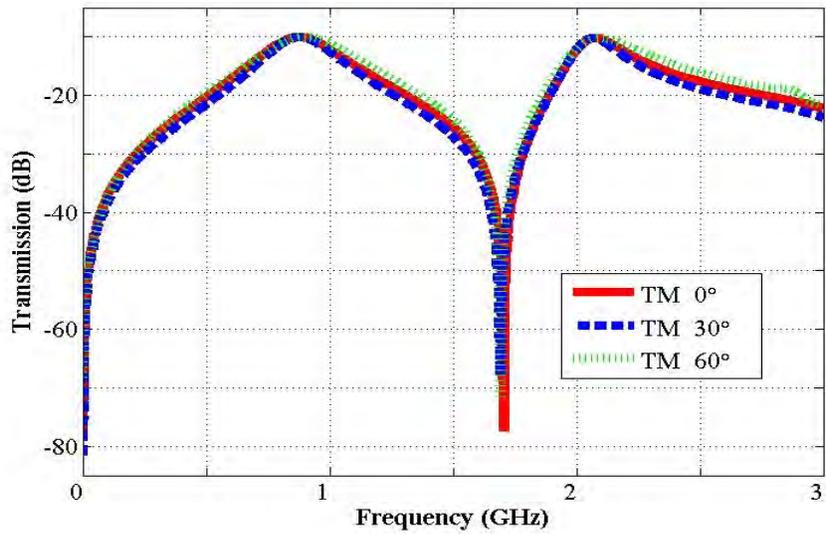
Figure 6.8: Theoretical TM transmission results of dual band-pass FSS, modeled on hard coated energy saving glass.

	887 MHz		2112 MHz	
Angle	Resonance (MHz)	BW (MHz)	Resonance (MHz)	BW (MHz)
0^0	861	749	2055	860
30^0	870	694	2065	620
60^0	888	44	2027	400

Table 6.6: -10dB transmission bandwidth at f_c= 887 MHz and f_c = 2112 MHz for TE polarisation.

	887 MHz		2112 MHz	
Angle	Resonance (MHz)	BW (MHz)	Resonance (MHz)	BW (MHz)
0^0	875	450	2075	375
30^0	870	425	2070	300
60^0	885	500	2075	525

Table 6.7: -10 dB transmission bandwidth at f_c= 887 MHz and f_c= 2112 MHz for TM polarisation.

the increase of the incident angle, these bandwidths were still sufficient for passing commonly used UMTS-FDD and Wi-Fi signals. In the case of a higher bandwidth requirement, other parameters can be adjusted to achieve the desired frequency responses. There might be a slight change in resonant frequency, however the effect would have negligible impact on the overall performance in practical applications.

TM Polarisation

Fig. 6.8 shows theoretical transmission coefficient response (dB) for parallel polarization (TM). The resonant frequency points at various angles (0^0, 30^0 and 60^0) and the corresponding bandwidths are presented in Table 6.7. In this case, the first passband filter (tuned for $f_c = 887$ MHz) was able to fully transmit UMTS-FDD 800 and 850 frequency bands ranging from 824 $\sim$ 894 MHz (Table 6.5) with only 2 dB transmission loss. The bandwidth variation in the first passband ranged between 450 $\sim$ 500 MHz, which is about 40% less than that of TE for the first two angles. For the second passband (tuned for $f_c = 2112$ MHz), the total bandwidth varied between 375 $\sim$ 525 MHz, with respect to -10 dB transmission coefficient. Thus, a loss of 50% bandwidth between the first two angles, as well as a slight increase at 60^0, was observed. This band-pass filter is capable of transmitting the full 2100 band (UMTS-FDD) with negligible transmission loss (1 dB); but for1900 MHz band, the maximum loss reached 16 dB for UL frequencies and 3 dB for DL frequencies (Table 6.5).

In summary, the transmission curves for both polarisations (TE & TM) at different incident angles satisfy the design requirements (transmitting all UMTS-FDD bands). This particular design can be optimised for different frequencies by changing certain parameters, for example, FSS element dimension, substrate
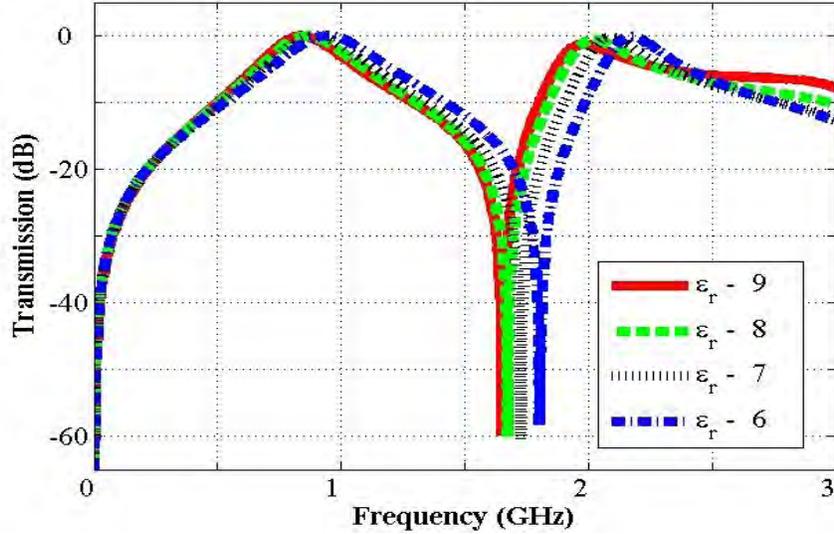
Figure 6.9: Transmission curve at normal incidence angle for TE polarisation using different permittivity values.

thickness, or by using substrate of different permittivity.

6.2.5 Parametric Study

Transmission through a FSS can be affected by several factors, including element dimensions, substrate thickness and variations in permittivity (ϵ_r). In this section, the results of parametric study are presented using all the aforementioned parameters:

Dimension Effect of the Top-Loaded Cross Dipoles

The width of the loaded top was parametrically scanned from $0.60 \sim 1.30$ mm, in 0.10 mm steps, for both TE and TM polarisations and at different incident angles. At 0^0 angle and thickness of 0.60 mm, a bandwidth of 808 MHz was achieved for the first passband, which gradually reduced with the increase in the width for both polarisations. The same effect was also observed for the second passband. At 30^0 angle of incidence, the bandwidth increased for the first passband, and became steady for the second passband. Meanwhile, the resonance points moved backward with the increase of the width in the second passband, but remained unchanged in the first passband for both polarisations. Furthermore, some unwanted resonances, attenuating some particular frequency ranges within the first passband by 12 dB to 16 dB were also seen in perpendicular polarisation at 30^0. In the case of 60^0, bandwidth was not changed in
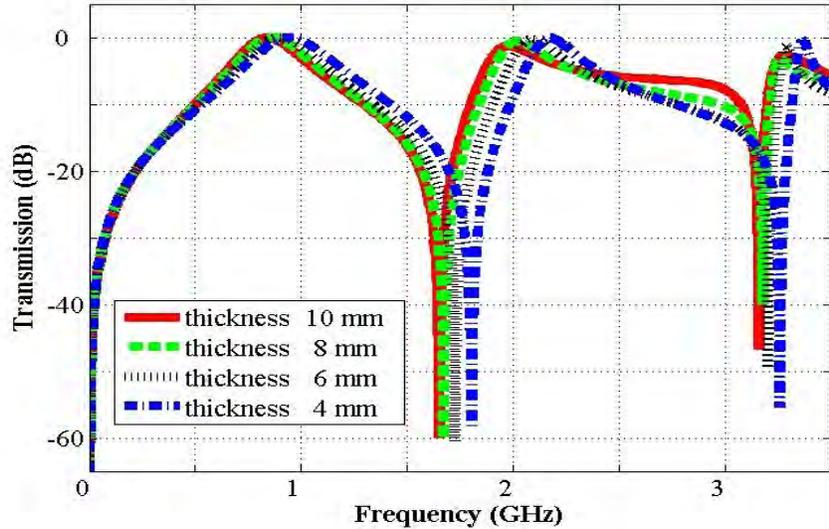
Figure 6.10: Transmission curve at normal incidence angle for TE polarisation using different thickness values of glass.

TE polarisation for both passbands, but a slight decline was observed in TM polarisation for the second passband. Resonance points steadily moved backwards with the increase in the thickness. The most important observation here is that the number of unwanted resonance peaks increased substantially, once the width was outside of the range 0.80 - 1.20 mm.

Dipole thickness was also parametrically analysed from 0.60 ~ 1.10 mm, in 0.10 mm steps. For 0^0 angle of incidence, bandwidth and resonance points did not change in the first passband for both polarisations, but a gradual decline ($\sim$ 100 MHz) in the bandwidth was observed in the second passband during the increase of dipole thickness from 0.60 mm to 1.10 mm. At incident angle of 30^0, resonance points and the bandwidth remained unchanged for TE polarisation, but for TM polarisation bandwidth was increased steadily up to an additional 100 MHz. With the second passband, the resonance frequency point shifted as thickness increased. Unwanted resonances were also seen at lower thickness for both polarisations, which becomes more prominent in TM when the thickness exceeded 1 mm. For 60^0 angle of incidence, the bandwidth and the resonance point in the first passband remain unchanged, but unwanted resonances appeared at lower and higher thickness for both polarisations. A bandwidth increase by 100 MHz in the first passband and a shift of the resonance points were also observed.

Permittivity Analysis

The transmission coefficient of the FSS with the unit cell (Fig. 6.6) was also analysed, using different relative permittivity values of the substrate at normal incident angle. Larger bandwidth within the first passband was achieved by reducing the permittivity value, for example, 60 MHz addition to the bandwidth after reducing permittivity by one unit, as illustrated in Fig. 6.9. Meanwhile, the resonance point only changed with a large change of the permittivity. For the second passband, both the bandwidth and resonance point reduced drastically for higher permittivity values, Hence, permittivity plays an important role in deciding the transmission characteristic of an FSS, particularly at higher frequencies.

Substrate Thickness Effect

The transmission characteristic of the FSS was also studied using the thickness of the substrate (glass) as a parameter. Within the first passband, a steady increase in thickness value from 4 mm to 6 mm reduced the bandwidth by 70 MHz, while reductions of the resonance frequency and the bandstop point were also observed, as shown in Fig. 6.10. However, no significant change was seen during the change of the thickness between $8 \sim 10$ mm. For the second passband, the bandwidth increased progressively as the thickness values increased, however, bandstop and resonance point were reduced as the thickness increases.

In summary, improved transmission frequency curves can be obtained by altering the dimensions of a unit cell, substrate thickness, and permittivity value of the substrate. The results of these parametric analysis can be used for optimising the configuration of the FSS elements, in order to achieve particular design objectives.

6.3　Conclusion

This chapter describes two typical FFS design which are used for improving the mobile and Wi-Fi signal transmission while maintaining the energy saving property of ESG.

The first design is of a DSL type, with the absorbing and transmitting properties of bandpass FSS filters based on hard-coating ESG to improve the transmission of UMTS bands. The design has been optimised according to the particular scenarios being used at ECU, where the full wave simulation technique has been utilized to evaluate the response of the FSS. The design has achieved transmission requirements for the two specific frequency bands, with stable frequency response for both TE and TM polarisation at normal and oblique incident angles up to 60^0. The DSL-FSS unit cell design sustains 92.7% efficiency of ESG by attenuating IR radiations, which fulfills the overall design objectives. Details about the effects of parameters have been discussed, with concrete suggestions

for variations in similar design work. This design can be adapted as a general reference, which is suitable for applications under similar circumstances.

The second design is of a combination type,which is used to improve the transmission of UMTS and Wi-Fi signals through hard coated ESG. A combination of square loop and TLCD were adapted for a novel DBP-FSS. An optimized design was presented, which attenuates less than 10 dB within the required microwave bands, with a reduction of 12.35% IR attenuation capability. For TE polarisation with different incident angles up to 60^0, promising -10 dB bandwidths of 444 and 400 MHz were achieved for center frequencies of 887 MHz and 2112 MHz respectively. The corresponding TM bandwidths being 450 and 300 MHz, respectively. Parametric studies were carried out with respect to the geometric dimensions, substrate permittivity and thickness. The width of the loaded top of the dipole FSS plays an important role in reducing the unwanted sharp resonances, with the optimum point located between 0.8 - 1.0 mm. An increase in permittivity shifts the resonance peaks towards the lower frequency end, and concurrently narrowing the lower pass-band and widening the higher pass-band. An increase in the thickness of the substrate has similar effects. The results presented in this chapter are expected to help clarify the effects of different parameters, and optimise designs under similar circumstances. Furthermore, they indicate that appropriately designed hard coated ESG can maintain its energy saving property, while avoiding excessive attenuation of the microwave frequency needed to allow mobile phone and Wi-Fi communication across external building walls.

Chapter 7

Conclusion

This thesis shows my effort to measure, evaluate, and rectify issues related to microwave radiation risks, generated from different sources (specifically 3G mobile base stations, mobile handsets, and microwave ovens). In this chapter a summary is presented of the achievements, contributions, and suggestions for future work.

Measurements around RBSs were conducted, results were recorded for different periods of time at multiple locations and angles, the results were then compared with ARPANSA standards. Microwave oven measurements have been conducted for: 1) different brands, 2) distance, and 3) measurement angles. ESG is utilised in the front panel as a shield to reduce direct radiation exposure. Mobile handsets were measured in both idle and active states to analyse their behavior. The solution for reducing excessive amount of infrared and unwanted microwave radiation has been suggested by using hard coated ESG, which is easy to handle and provides 70 dB signal attenuation. Useful signals transmission through ESG has been improved by designing DBP-FSS filters of varying elements shapes, fabricated onto the hard coated ESG.

7.1   RF-EME Measurements

Chapter 3 presents the measurement results of RF-EME levels at the ECU, Joondalup campus, resulting from RBSs. Telstra (WCDMA850) and 3GIS (WCDMA2100) RBS radiations have been individually measured for 2 hours, at 4 specific points selected from a group of multiple short measurement points; and for 24 hours at highly exposed locations closer to the RBS. Measured results have been compared to the ARPANSA standards. The objective was to identify high risk areas. Generally speaking, locations closer to the RBS and at the same elevation as the transmitting antenna will receive higher levels of radiation, compared to those which are located at oblique incident angles. Here are the main contributions of this research work:

- In previous research, measurements for GSM frequency bands have been

normally conducted only for short periods of time. Similarly for UMTS base stations, only very limited measurements have been carried out either in peak time or during off peak time. This is the first time that detailed EMI measurements have been conducted for 3G (UMTS) networks; these networks operate at frequency bands which are different from those used in traditional GSM networks.

- Comparisons between the radiation levels at varying distances and elevations have never been conducted before. Without investigating the influence of the angle formed between the transmitting antenna and the user position, it is difficult to identify the high risk regions and to provide EMI shielding solutions. EMI shielding is specifically required for those building closer to a RBS. This research is not limited to the ARPANSA standards when specifying the need for shielding material, but it suggests to implement shielding solutions even before the defined level is reached, since researchers have already proved that health hazards could exist below the recommended standards.

- Considerations have been given to those locations where different RF radiation sources are in close proximity, such as weather radar, emergency services communication systems, radio broadcasting stations, satellite TV stations, and power transmission lines; and where people are spending a sufficiently long time; for example, Universities, Hospitals, research and child care centers. This research work has considered all of these scenarios for providing the best possible solution to reducing unwanted radiation exposure. We have proposed that ESG be employed in order to block unwanted microwave signals, while the maintaining original beauty of the buildings and enabling the transmission of useful signals.

7.2 Radiations from Microwave Oven and Mobile Phone

Other sources of microwave radiation are appliances used in everyday life, e.g., microwave ovens and mobile phones, etc. Chapter 4 illustrates the measurement results of the radiation levels originating from microwave ovens and mobile phones; during both idle and operating modes. Microwave oven exposure at various distances and angles has been analysed to provide safety recommendations in order to reduce direct radiation exposure. Furthermore, the attenuating capability of ESG, when applied as a shield to microwave ovens has also been measured. The transmission power of different brands of mobile phones when communicating with base station has been measured and compared for evaluation purposes. The contributions from this chapter are summarised below:

- Measurement results of radiation power density from microwave ovens of different brands have been analysed and compared with ARPANSA safety standards. All measurements have been conducted for the best case

scenario (minimum reflection inside the room and water placed inside oven which can absorb radiation), where minimum radiation should be leaked into the environment.

- Influence of direct radiation exposure at various distance and angles for different brands of microwave ovens has been discussed in order to rectify higher exposure issues. Suggestions and recommendations have been proposed to reduce health hazards immediately after the microwave oven begins to operation.

- The radiation level was measured in front of the microwave oven, both with and without additional ESG shielding, and the results were compared. The fitting of ESG to oven doors was recommended due to its significant shielding effect.

- Mobile phone radiation power density level of different brands, before and during the call, was measured and compared.

- Most of the older mobile phones transmit at a higher power when communicating with the base station, and even transmit power during idle time. By comparison, the newer smart phones have the capability of maintaining a low power level before and after a connection has been made. It was strongly recommended that manufacturers specify the transmitting power on mobile handsets.

7.3   FSS for Energy Saving Glass

Being an excellent microwave signals attenuator, ESG also attenuates the desired mobile phone and Wi-Fi signals. Chapter 6 describes the design of two FSS bandpass filters on hard coated ESG, which enable the desired signals to be received while attenuating unwanted infrared and microwave radiation.

For the first design, only 7.30% of glass coating area was removed, while 92.70% original coating area was maintained. This design allows the locally used frequency band (WCDMA850 and WCDMA2100) to be transmitted. In comparison, the second FSS bandpass design allowed transmission of most of the UMTS frequency bands currently in use worldwide (WCDMA800, WCDMA850, WCDMA1900, WCDMA2100) by removing 12.35% of the coating area. Both designs show stable frequency response for TE (perpendicular) and TM (parallel) polarisation at normal and oblique incident angles. Listed below are the main contributions of this research work:

- This is the first FSS spatial filter design on hard coated ESG, which transmits the required signals within specific frequency bands, while stops wave propagation at unnecessary frequencies, including IR radiation.

- A combination of square loop and TLCD-FSS has been suggested for obtaining stable resonance curve for higher bandwidth, where incoming

waves approach from arbitrary directions. On the other hand, DSL-FSS spatial filters does not give higher bandwidth, but requires the removal of less coating area while providing angular stability at both polarisations.

- A parametric analysis of: 1) substrate permittivity, 2) substrate thickness, 3) width of square loop and TLCD-FSS has also been conducted to optimise frequency response for obtaining the required bandwidth.

- In traditional FSS designs, resonance occurs if the length of the element is equal to $\lambda_g/2$. This research shows that further reduction of element size can provide better angular stability for different polarisations. The compact element size is an important requirement at lower frequencies.

7.4 Suggestions for Future Research

Based on the results presented in this thesis, further research works are suggested, as listed below.

- It is recommended that radiation measurements be conducted over a longer measurement period (for example, 24 hours), under extreme weather conditions (winter and summer), and in the metropolitan areas where network traffic load is much higher and RBSs are closer to each other. It is also desirable that the power density level be measured for the newly deployed Long Term Evolution (LTE) network; which operates at different frequency bands, such as LTE band number 7 (for Asia and Europe) in the frequency range 2500-2690 MHz.

- Measurement and evaluation of Femto cell radiation is recommended, which is an access point for the home users to receive better mobile phone coverage via a DSL line. It works as an individual RBS in each house and continuously transmits radiation inside the home or commercial building.

- A feasibility study for using ESG as microwave oven window shielding instead of normal float glass is desirable.

- Measurements should be conducted after applying a radiation attenuator polymer to the back surface of the mobile handset, in order to ascertain whether the EME level can be significantly reduced.

- Due to rapid growth in wireless technology and implementation of new frequency bands, the demand for active FSS filters will increase. As the desired frequency response can be tuned using PIN or varacter diodes, it is desirable to further investigate inclusion of these diodes in FSS.

- Modern trains and cars are also using ESG and tinted window solutions which affect the transmission of mobile phone signals. Therefore, research should also further expand into this area.

- In modern architecture, buildings are often constructed in curved shapes, hence conventional FSS design may not work precisely for waves coming at oblique incident angles. As such, further research work in design and development is required for curved shape FSS, in addition to the planar structures which have been presented in this work.

Bibliography

[1] V. Agrawal and W. Imbriale. Design of a dichroic Cassegrain subreflector. *IEEE Transactions on Antennas and Propagation*, 27(4):466–473, 2002.

[2] N. Amitay, V. Galindo, and C.P. Wu. Theory and analysis of phased array antennas. *Top. Astrophys. Astron. Space Sci.*, 1, 1972.

[3] I. Anderson. On the theory of self-resonant grids. *The bell System Technical Journal*, 54(10):1725–1731, Dec 1975.

[4] ARPANSA. Australian radiation protection and nuclear safety agency, maximum exposure levels to radio frequency fields 3 KHz to 300 GHz. *Radiation protection standard, Series No 3*, 2002.

[5] Nikolai Atanasov and Gabriela Atanasova. An investigation impact of user's positions in closed space over SAR in the head induced from mobile phone. *The Environmentalist*, 31:181–186, 2011.

[6] P. W. B. Au, L. S. Musa, E. A. Parker, and R. J. Langley. Parametric study of tripole and tripole loop arrays as frequency selective surfaces. *Microwaves, Antennas and Propagation, IEE Proceedings H*, 137(5):263 – 268, Oct 1990.

[7] A. Barth, R. Winker, E. Ponocny-Seliger, W. Mayrhofer, I. Ponocny, C. Sauter, and N. Vana. A meta-analysis for neurobehavioural effects due to electromagnetic field exposure emitted by GSM mobile phones. *Occupational and environmental medicine*, 65(5):342, 2008.

[8] S.C. Bundy and Z.B. Popovic. A generalized analysis for grid oscillator design. *Microwave Theory and Techniques, IEEE Transactions on*, 42(12):2486 –2491, Dec 1994.

[9] R. Cahill and E. A. Parker. Concentric ring and jerusalem cross arrays as frequency selective surfaces for a 45 incidence diplexer. *Electronics Letters*, 18(8):313 –314, Apr, 1982.

[10] A. Caprani, A. Richert and P. Flaud. Experimental evidence of a potentially increased thrombo-embolic disease risk by domestic electromagnetic field exposure. *Bioelectromagnetics*, 25(4):313–315, 2004.

[11] Carol. Energy saving facts, www.calor.co.uk/home/central-heating/energy-efficiency/energy-saving-facts.htm.

[12] F. Che Seman, R. Cahill, V. F. Fusco, and G. Goussetis. Design of a salisbury screen absorber using frequency selective surfaces to improve bandwidth and angular stability performance. *Microwaves, Antennas Propagation, IET*, 5(2):149 –156, 31 2011.

[13] Hsing-Yi Chen, Yu Tao, Kuo-Lun Hung, and Hsi-Tseng Chou. Bandwidth enhancement using dual-band frequency selective surface with jerusalem cross elements for 2.4/5.8 GHz WLAN antennas. pages 1 –4, Sep 2010.

[14] David Keun Cheng. *Field and wave electromagnetics*. Addison-Wesley, 2nd edition, 1989.

[15] C.C. Chong, C.C. Tan, D.I. Laurenson, S. McLaughlin, M.A. Beach, and A.R. Nix. A new statistical wideband spatio-temporal channel model for 5-GHz band WLAN systems. *Selected Areas in Communications, IEEE Journal on*, 21(2):139 − 150, 2003.

[16] A. D. Chuprin, E. A. Parker, and J. C. Batchelor. Convoluted double square: single layer FSS with close band spacings. *Electronics Letters*, 36(22):1830 –1831, Oct 2000.

[17] M. Clemens, E. Gjonaj, P. Pinder, and T. Weiland. Numerical simulation of coupled transient thermal and electromagnetic fields with the finite integration method. *IEEE Transactions on Magnetics*, 36(4):1448 –1452, Jul 2000.

[18] D. B. Davidson, A. G. Smith, and J. J. van Tonder. Measurement and design of frequency selective surfaces. In *Tenth International Conference on Antennas and Propagation, (Conf. Publ. No. 436)*, volume 1, pages 156 –160, Apr 1997.

[19] A. Demenko, J.K. Sykulski, and R. Wojciechowski. On the equivalence of finite element and finite integration formulations. *IEEE Transactions on Magnetics*, 46(8):3169 –3172, Aug 2010.

[20] H. Dolk, G. Shaddick, P. Walls, C. Grundy, B. Thakrar, I. Kleinschmidt, and P. Elliott. Cancer incidence near radio and television transmitters in great britain i. sutton coldfield transmitter. *American Journal of Epidemiology*, 145(1):1, 1997.

[21] T. F. Eibert, J. L. Volakis, D. R. Wilton, and D. R. Jackson. Hybrid FE/BI modeling of 3-D doubly periodic structures utilizing triangular prismatic elements and an MPIE formulation accelerated by the ewald transformation. *IEEE Transactions on Antennas and Propagation*, 47(5):843 –850, May 1999.

[22] R.B. Ertel, P. Cardieri, K.W. Sowerby, T.S. Rappaport, and J.H. Reed. Overview of spatial channel models for antenna array communication systems. *Personal Communications, IEEE*, 5(1):10 –22, 1998.

[23] K.L. Ford and B. Chambers. Improvement in the low frequency performance of geometric transition radar absorbers using square loop impedance layers. *IEEE Transactions on Antennas and Propagation*, 56(1):133 –141, Jan 2008.

[24] K.R. Foster. Thermal and nonthermal mechanisms of interaction of radiofrequency energy with biological systems. *Plasma Science, IEEE Transactions on*, 28(1):15 –23, 2000.

[25] K.R. Foster and J.E. Moulder. Are mobile phones safe? *Spectrum, IEEE*, 37(8):23 –28, Aug 2000.

[26] J.K. Grayson. Radiation exposure, socioeconomic status, and brain tumor risk in the US Air Force: a nested case-control study. *American Journal of Epidemiology*, 143(5):480, 1996.

[27] The INTERPHONE Study Group. Brain tumour risk in relation to mobile telephone use results of the interphone international case-control study. *International Journal of Epidemiology*, 39(3):675–694, 2010.

[28] S. M. A. Hamdy and E.A. Parker. Current distribution on the elements of a square loop frequency selective surface. *Electronics Letters*, 18(14):624–626, 1982.

[29] T. Haumann, U. nzenberg, W. Maes, and P. Sierck. HF-radiation levels of GSM cellular phone towers in residential areas. pages 327–333. 2nd International Workshop on Biological effects of EMFS, Rhodes, Greece, 2002.

[30] Sabine Heinrich, Silke Thomas, Christian Heumann, RÃŒdiger von Kries, and Katja Radon. The impact of exposure to radio frequency electromagnetic fields on chronic well-being in young people – a cross-sectional study based on personal dosimetry. *Environment International*, 37(1):26 − 30, 2011.

[31] H. Hinrichs, H.J. Heinze, and M. Rotte. Human sleep under the influence of a GSM 1800 electromagnetic far field. *Somnologie*, 9(4):185–191, 2005.

[32] B. Hocking, I.R. Gordon, H.L. Grain, and G.E. Hatfield. Cancer incidence and mortality and proximity to TV towers. *Medical Journal of Australia*, 165(11):601–605, 1996.

[33] H.D. Hopfe, H. Dorn, A. Bahr, P. Anderer, and C. Sauter. Effects of electromagnetic fields emitted by mobile phones (GSM 900 and WCDMA/UMTS) on the macrostructure of sleep. *Journal of Sleep Research*, 20(1pt1):73–81, 2011.

[34] ICNIRP. International commission on non-ionizing radiation protection. guidelines for limiting exposure to time-varying electric, magnetic, and electromagnetic fields up to 300 GHz. *Health Phys*, 74:494–522, 1998.

[35] IEEE. IEEE standard for safety levels with respect to human exposure to radio frequency electromagnetic fields, 3 kHz to 300 GHz. *IEEE Std C95.1, 1999 Edition*, 1999.

[36] Jugalbandi. Microwave Q and A, http://jugalbandi.info/2007/08/microwave-q-a. Aug 2007.

[37] C. Kargel. Infrared thermal imaging to measure local temperature rises caused by handheld mobile phones. *IEEE transactions on Instrumentation and Measurement*, 54(4):1513 − 1519, 2005.

[38] G. I. Kiani. Passive, active and absorbing frequency selective surfaces for wireless communication applications. 2009.

[39] G. I Kiani, K. L Ford, L. G Olsson, K. P Esselle, and C. J. Panagamuwa. Switchable frequency selective surface for reconfigurable electromagnetic architecture of buildings. *Antennas and Propagation, IEEE Transactions on*, 58(2):581–584, 2010.

[40] G. I. Kiani, A. Karlsson, L. G. Olsson, and K. P. Esselle. Glass characterization for designing frequency selective surfaces to improve transmission through energy saving glass windows. In *Asia Pacific Microwave Conferenc*, 2007.

[41] G. I. Kiani, A. Karlsson, L. G. Olsson, and K. P. Esselle. Glass characterization for designing frequency selective surfaces to improve transmission through energy saving glass windows. In *Asia Pacific Microwave Conference Proceedings*, 2007.

[42] G. I. Kiani, L. G. Olsson, A. Karlsson, and K. P. Esselle. Transmission of infrared and visible wavelengths through energy-saving glass due to etching of frequency selective surfaces. *IET Microwaves, Antennas and Propagation*, 4(7):955 −961, 2010.

[43] G. I. Kiani, L. G. Olsson, A. Karlsson, K. P Esselle, and M. Nilsson. Cross-dipole bandpass frequency selective surface for energy-saving glass used in buildings. *IEEE Transactions on Antennas and Propagation*, 59(2):520–525, 2011.

[44] G. I. Kiani, A. R. Weily, and K. P. Esselle. Frequency selective surface absorber using resistive cross-dipoles. In *Antennas and Propagation Society International Symposium 2006, IEEE*, pages 4199 −4202, 2006.

[45] G. I. Kiani, A. R. Weily, and K. P. Esselle. A novel absorb/transmit FSS for secure indoor wireless networks with reduced multipath fading. *Microwave and Wireless Components Letters, IEEE*, 16(6):378 − 380, 2006.

[46] E.F. Knott, J.F. Shaeffer, and M.T. Tuley. *Radar cross section*. Sci Tech Publishing, 2nd edition, 2004.

[47] A. Kondo. Design and characteristics of ring-slot type FSS. *Electronics Letters*, 27(3):240 –241, Jan 1991.

[48] J. A. Kong. *Electromagnetic wave theory*. EMW publishing, Cambridge, 2000.

[49] R. J. Langley and E. A. Parker. Double-square frequency selective surfaces and their equivalent circuit. *IET Electronics Letters*, 19(17):675–677, 1983.

[50] C.K. Lee and R.J. Langley. Equivalent-circuit models for frequency-selective surfaces at oblique angles of incidence. *Microwaves, Antennas and Propagation, IEE Proceedings H*, 132(6):395 –399, 1985.

[51] S. W. Lee and T. T. Fong. Electromagnetic wave scattering from an active corrugated structure. *Journal of Applied Physics*, 43(2):388 –396, Feb 1972.

[52] E. W. Lucas and T. P. Fontana. A 3-D hybrid finite element/boundary element method for the unified radiation and scattering analysis of general infinite periodic arrays. *IEEE Transactions on Antennas and Propagation*, 43(2):145 –153, Feb 1995.

[53] X. F. Luo, P. T. Teo, A. b Qing, and C.K Lee. Design of double-square-loop frequency-selective surfaces using differential evolution strategy coupled with equivalent-circuit model. *Microwave and Optical Technology Letters*, 44(2):159–162, 2005.

[54] VR Makar, MK Logani, A. Bhanushali, M. Kataoka, and MC Ziskin. Effect of millimeter waves on natural killer cell activation. *Bioelectromagnetics*, 26(1):10–19, 2005.

[55] K. Mann and J.R. oschke. Effects of pulsed high-frequency electromagnetic fields on human sleep. *Neuropsychobiology*, 33(1):41–47, 1996.

[56] Tom Martin. Wireless quick facts, the wireless association, http://www.ctia.org. June 2010.

[57] A. E. Martynyuk and J. I. M. Lopez. Frequency-selective surfaces based on shorted ring slots. *Electronics Letters*, 37(5):268 –269, Mar 2001.

[58] D. A. A. Mat, F. K. W. Tat, K. Kipli, A. Joseph, K. Lias, and A. S. W. Marzuki. Visulization and analytical measurement of electromagnetic radiation from handheld mobile phones. Second International conference on computer engineering and application, March 2010.

[59] F. Mayer, T. Ellam, and Z. Cohn. High frequency broadband absorption structures. *IEEE International Symposium on Electromagnetic Compatibility*, 2:894 –899, Aug 1998.

[60] K. Merewether, R. Mittra, T. Cwik, and T. Wu. Relative convergence of the spectral-galerkin solution for the frequency response characteristics of the jerusalem cross FSS. In *Antennas and Propagation Society International Symposium, 1986*, volume 24, pages 859 – 862, June 1986.

[61] C. Mias, C. Tsakonas, and C. Oswald. An investigation into the feasibility of designing frequency selective windows employing periodic structures. *Final Report for the Radiocommunications Agency, The Nottingham Trent University, Nottingham, UK*, 2001.

[62] P. Michelozzi, A. Capon, U. Kirchmayer, F. Forastiere, A. Biggeri, A. Barca, and C.A. Perucci. Adult and childhood leukemia near a high-power radio station in Rome, Italy. *American journal of epidemiology*, 155(12):1096, 2002.

[63] Microwave Studio2010. Computer simulation technology, http://www.cst.com.

[64] M. M. Mokhtar and E. A. Parker. Conjugate gradient computation of the current distribution on a tripole FSS array element. *Electronics Letters*, 26(4):227 –228, Feb 1990.

[65] D. Molkdar. Review on radio propagation into and within buildings. *Microwaves, Antennas and Propagation, IEE Proceedings H*, 138(1):61 – 73, Feb 1991.

[66] S. Monni, N. L. Juan, A. Neto, and G. Gerini. A closely spaced waveguide phased array integrated with a frequency selective surface. modeling and design. In *IEEE Antennas and Propagation Society International Symposium*, volume 2, pages 829 – 832, Jun 2003.

[67] JE Moulder, KR Foster, LS Erdreich, and JP McNamee. Mobile phones, mobile phone base stations and cancer: a review. *International journal of radiation biology*, 81(3):189–203, 2005.

[68] A. Mousa. Electromagnetic radiation measurements and safety issues of some cellular base stations in nablus. *Journal of Engineering Science and Technology Review*, 4(1):35–42, 2011.

[69] B. Munk, R. Luebbers, and R. Fulton. Transmission through a two-layer array of loaded slots. *Antennas and Propagation, IEEE Transactions on*, 22(6):804 – 809, Nov 1974.

[70] B. A. Munk. *Frequency selective surfaces: theory and design*. Wiley-Interscience, 2000.

[71] Benedikt A. Munk. Periodic surfaces for large scan angles, united states patent 3789404. Jan 29 1974.

[72] H. M. Musal, Jr, and H. T. Hahn. Thin-layer electromagnetic absorber design. *IEEE Transactions on Magnetics*, 25(5):3851 –3853, Sep 1989.

[73] J.E. Muscat, M.G. Malkin, S. Thompson, R.E. Shore, S.D. Stellman, D. McRee, A.I. Neugut, and E.L. Wynder. Handheld cellular telephone use and risk of brain cancer. *Jama*, 284(23):3001, 2000.

[74] Narda. Narda safety test solution, Pfullingen, Germany, http://www.narda-sts.de.

[75] Netherland environmental assessment agency. Global CO2 emissions, http://www.pbl.nl/en/publications/2008/globalco2emissionsthrough2007.

[76] Q.T. Ostrom and J.S. Barnholtz-Sloan. Current state of our knowledge on brain tumor epidemiology. *Current neurology and neuroscience reports*, pages 1–7, 2011.

[77] E. A. Parker, A. D. Chuprin, J. C. Batchelor, and S. B. Savia. GA optimisation of crossed dipole FSS array geometry. *Electronics Letters*, 37(16):996 –997, Aug 2001.

[78] E. A. Parker, S. M. A. Hamdy, and R. J. Langley. Arrays of concentric rings as frequency selctive surfaces., 1981. cited By (since 1996) 7.

[79] E. A. Parker, S. M. A. Hamdy, and R. J. Langley. Modes of resonance of the jerusalem cross in frequency-selective surfaces. *Microwaves, Optics and Antennas, IEE Proceedings-H*, 130(3):203–208, 1983.

[80] E. A. Parker, S. M. A. Hamdy, and R. J. Langley. Modes of resonance of the jerusalem cross in frequency-selective surfaces. *IET Proceedings, Microwaves, Optics and Antennas*, 130(3):203–208, Apr 1983.

[81] EA Parker, C. Antonopoulos, and NE Simpson. Microwave band FSS in optically transparent conducting layers: Performance of ring element arrays. *Microwave and Optical Technology Letters*, 16(2):61–63, 1997.

[82] E. Pelton and B. Munk. Scattering from periodic arrays of crossed dipoles. *IEEE Transactions on Antennas and Propagation*, 27(3):323 – 330, May 1979.

[83] M Philippakis, C Martel, D Kemp, M Allan, S Appleton, W Damerell, C Burton, and EA Parker. Application of FSS structures to selectively control the propagation of signals into and out of buildings. *ERA Technology, report 2004-0072 A3*, 2004.

[84] J.L. Phillips, O. Ivaschuk, J. T. Ishida, R.A. Jones, B. M. Campbell, and W. Haggren. DNA damage in molt-4 t-lymphoblastoid cells exposed to cellular telephone radiofrequency fields in vitro. *Bioelectrochemistry and Bioenergetics*, 45(1):103–110, 1998.

[85] Adriano Pedro. Raiva. *Frequency selective surfaces:design of broadband elements and frequency stabilization techniques.* PhD thesis, 1998.

[86] G. S. N. Raju. *Electromagnetic field theory and transmission lines.* Dorling kindersley Pvt. Ltd., Delhi 2005.

[87] M.H. Repacholi, A. Basten, V. Gebski, D. Noonan, J. Finnie, and AW. Harris. Lymphomas in e mu-pim1 transgenic mice exposed to pulsed 900 mhz electromagnetic fields. *U.S. National Library of Medicine National Institute of Health*, 1997.

[88] L.G. Salford, A. Brun, K. Sturesson, J.L. Eberhardt, and B.R.R. Persson. Permeability of the blood-brain barrier induced by 915 mhz electromagnetic radiation, continuous wave and modulated at 8, 16, 50, and 200 hz. *Microscopy Research and Technique*, 27(6):535–542, 1994.

[89] R. Santini, P. Santini, J.M Danze, P. Le Ruz, and M. Seigne. Study of the health of people living in the vicinity of mobile phone base stations: I. influences of distance and sex. *Pathol. Biol*, 50:369–373, 2002.

[90] K. Sarabandi and N. Behdad. A frequency selective surface with miniaturized elements. *Antennas and Propagation, IEEE Transactions on*, 55(5):1239 –1245, May 2007.

[91] RD Saunders, ZJ Sienkiewicz, and CI Kowalczuk. Biological effects of electromagnetic fields and radiation. *Journal of Radiological Protection*, 11:27, 1991.

[92] G. H. Schennum. Frequency Selective Surfaces for multiple-frequency antennas Design data plus experimental results. *Microwave journal*, 16(4):55–57, 1993.

[93] J. Shaker and L. Shafai. Removing the angular sensitivity of FSS structures using novel double-layer structures. *IEEE Microwave and Guided Wave Letters*, 5(10):324 –325, Oct 1995.

[94] M. Siegrist, T.C. Earle, H. Gutscher, and C. Keller. Perception of mobile phone and base station risks. *Risk Analysis*, 25(5):1253–1264, 2005.

[95] S. Simms and V. Fusco. Tunable thin radar absorber using artificial magnetic ground plane with variable backplane. *IET Journal*, 42(21):1197–1198, 2006.

97

[96] I. Ullah, G. I. Kiani, X. Zhao, and D. Habibi. Transmission improvement of mobile Phone signals through energy saving glass using frequency selective surface. In *12th Australian Symposium on Antennas*, Sydney, Australia, 2011.

[97] I. Ullah, G. I. Kiani, X. Zhao, and D. Habibi. Selective transmission of RF signals through energy saving glass using FSS. 12th Australian symposium on Antenna, Sydney, Australia, Feb 2011.

[98] R. Ulrich. Far-infrared properties of metallic mesh and its complementary structure. *Infrared Physics*, 7(1):37–55, 1967.

[99] J. C. Vardaxoglou and E. A. Parker. Performance of two tripole arrays as frequency-selective surfaces. *Electronics Letters*, 19(18):709 –710, Sep 1983.

[100] J.C. Vardaxoglou. *Frequency selective surfaces: analysis and design.* Research Studies Press, 1997.

[101] K. J. Vinoy, J. V. Kalarickaparambil, and R. M. Jha. *Radar absorbing materials: theory to design and characterization*, volume 1. Boston, Kluwer Academic Publishers, 1996.

[102] Viridian. Viridian glass comfortsave, dandenong, Vic, australia, http://www.viridianglass.com.

[103] J. D. Walton. *Radome engineeing handbook design and principles*. Marcel dekker, Inc, New York, 1970.

[104] W. T. Wang, S. X. Gong, X. Wang, H. W. Yuan, J. Ling, and T. T. Wan. RCS reduction of array antenna by using bandstop FSS reflector. *Journal of Electromagnetic Waves and Applications*, 11(12):1505–1514, 2009.

[105] A. Watilliaux, J.M. Edeline, Philippe Leveque, T. Jay, and M. Mallat. Effect of exposure to 1800 MHz electromagnetic fields on heat shock proteins and glial cells in the brain of developing rats. *Neurotoxicity Research*, pages 1–11, 2010.

[106] Thomas Weiland. Discretization method for the solution of maxwell's equations for six-component fields. [Eine methode zur loesung der maxwellschen gleichungen fuer sechskomponentige felder auf diskreter basis]. *AEU-Archiv fur Elektronik und Ubertragungstechnik*, 31(3):116–120, 1977.

[107] A. Wexler. Solution of waveguide discontinuities by modal analysis. *IEEE Transactions on Microwave Theory and Techniques*, 15(9):508 – 517, Sep 1967.

[108] WHO. "fact sheet N" world health organisation," 2010.

[109] B. Widenberg, S. Poulsen, and A. Karlsson. Thick screens perforated with a periodic array of apertures with arbitrary cross-section. *Journal of electromagnetic waves and applications*, 14(9):1303, 2000.

[110] B. Widenberg and J.V.R. Rodriguez. Design of energy saving windows with high transmission at 900 MHz and 1800 MHz, technical report lutedx teat-7110. pages 1–14, 2002.

[111] Wikipedia. Mobile phone subscribers per 100 inhabitants, http://en.wikipedia.org. Jul 2008.

[112] T. K. Wu. *Frequency Selective Surface and grid array.* Wiley, New York, 1995.

[113] T. K. Wu. Four-band frequency selective surface with double-square-loop patch elements. *IEEE Transactions on Antennas and Propagation*, 42(12):1659 –1663, Dec 1994.

[114] C. F. Yang, W. D. Burnside, and R. C. Rudduck. A periodic moment method solution for tm scattering from lossy dielectric bodies with application to wedge absorber. *IEEE Transactions on Antennas and Propagation*, 40(6):652 –660, Jun 1992.

[115] C. F. Yang, W. D. Burnside, and R. C. Rudduck. A doubly periodic moment method solution for the analysis and design of an absorber covered wall. *Antennas and Propagation, IEEE Transactions on*, 41(5):600 –609, May 1993.

[116] H. Q. Yang and X. F. Luo. The design of band-stop filter with jerusalem-cross periodic array with four additional circular rings. In *International Conference on Advanced Infocomm Technology*, 2008.

[117] Yshield. Yshield EMR protection, Germany, http://www.yshield.com.

[118] A. F. M. Zain, Z. A. Rhazali, and S. Mohamad. Measurements and radiation distribution along the structure of a mobile phone. Asia-pacific conference on applied electromagnetics (APACE), Shah Alam, Malaysia, 2003.